MODELLING AND COMPUTER SIMULATION OF THE BEHAVIOUR OF SOLDER PASTE IN STENCIL PRINTING FOR SURFACE MOUNT ASSEMBLY

DA HE

B.Eng., M.Sc.

Ph.D. Thesis **1998**

Modelling and Computer Simulation of the Behaviour of Solder Paste in Stencil Printing for Surface Mount Assembly

Da He

B.Eng., M.Sc.

T.I.M.E. Research Institute

Department of Aeronautical, Mechanical and Manufacturing Engineering

University of Salford, Salford, UK

Submitted in Partial Fulfilment of the Requirements of the

Degree of Doctor of Philosophy, April 1998

Table of Contents

Acknowledgement

I would like to thank my supervisor Dr N N Ekere for having identified this research project and given me the opportunity to carry out this work. His help and expert guidance throughout the period of writing up is gratefully acknowledged.

I also extend my gratitude to the following people: Dr A M Dore who supported me to apply for the Overseas Research Student Award, Mark and Mike for their help and advise during my study at Salford, N Clark, B Wroe, R Gardner, S Kenway, H Pendlebury and the Department Workshop staff for their assistance to carry out the experiments.

Finally, a special thank is given to my family for their warm and loving support.

List of Figures

List of Tables

Abstract

One of the main challenges facing the electronics manufacturing industry in solder paste printing for ultra-fine pitch surface mount and flip-chip assembly is the difficulty in achieving consistent paste deposit volumes from pad-to-pad. At the very small aperture geometries required for ultra-fine pitch and flip chip assembly, flow properties of the paste becomes one of the dominant factors in the printing process. It is widely accepted that over 60% of assembly defects originate from the solder paste printing stage, and hence the urgent need for a better understanding of solder paste rheology, its behaviour during printing, and its impact on defect generation. This understanding is essential for achieving proper control of the printing process.

This thesis presents the result of work on the modelling and computer simulation of solder paste behaviour during printing, and consists of three main parts. The first part concerns the modelling of paste behaviour in stencil printing using a vibrating squeegee. The performance of the vibrating squeegee is analysed and process models developed for predicting the ideal printing conditions. In the second part, the random packing of solder powder and the microstructure of solder paste are numerically simulated by applying Monte Carlo method. The effect particle size distributions on the paste microstructure is studied in this part. Based on the simulation results of the second part, the third part concerns the study of the effect of particle size distribution on the paste viscosity and the hydrodynamic interaction between adjacent particles during paste flow. A theoretical enhanced model for predicting the viscosity of dense suspensions such as solder pastes has been developed. This correlates relative viscosity with particle size distribution and with solid volume fraction of dense suspensions.

The results of the work have wide applicability: firstly for solder paste manufacturers in optimising paste printing performance at the development stage and for stencil printing equipment manufacturers in specifying the ideal conditions for defect free printing. The simulation algorithm and the viscosity model are also applicable for a wide range of industrial processing applications; in particular metal or ceramic powder compaction, material surface coating, chemical or food material transportation.

Chapter One

Introduction

1.1 Overview and problem description

The stencil printing of solder paste is one of the key steps in the reflow soldering of electronic components and Printed Circuit Boards (PCB's) using the Surface Mount Technology (SMT) technique. In general, the stencil printing process must transfer accurate and consistent volumes of solder paste deposits onto the pads on the PCB. The components are then placed onto the PCB before the populated board is passed through an Infra-red reflow oven to complete the soldering process. Figure 1.1 shows a schematic of the stencil printing process and the key sub-processes in the printing process (Ekere, 1994).

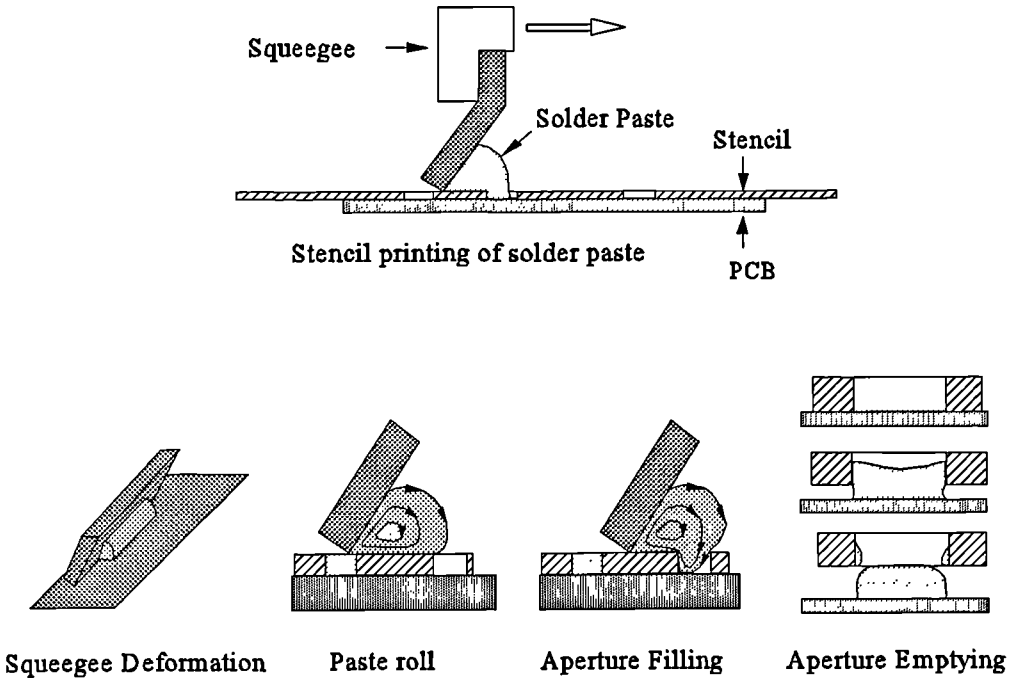

Figure 1.1 Stencil printing of solder paste and sub-processes.

As can be seen in Figure 1.1, the process can be divided into four main stages:

a). The squeegee is lowered onto the stencil to a pre-set squeegee pressure;

b). The squeegee pushes solder paste to produce a paste roll in front the squeegee;

c). The paste ahead of the paste roll is squeezed by the squeegee into the apertures;

d). Paste is transferred onto the pads on the PCB as stencil is separated from PCB.

As the trend towards miniaturisation of electronic products continues, depositing precise volumes of solder paste onto the PCB from pad-to-pad, and from board-to-board is becoming increasingly difficult at the fine-, and ultra-fine-pitch level. The importance of the paste printing process is underlined by the fact that over 60% of the surface mount assembly defects are estimated to originate from the stencil printing process (Currie, 1997). The stencil printing process is still not very well understood, and is known to be governed by complex interactions between a large number of process parameters and variables. These factors can be classified into three groups:

a). Printing equipment variables (eg. stencil material and aperture fabrication);

b). Printing process parameters (eg. printing speed and squeegee pressure);

c). Solder paste properties (eg. viscosity and creep recovery).

The main difficulty is in understanding the effect of each parameter/variable and also the nature of their interactions. The interactions between the printing process parameters **b)** and the solder paste properties **c)** have been shown to be more significant than the others (Haslehurst, 1997). The effect of the paste properties, such as its viscosity is of immense interest, as the paste property provides the link between the various sub-processes, with paste properties such as the viscosity varying from one sub-process to another depending on the applied stress/strain. The paste properties are also important even after the paste has been deposited onto the pads, to ensure that the paste deposit maintains its resolution (does not slump), and but remain tacky enough to hold onto the components after placement. As a dense suspension, the solder paste properties are directly related to the properties of the

flux/vehicle system and are determined by the solid volume fraction, the solder powder particle size and size distribution. There is thus a need for a proper understanding of the effects of various paste properties and paste microstructure as it passes through the various sub-processes, and to correlate the microstructure to the printing process performance.

As the demand for miniature hand-held and pocket electronic products continue, the major challenge facing the electronics manufacturing industry is to put more and more components into a unit area on a PCB. To meet the challenges posed by consumer's requirement for miniature products, high density components with as many as 500 input and output (I/O) leads, and with pitch sizes as small as 0.3 mm are now being designed into new products. In response, the electronics manufacture and assembly industry is forced to develop innovative processing techniques to deal such fine-pitch components. An example of one of the recent developments is the application of sinusoidal vibration to the squeegee system in the solder paste stencil printing process (Anon, 1994). The use of vibrating squeegee can provide several benefits to the stencil printing process, and this is made possible by the changes in the solder paste properties and its behaviour as it experiences sinusoidal vibration. A review of the literature shows no records of any studies on this new technique. Proper understanding of the pastes' viscoelastic properties under the action of the vibrating squeegee is important for optimising the printing quality.

In previous studies of the modelling of solder paste behaviour in stencil printing (Riemer, 1988), one of the key assumptions is that the solder paste is homogeneous, and is a single phase and continuous material. Although this assumption is reasonable in some cases (such as for modelling the paste roll in front of the squeegee), it is not be suitable in other cases (such as in the modelling of aperture emptying in fine-pitch printing, in which the aperture dimension is only an order of magnitude larger than the solder particle). In the aperture emptying case, the interactions between the particles and between the particles and aperture wall must be taken into account; this means that the paste must be considered as a discrete system. The proper modelling of the aperture emptying process requires the understanding of the nature of the particle-to-particle, and particle-to-wall interactions, and the particle

packing structure inside the aperture.

1.2 Research objectives

As stated earlier, the solder paste stencil printing process is a very critical stage in the SMT assembly process, and the printing performance is directly influenced by the properties of the solder paste. Although a number of papers on the modelling of solder paste printing have been reported in the literature (see Literature Review in Chapter two), there are no records of any previous work on the application of sinusoidal vibration to the stencil printing process, and specifically on the behaviour of the paste under the action of the vibrating squeegee. The literature search also showed that there are very few reports on the paste microstructure and its effect on the solder paste viscosity.

In this study, the following research issues and questions were addressed:

a). The behaviour of solder paste in stencil printing using a vibrating squeegee;
b). The effects of squeegee vibration parameters such as frequency and amplitude on the printing quality;
c). The pastes microstructure and the random distribution of solder particles within the flux/vehicle system;
d). The effect of solder powder particle size distribution on the hydro-dynamic interactions between neighbouring particles within the solder paste;
e). The effect of solder powder particle size distribution on the solder paste viscosity.

The main research objectives are as follows:

a). To gain an understanding of the response of solder paste to sinusoidal vibration and to develop process model of the vibrating squeegee printing process;

b). To evaluate the effects of the vibration parameters, and to determine the process window;

c). To develop computer simulation models of solder powder packing, and to study the random packing of dispersed particles, and the microstructure of solder paste;

d). To develop models for predicting solder paste viscosity based on the solder powder particle size distribution and the solid volume fraction.

1.3 Overview of thesis

The thesis contains seven chapters, and **Chapter 1** covers the project background and problem description. It also reviews the research objectives and gives an overview of the thesis. **Chapter 2** presents the literature review on stencil printing of solder pastes, and on solder paste characterization. Theoretical analysis of the behaviour of solder paste in stencil printing using vibrating squeegee and the development of the predictive models of the vibrating squeegee performance is presented in **Chapter 3**. **Chapter 4** gives a description of the vibration experiments and oscillatory shear measurements carried out on solder paste samples. It also presents the discussion on the experimental results and optimisation of the vibration squeegee parameters. **Chapter 5** presents a unique computer simulation model, which can be used to simulate the random packing of dispersed spherical particles and the micro-structure of dense suspensions such as solder pastes. **Chapter 6** is devoted to the study of the effects of particle size distributions on the particle interactions and on the relative viscosity of solder paste. **Chapter 7**, the final chapter presents a summary of the thesis, the conclusions and suggestions for future work.

Chapter Two

Review of Relevant Literature

This chapter presents a literature review on the stencil printing of solder pastes used in the reflow soldering of SM assemblies. The review covers the period from the introduction of the SMT assembly technique to date and is organised under three different headings: the characterisation of solder pastes, the modelling of solder paste printing and the experimental work on the printing.

2.1 Characterization of solder pastes

As was stated earlier in section **1.1** the majority of SM assembly defects are thought to originate at the solder paste printing process stage, and proper understanding of the effect of the paste properties and their interactions with process and equipment parameters holds the key to control the printing process. To this end, a great deal of the work on solder pastes reported in the literature concerns the characterisation of paste rheology. A good understanding of the paste processing behaviour is essential for achieving defect free SM assembly and reliable solder joints.

Most of the early work, notably Roos-Kozel (1983,1984), MacKay (1981), Daebler (1981), Hwang (1989), Park (1993), concentrated on determining the effect of the solder powder particle size distribution, shape, metal loading, and the rheology of the flux/vehicle system on the viscosity and printing.

2.1.1 Solder particles

Particle size and size distribution have been identified as being important to solder paste behaviour. Evans et al (1987) characterized the particle morphology and indicated that a tight particle size distribution without 'fines' is generally desirable. Particles below 20 μm

would tend to produce greater numbers of extraneous solder balls during paste reflow which are highly undesirable as they may result in electrical shorting of the circuit. The particle size may also influence the oxide content of the paste. Smaller particles will intrinsically have a greater oxide content due to increased surface area per gram of powder. Consequently, flux activity may be wasted on breaking down powder oxides rather than substrate oxides. This may result in poor solderability. Rubin (1983) showed that high oxide content, which may be present in small solder powder particles tends to increase solder ball formation. The similar result was reported by Lee et al (1994), but their work also indicated that finer powder can help to reduce slumping which is the major cause of bridging defects in reflow soldering.

In another study of solder pastes for fine pitch printing, Morris et al (1991) suggested a rule for achieving good stencil printing performance is that the diameter of the largest particle should not be larger than one-half the thickness of the stencil (i.e., for a 102 μm thick stencil, the largest solder particles should be smaller than 51 μm). Hwang (1994) also indicated that it is alway advantageous to use the coarsest powder allowed for achieving the desired printability so the lowest possible cost and proper fluxing can be obtained. However, it should be noted that the finer powders offer more latitude in the printing process. Lee et al (1994) investigated the effect of solder particle size on the defect rate of fine pitch printing. Their result showed that both smear and insufficient deposit defects can be reduced by decreasing the particle size. Figure 2.1 shows the relationship between pitch size and maximum particle size of solder powder for achieving a printing defect rate of less than 0.1%.

There is a wide agreement that particle shape is one of the important variables which affects the paste behaviour, and this is widely covered in the literature. However, there are still some disagreements regarding the desirability of shape variation for different aspects of the printing process. Socolowski and Roos-Kozel (1983) suggested that non-spherical or elongated particles are undesirable as they may cause aperture clogging; whilst Rubin (1983) and Daebler (1981) suggested that the introduction of a small number of elongated

or non-spherical particles can help to reduce slumping (and flowing out during paste heating) as the elongated particles enhance mechanical interlocking. Evan et al (1987) and Hwang (1994) suggested that smooth surface and spherical shape are the desired characteristics of solder particles for good stencil printing and soldering performance. Evan et al also agreed that spherical particles provide the most consistent rheological behaviour and may increase screen or stencil life when compared with non-spherical particles. Mannan et al (1995) measured the particle size distribution and shape. They found that there exists a small percentage of particles which are dumbbell shaped, ellipsoidal or more irregular. They also indicated that irregular particles will tend to cause the formation of particle clusters and agglomeration, which may contribute to the clogging of stencil apertures.

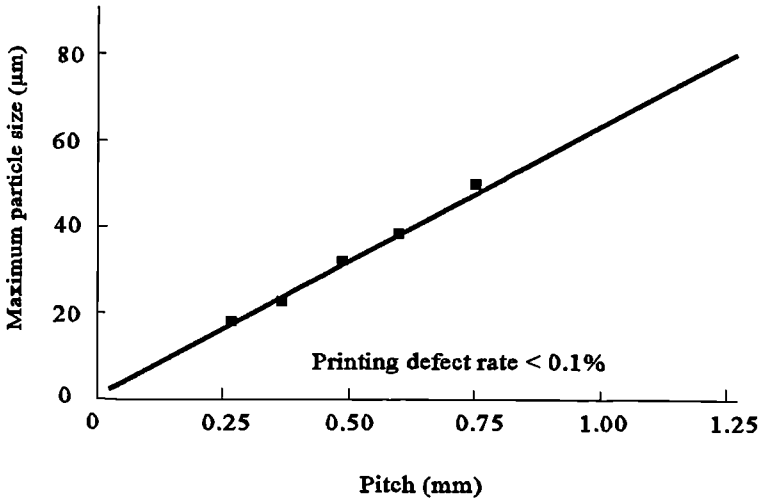

Figure 2.1 Relation between pitch and maximum particle size.

The effect of particle size distribution on the rheology of solder paste is covered in the next section.

2.1.2 Rheology of solder paste

The rheology of solder pastes is influenced by two main factors: the rheology of the flux/vehicle system, and the solder powder particle characteristics (size, size distribution, shape solid volume fraction). In practice, the major elements used by the solder paste manufacturers for controlling the rheology of the solder paste are the solder particle size distribution, metal loading and flux/vehicle rheology. In this section, four key properties of solder paste: viscosity, thixotropy, pseudoplasticity and yield point will be examined.

Thixotropy implies the paste will change viscosity over time under a constant shear rate. This behaviour may be exemplified by the presence of a hysteresis loop in the shear stress *vs* shear rate curves for increasing and decreasing shear rate, as shown in Figure 2.2 (Hwang, 1994). Lapasin et al (1994) measured the shear stress in solder paste under constant shear rate, as shown in Figure 2.3. Note that, under constant shear rate, the shear stress decreases with time. Hwang (1994) indicated that although the thixotropic nature of solder paste is assumed, the measure of the thixotropy is important to the resolution of

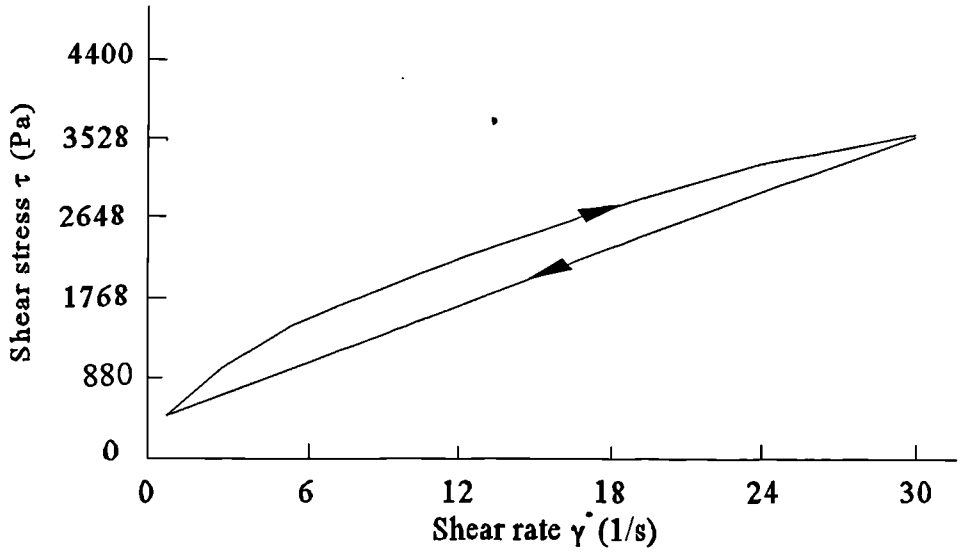

Figure 2.2 Hysteresis loop of solder paste

paste deposition. Excessive thixotropy hinders the viscosity recovery process, causing post-print slumping. On the other hand, shear thinning is advantageous, facilitating the transfer of paste through the narrow stencil apertures. Evans et al (1987) believed that thixotropic behaviour of solder paste is undesirable as it causes the paste to fluctuate in viscosity over the course of a working day as the paste is agitated by mixing, handling, and printing. Thixotropy may also make reproducible viscosity measurement difficult depending on how much recovery time occurs after initial agitation of the paste.

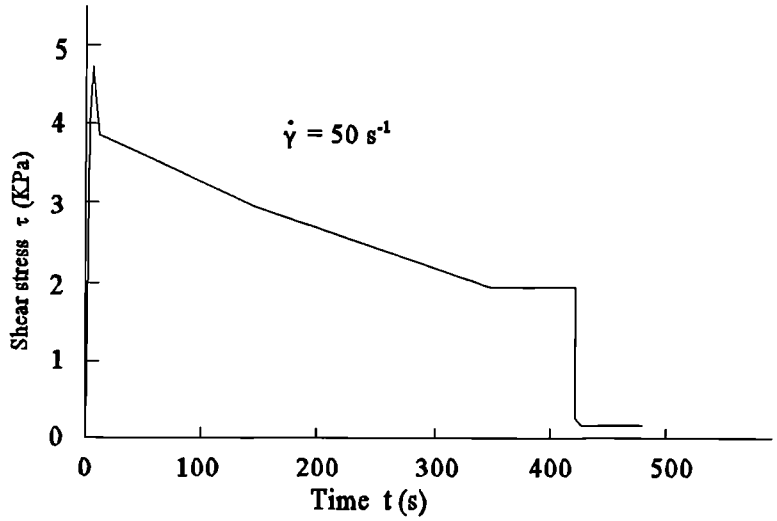

Figure 2.3 Time-dependent effect under constant shear rate

Pseudoplasticity implies that viscosity of solder paste will drop dramatically on the application of shear stresses and subsequently recover when the stresses are removed. This behaviour is illustrated in Figure 2.3. Lapasin et al (1994) measured the pseudoplasticity of solder paste and fitted the experimental data with the Casson model as:

$$\sqrt{\tau} = \sqrt{\tau_0} + \sqrt{\eta_\infty}\sqrt{\gamma'} \qquad (2.1)$$

where τ_0 is the yield point or yield stress as $\gamma' \rightarrow 0$ and η_∞ is the infinite viscosity as $\gamma' \rightarrow \infty$. Figure 2.4 shows the fitting of measurement data with the Casson model. A review of the work by Hwang, Evans et al, Lapasin et al shows that they agree that the plastic flow behaviour of solder paste is desirable for both screen and stencil printing. This behaviour facilitates the filling of solder paste into the apertures under high shear stress and allows the paste deposits to retain the desired shape on the PCB pads after the shear stress is removed.

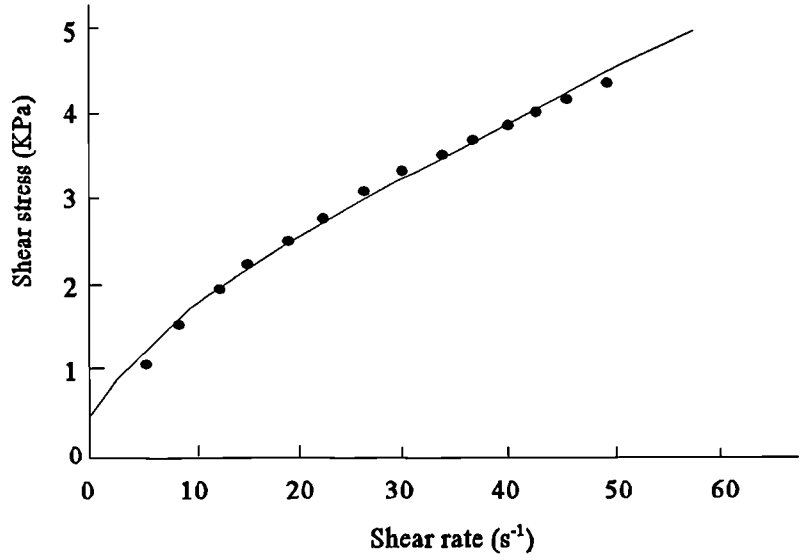

Figure 2.4 Pseudoplasticity of solder paste fitting with Casson model. (Lapasin)

The yield point or yield stress refers to the maximum shear stress that the material can withstand without flowing. There exist yield points for solder pastes, which can be found from Figure 2.2 and Figure 2.4 at zero shear rate. Usually, at a given temperature, the yield point is proportional to the solid volume fraction of a dense suspension. With solder paste, a high yield point will demand a high shear stress to generate flow. Conversely, a low yield point tends to generate deposit slumping. Morris et al (1994) investigated the relationship between the yield point of solder paste and the minimum pad pitch, and they indicated that as the yield point increases the minimum pad pitch decreases, as shown in Figure 2.5.

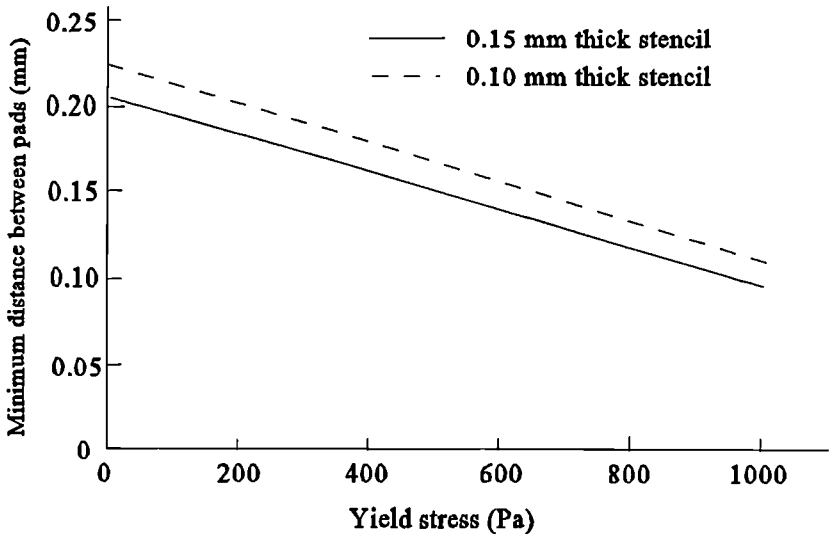

Figure 2.5 Relationship between min. pad separation and yield point.

The viscosity of the solder paste is widely considered to be the most important rheological property. The viscosity influences the paste roll in front the squeegee, the filling of the apertures and the paste release from the apertures. The viscosity of solder paste is affected by a lot of factors such as the shear rate, the temperature, the metal load and particle size distribution. Hwang (1994) indicated that "As a convenience, a single-point viscosity has been used as an indicator of paste consistency. It is a useful measurement when the following conditions are met:

- The rheology of the paste is known;
- The paste handling technique immediately prior to measurement is specified;
- The measurement technique and equipment are specified;
- The measurement temperature is specified."

If other factors are constant, the metal load and the particle size distribution strongly affect

the viscosity of solder paste. Lee et al (1994) measured the viscosity of Sn63 solder paste as a function of the metal load (the volume fraction of solder powder) which is shown in Figure 2.6. They indicated that the volume fraction of solder powder appears to be more meaningful for a structure-property correlation study of solder paste. The maximum metal load for solder paste is 59%(v/v) or 92.5%(w/w). They attributed the rapid increase in viscosity for high volume fraction to the onset of formation of powder cluster. As result, the viscosity of a high metal load is dictated by the solder powder, and the variation in the flux/vehicle viscosity will have a relatively minor effect on the paste viscosity.

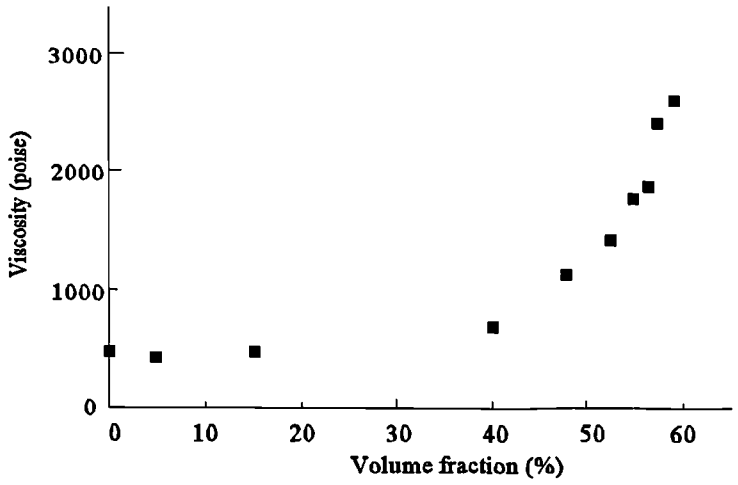

Figure 2.6 Viscosity vs solid volume fraction of Sn63 paste.

For dense suspensions, such as solder paste, since the variation in the flux/vehicle viscosity will have a relatively minor effect on the paste viscosity, it is more convenient to express the viscous property by relative viscosity, η_r, than apparent viscosity. Relative viscosity is defined as the ratio of the paste viscosity to the flux/vehicle viscosity. The relative viscosity of a dense suspension with spherical particles is affected by two variables: the solid volume fraction, ϕ, and the maximum solid volume fraction, ϕ_m, which is the limitation of ϕ. Mannan et al (1995) analysed the effect of particle size distribution on the relative viscosity of solder paste. The relationship between η_r and (ϕ/ϕ_m) can be generally expressed as:

$$\eta_r \propto [\ 1 - (\frac{\phi}{\phi_m})^a\ ]^{-b} \qquad (2.2)$$

where a and b are positive constants. Mannan et al indicated that, the maximum solid volume fraction, ϕ_m, of poly dispersed particles is higher than that of uniform particles, and hence the lowering of the viscosity. It can be observed from Equation (2.2) that as ϕ approaches ϕ_m, η_r tends to be infinite.

There are also some other paste properties that affect the stencil printing process. Lee et al (1994) studied the tack and tack time of solder paste which are indicators of the capability of paste deposits to hold the components on pads prior to reflow. Currie (1997) investigated the tensile strength of solder paste experimentally. In the experiment, paste samples were sandwiched between two parallel plates which were then separated. The force and time required for complete separation of the paste was measured. Experimental result showed that the tensile stress of solder paste depends on both the strain rate and the sample geometry. The empirically enhanced model developed can be used to predict the onset of skipping defect in the aperture emptying process, and it can be used to estimate when skipping is likely to occur for a given stencil aperture geometry and stencil and PCB separation speed.

2.2 Modelling of solder paste printing

The stencil printing of solder paste is a relatively new technique when compared with the well established screen printing technique which is used to produce thick film circuitry on PCB's. The screen printing process is illustrated in Figure 2.7. There are several models of screen printing in the literature which may be applied to stencil printing of solder paste when the differences between the two techniques are identified. Therefore, these screen printing models will be reviewed. Mannan et al (1993) identified the similarities and the differences between the two techniques and discussed the possibility of applying screen

printing models to stencil printing of solder paste. The similarities between the two techniques are:

i. A squeegee moves along the stencil or screen surface to drive a paste roll ahead (either solder paste or ink). The squeegee generates hydrostatic pressure in the paste roll, which injects the paste into the apertures, and the paste wets the substrate. The squeegee then shears off the paste inside the apertures from the paste roll as it moves over the apertures.

ii. Both the solder paste and the ink are non-Newtonian, and the rheological properties change dramatically during the different printing stages.

iii. In both processes, clogging of apertures and smearing of deposits are the main defects.

The differences between the two techniques are:

i. Screen printing is performed off-contact while stencil printing is generally on contact. Therefore, the screen/stencil and substrate separation patterns are different.

ii. In screen printing the pressure difference above and below the screen governs the transfer of ink through the screen and onto the substrate. Whilst, in stencil printing the adhesive forces of paste to the aperture wall and to the substrate are the decisive factors.

iii. The aperture geometries of stencils and screens are different.

iv. The viscosity of solder paste is higher than that of ink and ink can be modelled as a homogeneous fluid. However, for solder paste, the presence of solder particles in the paste can not be ignored, especially as it flows through narrow apertures.

Riemer (1988) indicated that, in screen printing of ink, the ink roll in front of the squeegee forms a hydrodynamic pump that generates a high pressure. This pressure injects viscous

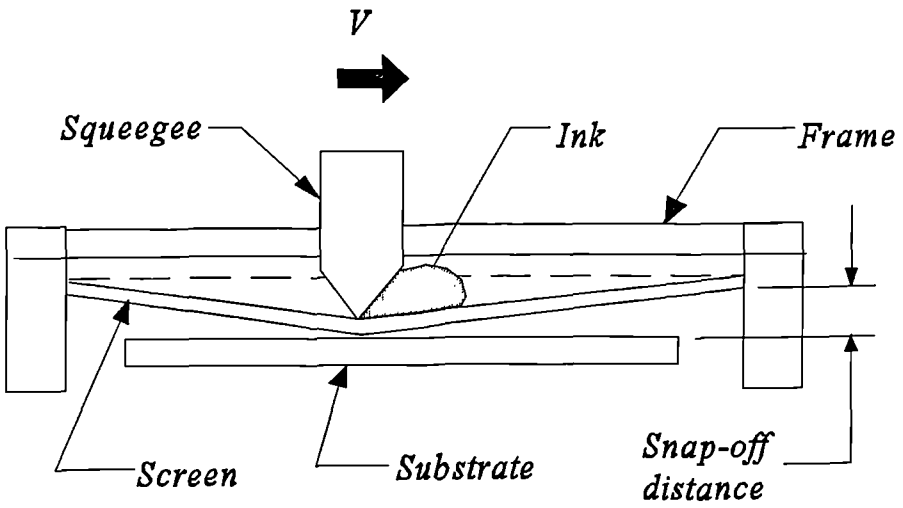

Figure 2.7 Off-contact screen printing of ink.

ink into the mesh openings. To model the ink roll he employed the simplified Navier-Stokes equation for high viscosity fluid which has the form:

$$-grad\ p + \eta \Delta v = 0 \qquad (2.3)$$

where p is the hydrostatic pressure (scalar), v is fluid velocity (vector), η is the viscosity of ink, grad $= \partial/\partial x\ \mathbf{i} + \partial/\partial y\ \mathbf{j}$, **I** and **j** are unit vectors, $\Delta = \partial^2/\partial x^2 + \partial^2/\partial y^2$. In this equation only viscous forces and pressure drop are considered (other relatively small forces such as gravity, centrifugal force and inertia are neglected) and Newtonian fluid is also assumed. For infinite amount of fluid, Taylor derived a stream function to solve the Stokes equation in cylindrical polar coordinates, r-φ. The stream function is presented as:

$$\Psi = r\ V\ T(\varphi,\ \alpha) \qquad (2.4)$$

where $T(\varphi,\alpha)$ is the Taylor's function composed of trigonometric functions, α is the wedge

angle between squeegee and screen surface and V is the squeegee speed. The velocity components v_r and v_φ are derived from the stream function as:

$$v_r = \frac{1}{r}\frac{\partial \Psi}{\partial \varphi} \qquad v_\varphi = -\frac{\partial \Psi}{\partial r} \tag{2.5}$$

The hydrostatic pressures on the squeegee and on the screen surface are derived as:

$$p_{sq} = \frac{1}{r}\frac{2\alpha \sin\alpha}{\alpha^2 - \sin^2\alpha}\eta V \qquad p_{sc} = \frac{1}{r}\frac{2\sin^2\alpha}{\alpha^2 - \sin^2\alpha}\eta V \tag{2.6}$$

The total force on the squeegee surface is represented by the integration of the pressure p_{sq} as:

$$F_{lift} = \int_0^Q p_{sq} dr = f(Q)\frac{2\alpha \sin\alpha}{\alpha^2 - \sin^2\alpha}\eta V \tag{2.7}$$

where $f(Q)$ is a factor increases with ink quantity (Q) in front of the squeegee. F_{lift} tends to lift the squeegee that may lead to increasing of ink deposit height on the substrate. Equation (2.5) (2.6) and (2.7) establish the effect of ink viscosity, squeegee angle and printing speed on the ink roll, the screen and squeegee surface pressures and lift force acting on the squeegee. Figure 2.8 is the simplified streamline and pressure distribution of Riemer's model.

Riemer's work makes significant contribution both to screen and stencil printings, and some useful common ideas can be taken over directly to model the stencil printing process, such as the paste/ink roll in front of the squeegee, the pressure distributions on the screen and on the squeegee surface and the shear rate in the paste/ink near the contact point between the squeegee and stencil/screen may also be predicted.

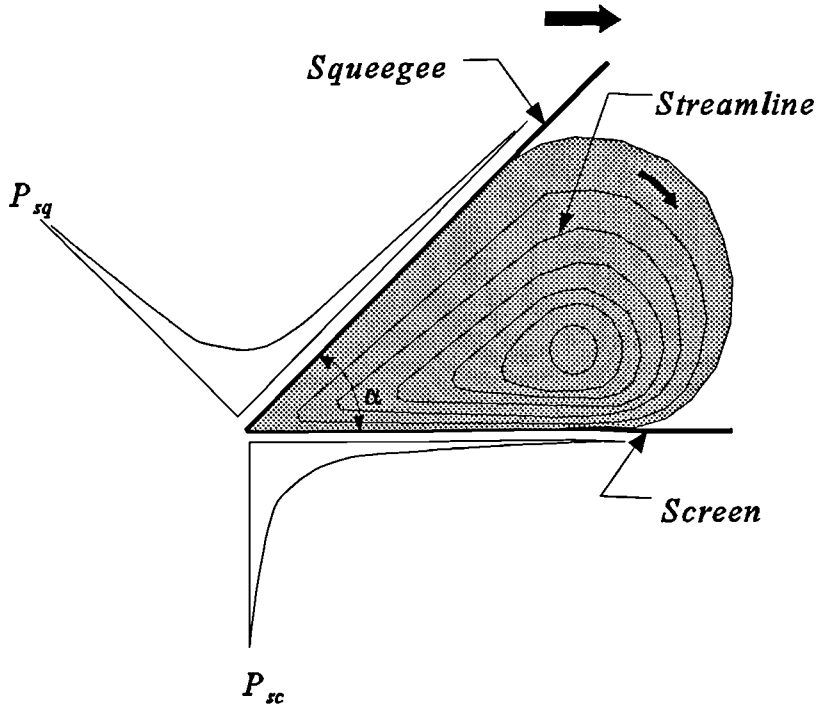

Figure 2.8 Streamline and pressure distribution of Riemer's model.

Harahan et al (1991, 1992) modelled the solder paste roll in front of a squeegee with infinite volume and with free surface. Several assumptions similar to that in Riemer's model were also made. The continuity and momentum equations were solved along with boundary conditions using a CFD package. There is close agreement between Riemer's model and Harahan's model. Harahan et al found that both infinite volume and free surface models predict similar shear rates across the entire stencil length as shown in Figure 2.9. But the pressures predicted by the two model are only similar near the squeegee and stencil contact point. Far from the contact point the pressure predicted by the free surface model is smaller than that predicted by the infinite model as shown in Figure 2.10. The Harahan et al work is very useful for predicting the pressure, the shear rate and paste flow near the squeegee and stencil contact point.

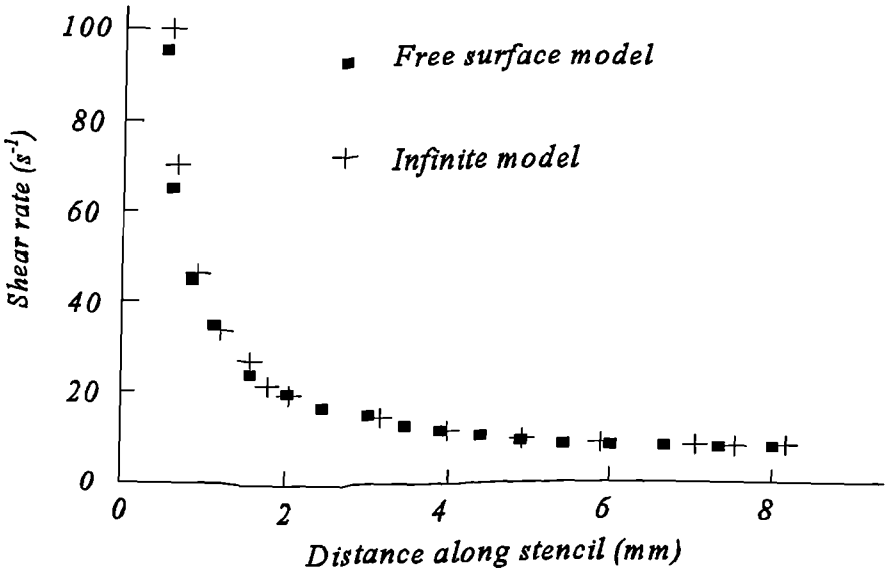

Figure 2.9 Solder paste shear rate at stencil surface

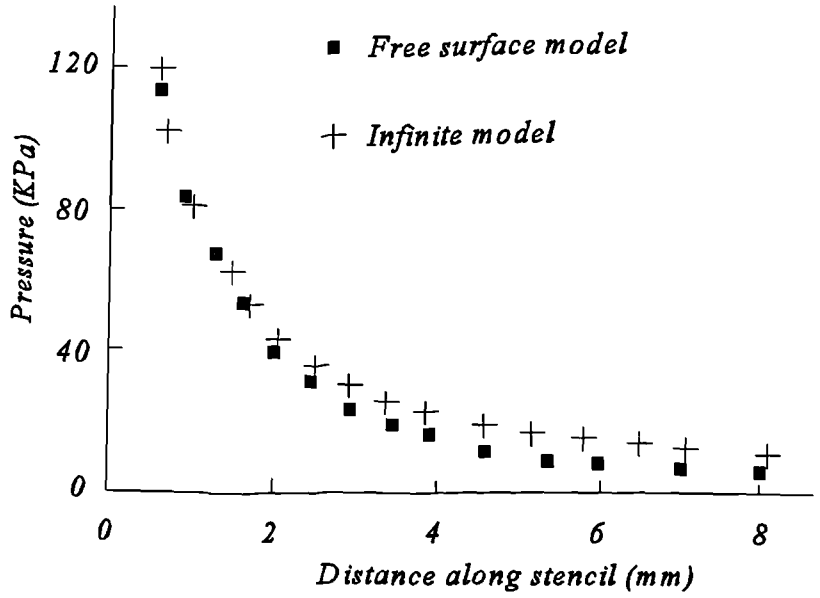

Figure 2.10 Solder paste pressure on the stencil surface

It is important to notice that both Riemer and Harahan et al assumed the ink and the paste to be Newtonian fluids. In fact both materials are non-Newtonian and the viscosities vary with shear rate, and usually decrease with an increase in the shear rate. This shear thinning property of both materials significantly affects the pressure and velocity near the squeegee and stencil (or screen) contact point because the shear rate in this region is very high. It is also important to notice that, Riemer and Harahan et al both assumed that there is no slipping at the interface between ink/paste and screen/stencil. However, it has been demonstrated by Kolli et al (1997) that it is only when the ink/paste is properly formulated and printing parameters are carefully selected that the no slipping assumption are true.

Owczarek and Howland (1990a) also modelled the screen printing process. Their model is focused on the flow pattern as ink/paste is injected into screen openings. The flow field ahead of the squeegee is divided into three regions: the pressurization region I, the downward screen cross-flow region II, and the paste accumulation region III, as shown in Figure 2.11. In this model Owczarek et al first raised the concept that underneath the squeegee there is a flow of paste with speed w relative to the substrate in the direction opposite to the squeegee motion, V. This flow is caused by the pressure build-up ahead the

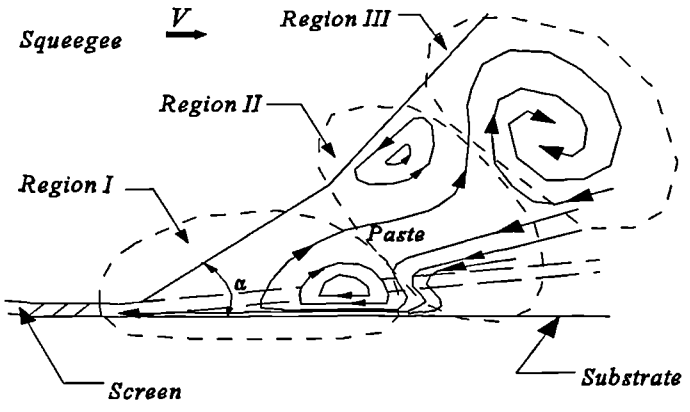

Figure 2.11 Motion of paste relative to squeegee.

squeegee. Using continuity equation they derived the relation between the thickness of deposited wet paste, H, and the average paste thickness, h, under the squeegee, as shown in Figure 2.12. The average speed, w, of paste underneath the squeegee is estimated between 0.1 and 0.2 of the squeegee speed. This opposite flow of paste leads to H being higher than h.

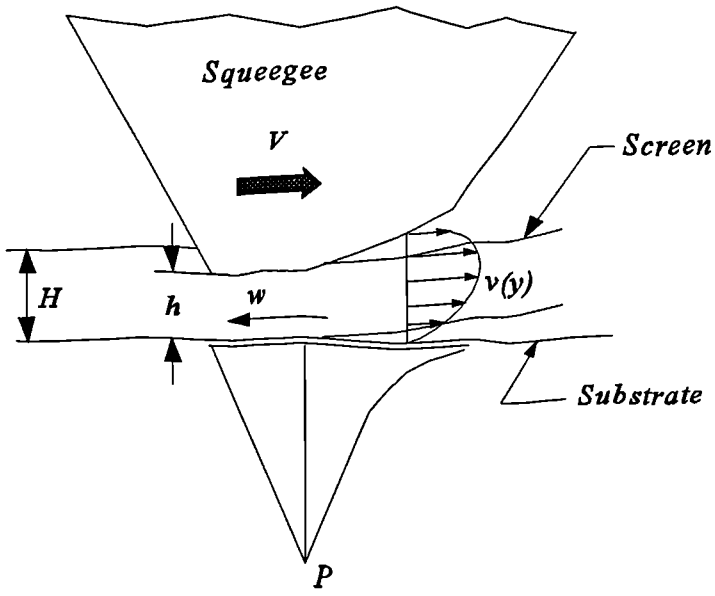

Figure 2.12 Deposit thickness H in relation with h, paste velocity and pressure profiles.

In a subsequent paper, Owczarek and Howland (1990b) derived the profiles of horizontal velocity, $v(y)$, and the pressure, P, near the squeegee tip by the application of the momentum equation to the paste element. The velocity and pressure are also shown in Figure 2.12. In the above derivation, a power law is used to represent the relationship between shear rate and shear stress in the paste, and the vertical component of the flow velocity is assumed to be very small relative to $v(y)$ because the squeegee and substrate contact angle α is very small. The squeegee tip deformation and the real contact angle can be estimated from the pressure distribution. Then the velocity of paste flow underneath the

squeegee tip, w, and deposit thickness, H, are calculated.

Mannan et al (1993) examined Owczarek and Howland's model and examined the idea of building into the model the distortion of the squeegee tip as applied to stencil printing. The power law fluid assumption leads to the calculation of velocity profile and pressure distribution more accurately than the Newtonian fluid assumption. The paste flow under the squeegee in the direction opposite to the squeegee motion is also one of the possible explanations of the observation in stencil printing that the deposits are often higher than the stencil thickness; there are also some assumptions in this model that are questionable such as the neglecting of the vertical velocity component near the squeegee tip and the effect of the screen on the paste flow not being taken into consideration.

In all of the above models, the ink/paste is treated as a uniform, continuous and homogenous liquid. Such a treatment to solder paste may be reasonable in cases where the concerned geometry and dimensions are much larger than the solder particle size, such as modelling the paste roll in front of the squeegee. However, when the particle size is comparable with the geometric dimension, such as the filling and emptying of stencil apertures, where the ratio of the thickness or width of stencil apertures to the particle size is less than 10, the effect of particle size cannot be ignored. In such case the interactions between individual particles should be taken into consideration.

Mannan et al (1994) investigated paste withdrawal from stencil apertures by considering the motion of each individual particle. For solder paste with 50% solid volume fraction of solder particles, the average gap between neighbour particles was estimated to be about 0.1 of the average particle size. Therefore, in this model the motion of each individual particle was assumed to be governed by lubricational forces between it and its nearest neighbouring particles. For particles near the aperture wall, lubricational forces between particles and aperture wall were also taken into account. Other forces, such as gravitational and inertial forces and far field particle forces were neglected; particle rotation was also neglected. For each particle the force balance equations could be written. Periodical boundary condition

was applied along the aperture length to reduce the number of particles considered. Applying explicit method, the particle positions, the tensile and shear forces in the paste at each step in time were determined by solving the group of force balance equations. Using this simulation technique Mannan et al examined the effects of aperture shape, solid volume fraction and particle size distribution on the tensile stress in the paste during withdrawal.

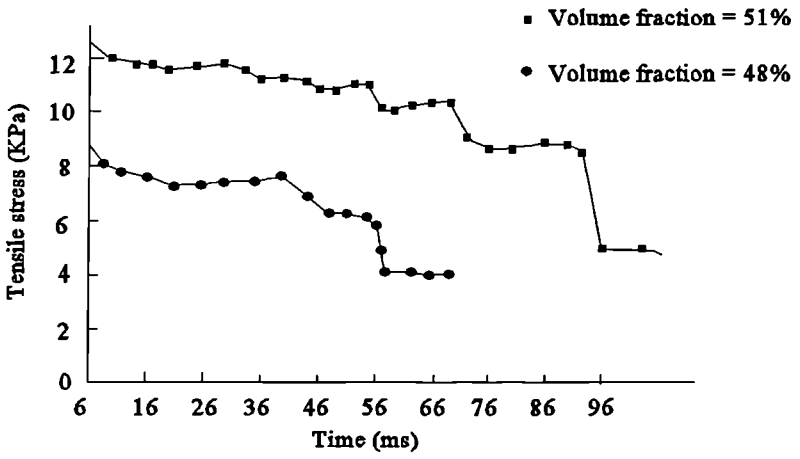

Figure 2.13 Effect of solid volume fraction of solder particles on tensile stress in the paste.

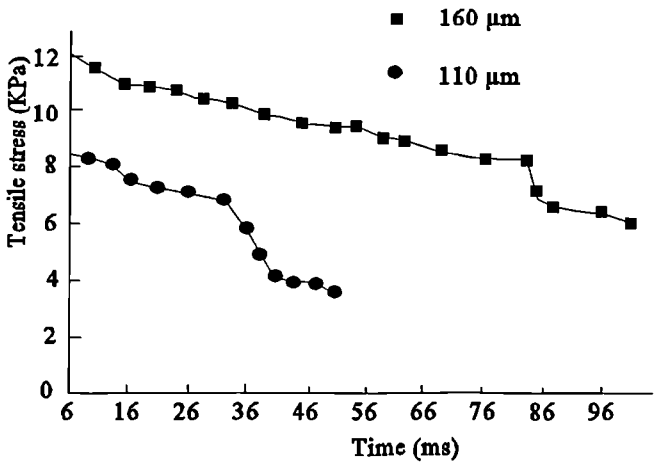

Figure 2.14 Effect of stencil thickness on tensile stress in paste.

The separation speed of the stencil from the substrate was assumed to be 1 mm/s. Then the tensile stress was compared with the tensile strength of solder paste to predict when skipping will occur. Figure 2.13 shows the effect of solid volume fraction and particle size distribution on the tensile stress in the paste and Figure 2.14 shows the effect of stencil thickness.

Mannan et al (1993, 1994) also theoretically investigated squeegee deformation during stencil printing. First, the static deformation was predicted using stencil material properties; for a squeegee of 90-94 hardness on the Shore A scale, and squeegee/substrate contact force of 480 N/m, Figure 2.15 shows the squeegee profile across a 0.25 mm wide aperture. Then the squeegee was treated as a damped harmonic oscillator and the dynamical deformation during the printing process was predicted by vibration theory. Mannan et al concluded that the use of a hard squeegee increases the defect rate of skipping compared with the use of a soft squeegee; the use of a soft blade tends to scoop more paste out of the aperture than the use of hard one. They suggested that a soft blade should be used for fine-pitch printing, while a hard blade being more suitable for large apertures.

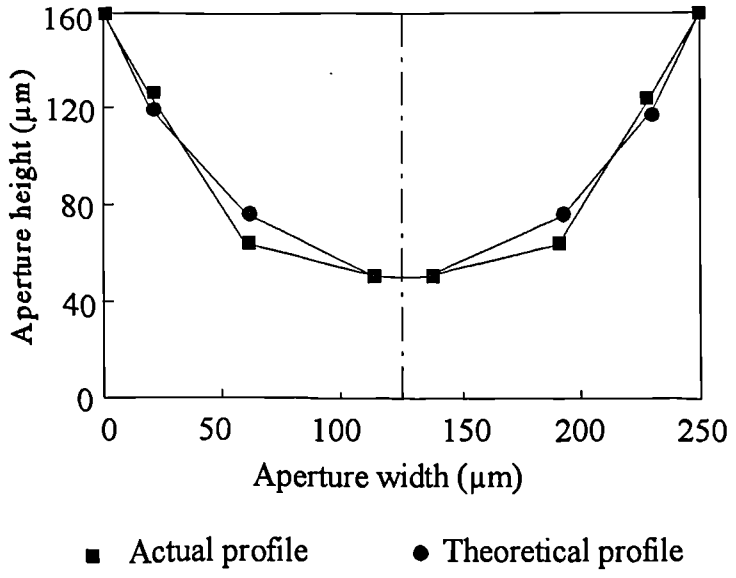

Figure 2.15 Comparison of squeegee profiles cross aperture

2.3 Experimental investigations

Since the introduction of the stencil printing technique into the assembly process of PCB's, theoretical analysis and numerical simulation models have been developed to study this process and investigate the effects of variables on the performance. Because the number of variables governing this process is very large and their interactions are too complex to be taken into account completely in the models, experimental studies have been and still are widely used. A lot of experimental investigations can be found in the literature. In this section some of the experimental investigations are reviewed.

There are three methods commonly used for fabricating stencils, electroforming, chemical etching and laser cutting. The fabrication can directly affect the paste printing quality. Clouthier (1995) appraised stencils made by different methods for fine-pitch printing. He indicated that electroform method allows for tight tolerance control and is geometrically blind which means different shapes can be produced. Laser cutting provides a fine geometry capability compared to chemical etching, but it tends to leave a rough aperture wall which may hinder the solder paste transfer efficiency. Chemical etching is the most economical means of producing stencils but as pitches continue to reduce, repeatability from aperture to aperture becomes difficult. The aperture's knife edges add to clogging and the deposition of too little solder paste. Measurement on the aperture sizes from 142 samples for each fabrication method, showed that for ultra-fine pitch aperture (0.0045″ width) chemical etching and laser cutting show a process variability of between two to four times the process variability for the electroforming method.

The ideal stencil will have aperture shapes optimized for the specific printing requirement, and it could be expected that shapes requested will be provided by the stencil manufacturer. As apertures and associated pitches become smaller, however, there is growing interest in evaluating alternative aperture shapes that may enhance the release of materials, provide flexibility to improve paste distribution on the pad and add to flexibility of pad design. Figure 2.16 shows a comparison of aperture shapes made by three different methods.

The laser-cut and chem-etch stencil apertures are ragged and the ends do not have well-defined corners or end segments as compared with that of electroformed stencil.

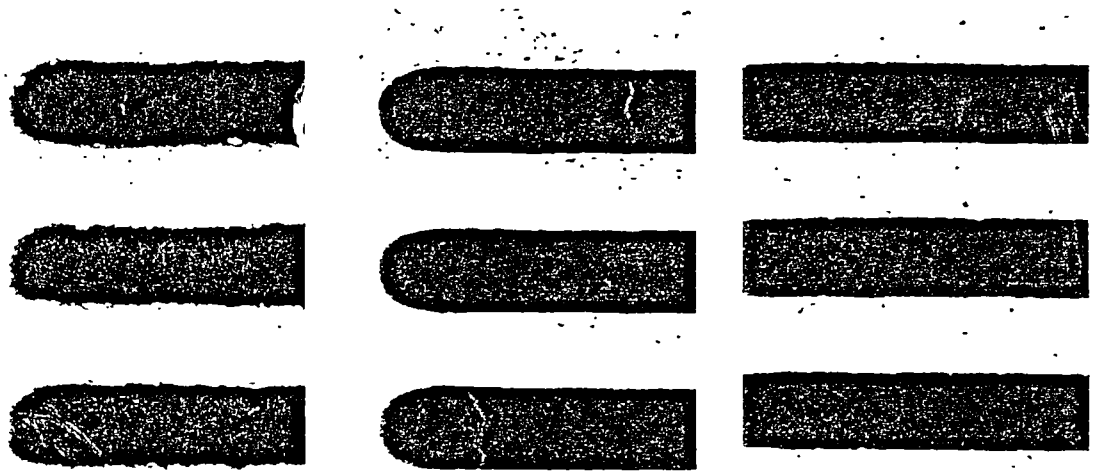

Chemical etched Laser cut Electroformed

Figure 2.16 Comparison of aperture shapes of three fabrication methods. (Clouthier)

The accuracy of aperture location is as important as the aperture size and shape. Inaccurate aperture location will cause major problems downstream in the pick-and-place and reflow processes. To evaluate the accuracy of aperture location of the three fabrication methods, Clouthier conducted actual printing experiments. The basic parameters were developed using Taguchi experimental design techniques. Experimental result demonstrated that the accuracy of aperture location of electroformed stencil is higher than that of the other two, which leads to high print image quality. Figure 2.17 shows a comparison of ultra-fine-pitch traces of three stencil printing processes. Experimental result showed that for ultra-fine-pitch, less than 0.38 mm, a 0.1 mm thick electroformed stencil yielded approximately 98% paste transfer while the paste transfer with laser cut stencil was 60% and less than 50% for chemical etched stencil. Clouthier concluded that electroformed stencil will achieve low variability and improve first-pass yields.

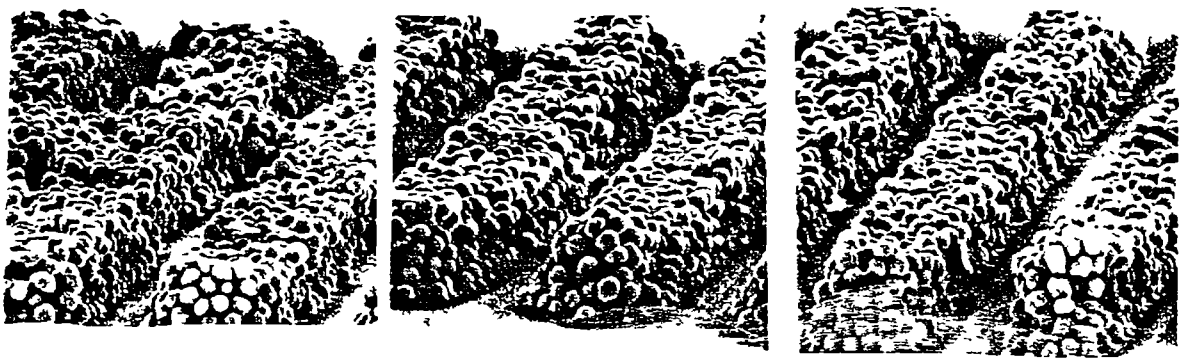

Chemical etched Laser cut Electroformed

Figure 2.17 Comparison of fine-pitch traces of three stencil printing processes. (Clouthier)

To meet the tight tolerance requirement for fine-pitch printing and to reduce the cost of the stencil manufacturing, Myklak and Coleman (1995) investigated the application of hybrid stencil: laser cut/chemical etched stencil. The stencil had some apertures laser cut and some apertures chemical etched. Both the laser cut and chemical etched apertures were electro polished. Due to the high cost of laser cutting process only the apertures of 0.5 mm pitch and less were laser cut and the remaining apertures were chemical etched. They experiments demonstrate that the hybrid stencil provides a high printing quality whilst the cost of stencil manufacture is still economical. In addition, this speeds up delivery, which is an essential factor in the fast paced SMT industry.

Besides the stencil fabrication method and the rheology of the solder paste, the paste withdrawal process from stencil apertures is also governed by the stencil/substrate separation speed. Ekere et al (1993) investigated the effect of separation speed on the paste withdrawal process experimentally. In the experiments a 0.125 mm thickness chemical

etched stencil was used with different ratios of aperture pitch to aperture width. The apertures were clustered in 100 groups with 100 apertures in each group. In each group of 100 apertures some were orientated perpendicularly and some parallel to the squeegee travel direction. Figure 2.18 shows the paste deposit height profile that the aperture was perpendicular to the squeegee travel direction. To eliminate the effect of other factors the underneath of the stencil was cleaned after each print stroke. Four solder pastes were used in this experiment. For each paste, three values of separation speed (1, 10, and 5 mm/s) were examined. The squeegee speed was 12 mm/s. Their experiment results confirmed that the effect of varying separation speed on the print quality is paste-dependent, but small. For some pastes a low separation speed is not favourable. But for other pastes there is no statistically significant effect of separation speed. For a 0.35 mm fine pitch, bridging is the most serious defect which indicates that either the paste flow underneath the stencil during separation (leading to bridging) is affected by separation speed or the paste deposits are likely to slump at different separation speeds. Compared with bridging, the skipping defect is insignificant and there is no correlation with separation speed which means that the adhesive force of the paste to the substrate dominates over the frictional forces at the aperture walls for all values of separation speed. The bridging defect rate, for 0.35 mm pitch, obtained by this experiment was from a minimum value of 7.5% up to a maximum value of 32.5%, which is in agreement with Clouthier's and Myklak and Coleman's conclusions that chemical etched stencils are unsuitable for fine/ultra-fine-pitch printing (see Figure 2.16 and Figure 2.17).

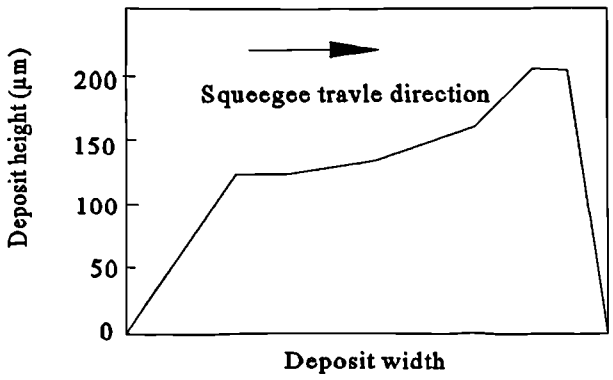

Figure 2.18 Paste deposit height profile.

To model the withdrawal process of solder paste from apertures, Head et al (1994) adapted and programmed a micro-mechanical testing device to measure the shear stress developed at the interface between the solder paste and the side wall of the stencil aperture as the stencil is separated from the substrate. The test set up is shown in Figure 2.19, which is very similar to a parallel plate rheometer. A paste sample was sandwiched between two horizontal parallel plates which were mounted in a mechanical stressing device; the bottom plate was stationary and the top one was driven at a constant speed of 1 mm/s (similar to the stencil/substrate speed) to shear the sample. The gap between the plates was adjustable between 0.16 and 1.5 mm to investigate the changes in the shear force required to overcome the shear strength of the paste for various aperture dimensions. The test was started from a full overlap of 1 cm of the two plates to the release of the overlap and the shear stress was recorded. Two paste samples were tested. Figure 2.20 shows one of the experimental results in which the shear stress is as function of the gap size between the two plates. As a stencil is separated from a substrate the aperture wall acts as a shearing plate which transfers shear stress to the paste. The shear stress is an important factor that affects the final deposit volume of paste on the pad of the PCB. Experimental result shows that the smaller the gap the higher the shear stress. This can be useful in assessing the applicability of the stencil for fine-pitch printing.

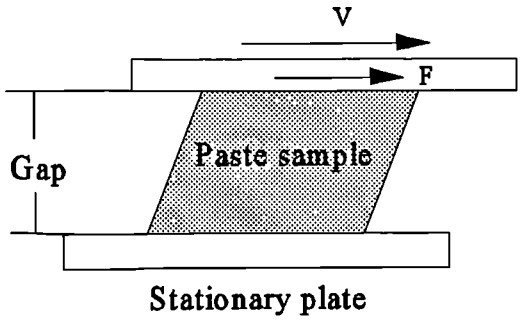

Figure 2.19 Shear stress applied to solder paste. (Head)

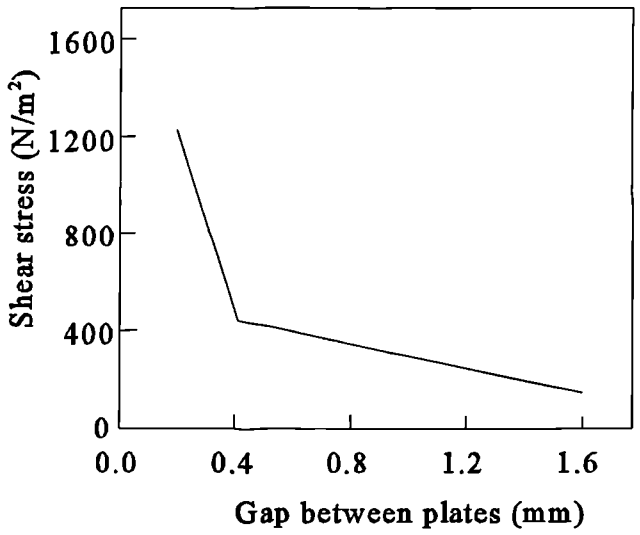

Figure 2.20 Shear stress vs gap between plates. (Head)

Head et al's work does provide useful information about the rheological properties of solder paste. However, it does not provide ideas on how to apply the experimental result to predict the stencil/substrate separation performance. In addition the experiment is more like a viscosity measurement than a measure of the stencil/substrate separation process. In the separation process the paste does not merely experience simply a shear force at the aperture wall there is also adhesive force exerted on the paste by the substrate which together with the shear force of the aperture side wall will generate tensile stress in the paste. If the adhesive force, which is affected by the surface energy of the pads and by the paste properties, is smaller than the shear force, the paste could not withdraw from the aperture to the pad, but will remain inside the aperture. If the tensile stress exceeds the tensile strength, the paste inside the aperture will deform and part of the paste will be deposited on the pad and part will be left inside the aperture. In both of these cases aperture clogging defects will occur.

Li et at (1996) investigated the effect of printing equipment parameters on the printing quality. The overall objective of their investigation was to determine the optimum settings

of the designing parameters, which would result in minimum solder paste height variation for new board designs with 0.5 mm, 0.625 mm and 1.25 mm pitch pad patterns. First, a Taguchi orthogonal array, L27, was designed to capture the main effects of six most important printing equipment parameters and the PCBs pad conditions. Some interaction between the parameters were also examined. Experimental data were used to construct neural network models to correlate the desired quality characteristics to the input design parameters. A modular approach was used to select the appropriate architecture for these models. These models in conjunction with the gradient descent algorithm were used to determine the optimum settings for minimum solder paste height variation. The optimum settings predicted by the model was validated by experiments on the production line. In addition to the combination of all three pad patterns, Li et al also built neural network models for individual and dual combinations of the three pad patterns. They concluded that there are different optimum settings for different pad pattern combinations.

Haslehurst et al (1996) intensively investigated the parameter interactions in stencil printing of solder paste. Eleven parameters, each at two levels, were examined. The parameters and the levels are given in Table 2.1. In order to reduce the number of experiments, a Fractional Factorial Design method was employed which uses only a fraction of the total possible combinations of levels and the highest order of interactions were assumed negligible. By this method all of two parameter interactions and some three parameter interactions could be estimated. The height of paste deposit was measured as the criterion of printing quality.

Figure 2.21 shows the main effect of individual parameter on the mean paste deposit height. Among the printer parameters, pressure (squeegee loading) and direction of print stroke are by far the most significant. Haslehurst et al indicated that high pressures are likely to reduce the deposit height because the squeegee is more likely to scoop paste out of the apertures as it passes over them. This experimental result agrees with the prediction of theoretical analysis by Mannan et al. Haslehurst et al attributed the significant effect of direction of print stroke to asymmetries in the printer mechanism or in the stencil. They also suggested that in order to compensate for this effect, the squeegee loading and speed should be set

independently for the forward and reverse print strokes. As mentioned earlier, the squeegee speed and separation speed are important parameters that affect the printing process, but Figure 2.21 shows the effects of these two parameter are not very significant. Haslehurst et al suggested this may be because the two levels were too close together for the effects to show up. Of aperture geometry parameters, aperture width produced the most significant main effect. Haslehurst et al suggested that both the filling and the emptying of narrower apertures may be more difficult than that of wider apertures which lead to insufficient paste deposit on the PCB. Aperture orientation was also important: the mean height for apertures with the long axis parallel to the squeegee blade was higher than that for the apertures perpendicular to the squeegee blade. This is also in agreement with Mannan et al's prediction. In the experiments Haslehurst et al also found that the mean deposit height was affected by the aperture pitch where the larger the pitch the higher the deposit. This suggests the paste roll may be affected by the distance between two apertures.

Table 2.1 Levels of parameters

Factor	Low level	High level	Factor	Low level	High level
Squeegee loading	5 kg	10 kg	Printing direction	Reverse	Forward
Squeegee speed	16 mm/s	25 mm/s	Pitch	0.4 mm	0.5 mm
Separation speed	2 mm/s	6 mm/s	Aperture length	1.5 mm	2.0 mm
Print gap	0.0 mm	0.1 mm	Aperture width	0.1 mm	0.2 mm
Print stroke	290 mm	333 mm	Orientation	0°	90°
Squeegee delay	2 s	8 s			

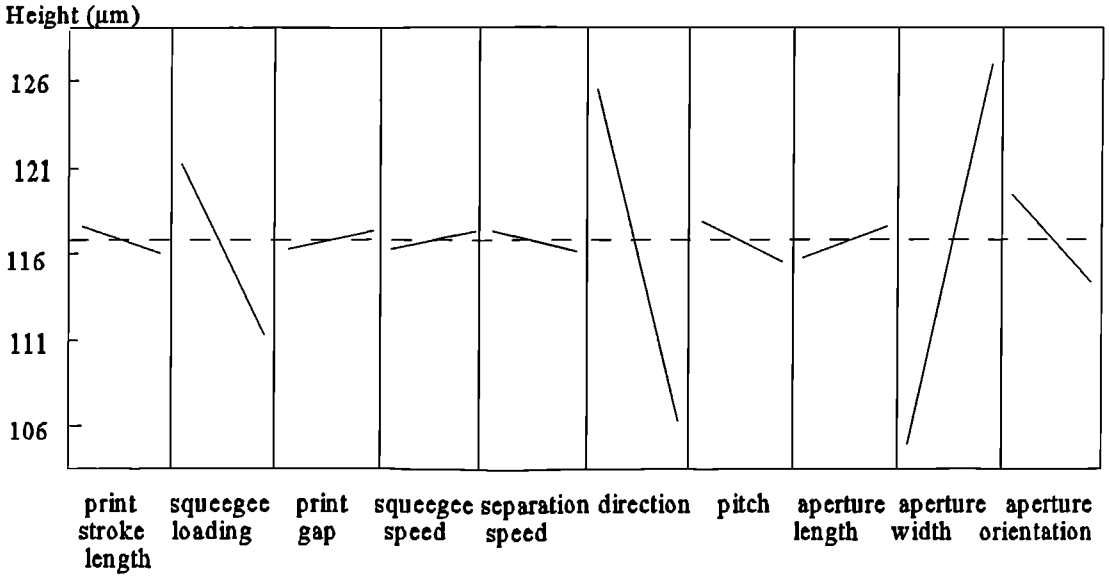

Figure 2.21 Main effect plot

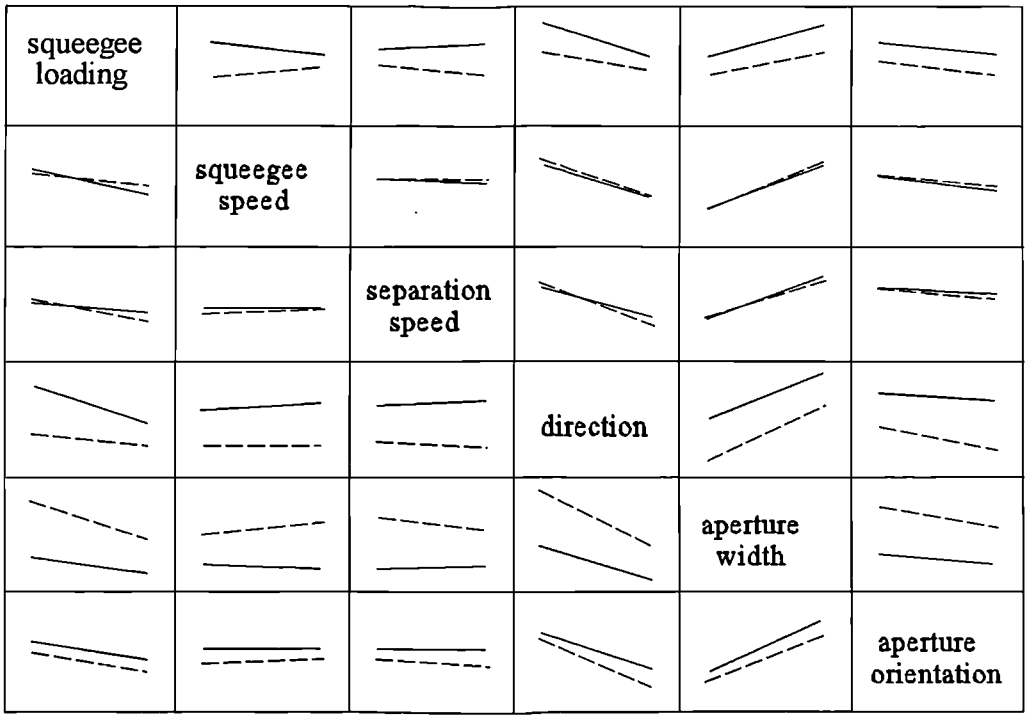

Figure 2.22 Interaction plot

Figure 2.22 shows a graphical overview of two-way interactions between the important parameters. Parallel lines in the interaction plot indicate that there is no interaction between the two parameters; crossing and divergent lines indicate an interaction is present. Haslehurst et al found that most of the significant two-way interactions were those involving either aperture width or pressure. Direction, separation speed, squeegee speed, and aperture orientation were also involved in several interactions. From Figure 2.22 it can be seen that the most significant interaction was between squeegee pressure and squeegee direction; changes from low pressure to high pressure made more difference to the reverse print than to the forward print. The second significant interaction was between pressure and separation speed; at low speed, mean deposit height was affected more by an increase in pressure than at high speed. The significant interaction of geometrical parameters was between pitch and aperture width; pitch made no difference to deposit height for narrow apertures, but for wide apertures, 0.4 mm pitch produced deposits 6 μm higher than 0.5 mm pitch. The separation speed also interacted with print gap; change of separation speed had less effect if there was a gap between stencil and substrate than that of contact print. Haslehurst et al also examined some three way-interactions and they found that these interactions were not significant compared with the main effects and some of the two-way interactions. However they indicated that the three-way interactions should be taken into account when fine-tunning the printing process.

Although it had been already recognized that the printing process is governed by the interactions of machine setting and stencil parameters, Haslehurst et al were the first to intensively investigate these interactions experimentally and provided quantitative relationships. Therefore, this work is very important for a full understanding of the interactions of process parameters on the stencil printing quality of solder paste.

Chapter Three

Modelling of the Behaviour of Solder Paste in Stencil Printing Using a Vibrating Squeegee

One of the most important developments in stencil printing technology in recent years is the use of vibrating squeegee (Anon, 1994). The idea for the vibrating squeegee is taken directly from that of a mason oscillating a float to level and pack the mortar. The vibrating squeegee utilises the same principle with solder paste. An important feature of the vibrating squeegee is its ability to assist the rolling motion of solder paste during printing. The vibration of the squeegee also ensures a smooth and level packing of solder paste into the stencil apertures, providing dense packing of solder particles. The other benefit claimed for the vibrating squeegee are longer stencil and blade life as less pressure is applied to the squeegee blade.

In this chapter a theoretical analysis of the behaviour of solder paste during printing with a vibrating squeegee is presented. The effect of the vibration on the paste roll in front of the squeegee is analysed in **3.1**. In **3.2** oscillatory shear theory is applied to analyse the packing of solder paste inside the apertures. The main conclusions are summarized in **3.3**.

3.1 Paste roll in front a vibrating squeegee

Printing of solder pastes using a constant speed squeegee has been introduced in **Chapter one**, and the process is illustrated in Figure 1.3. In this case, the squeegee moves at a constant speed with respect to a stationary stencil, and as the squeegee pushes the solder paste, a paste roll is formed, and very high pressures and shear rates are generated in the paste near the squeegee tip. Under the action of hydraulic pressure and shear force, the paste is injected into the stencil apertures. The paste roll in front of the squeegee plays a very important role in the aperture filling sub-stage. If paste slides on the stencil surface and there is no rolling action, then both the pressure and shear rate will be decreased. Modelling

of the paste roll in front of a constant speed squeegee has been reviewed in **Chapter two**. With a constant speed squeegee, if we ignore the small paste deposits injected into the apertures, then the paste roll in front of the squeegee can be assumed to be a steady state, in which the pressure and velocity at any given point on the paste roll are constants, as shown in Figure 2.8 to Figure 2.10. In contrast, with vibrating squeegee both paste pressure and velocity are not constants. This section presents an analysis of the characteristcs of paste roll in front of a vibrating squeegee.

3.1.1 The displacement, velocity and accelerate of the vibrating squeegee

Figure 3.1 shows the stencil printing of solder paste using a vibrating squeegee. Note that as the squeegee moves forwards with a constant speed V_0, it also vibrates sinusoidally. The motion of the vibrating squeegee relative to the stationary stencil is the superimposition of a vibration onto the constant squeegee motion, gives a squeegee displacement:

$$S = V_0\, t + A\, \sin(\omega t) = S_0 + A\, \sin(\omega t) \tag{3.1}$$

where S is the squeegee displacement, V_o is the constant velocity of the squeegee, t is time, A is the amplitude of vibration of the squeegee, and ω is the vibration frequency. Then the velocity of the squeegee can be derived from Equation (3.1) as:

$$V_t = V_o + A\omega\, \cos(\omega t) = V_o + V_s \cos(\omega t) \tag{3.2}$$

where the product $A\omega$ is the amplitude of vibration velocity. The acceleration of the squeegee is given by:

$$a_t = -A\omega^2\, \sin(\omega t) \tag{3.3}$$

$A\omega^2$ is amplitude of the vibration acceleration and is also called the acceleration modulus. The vibration frequency, ω, and amplitude, A are both important parameters that affect the performance of the vibrating squeegee.

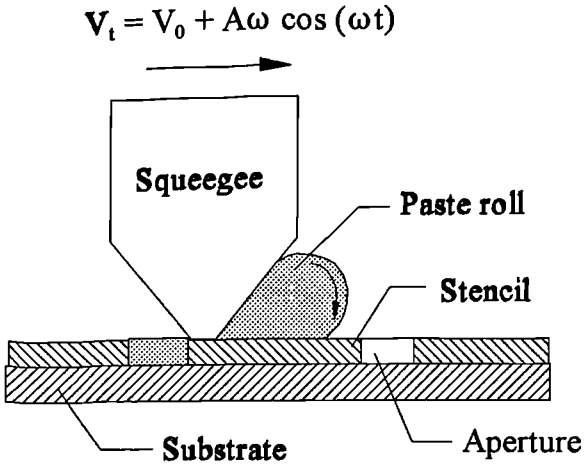

Figure 3.1 Stencil printing using a vibrating squeegee.

For constant speed squeegee printing, the printing speed, V_0, is usually between 20 mm/s and 40 mm/s. For vibrating squeegee printing, examination of Equation (3.2) shows that, for a given constant speed, V_0, taking different values of the vibration velocity, $A\omega$, will lead to three different types of the minimum values of the squeegee velocity, V_t. To express the minimum value of V_t by V_{min}, then V_{min} is dependent on the ratio of V_0 / V_s. Figure 3.2 illustrates the three typical squeegee velocities. From which it is seen that, if $V_0 > V_s$, then V_{min} is greater than zero; if $V_0 = V_s$, then V_{min} is equal to zero, and if $V_0 < V_s$, then V_{min} takes a negative value.

Figure 3.3 shows the displacements of the vibrating squeegee corresponding to the different values of V_{min}. For $V_{min} > 0$, the squeegee motion is always forward; however, if $V_{min} < 0$, then during each vibration cycle there is a backward motion; and if $V_{min} = 0$, there is a instantaneous stop during each vibration cycle.

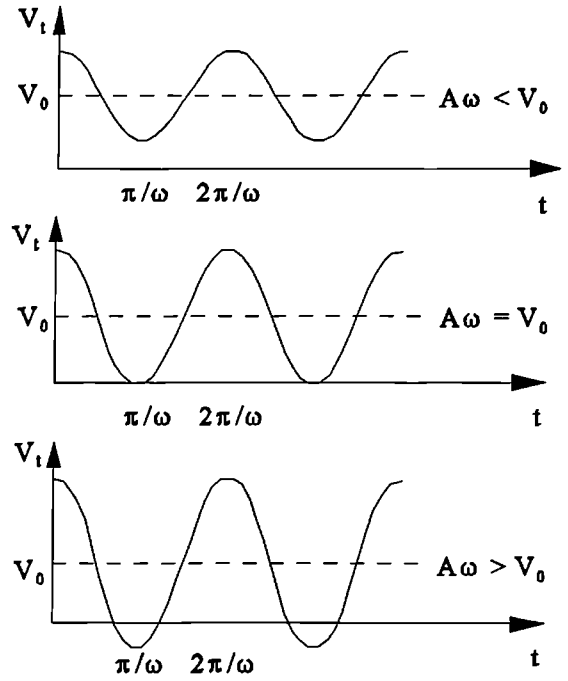

Figure 3.2 Comparison of squeegee velocities for different amplitudes.

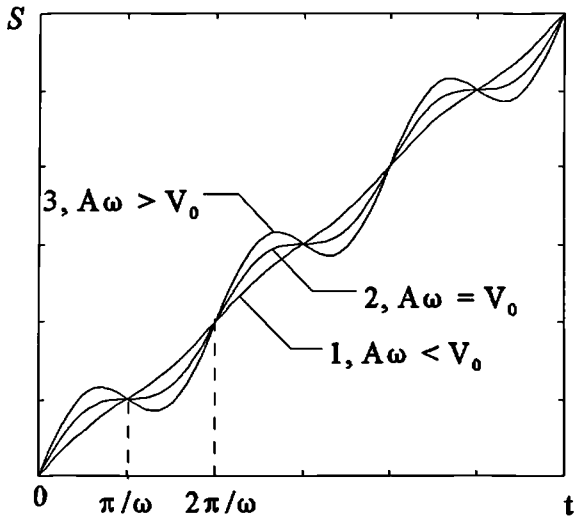

Figure 3.3 Comparison of squeegee displacements for different amplitudes.

3.1.2 The linear motion of the solder paste

The paste roll in front of the squeegee is produced by the motion of the squeegee blade which pushes the paste during stencil printing. To examine the linear motion of the paste, it is assumed that the paste in front of the squeegee is taken to be a point of mass. Interrupted printing tests were conducted by Owczarek and Howland (1990), where the printing process was stopped suddenly before the end of the stroke, and observations showed that the paste in contact with the leading edge of the squeegee largely retained its shape after the process was stopped. This implies that when the speed of squeegee is reduced to zero, the paste in front of the squeegee stops moving simultaneously with the squeegee. From this observation the paste would be expected to move in front of the vibrating squeegee in different patterns under different squeegee vibrating conditions. First consider the condition $V_{min} \geq V_0$, in which the squeegee always moves forwards, and the solder paste is in continuous contact with the leading edge of squeegee blade. This means that the displacement of the paste is the same as the squeegee displacement shown as *1* and *2* in Figure 3.3. For $V_{min} < V_0$, when $V_t > 0$, the squeegee remains in continuous contact with the paste as it moves forwards; but when $V_t < 0$, the squeegee oscillates backwards, and if the tack force between the squeegee and the solder paste roll is less than the squeegee pulling force exerted on the solder paste, then the solder paste would be separated from the squeegee. So it can be assumed that when the velocity of the squeegee is positive, the solder paste moves with the same velocity as the squeegee; but when the velocity of squeegee is zero or negative, then the velocity of the solder paste is zero. This means that when V_{min} is greater than or equal to zero, the paste will always move synchronously with the squeegee, but when V_{min} is less than zero, both the displacement and the velocity of the solder paste are not continuous functions of time. The velocity and displacement profile of the paste is illustrated in Figure 3.4. Notice that when $V_t < 0$, the squeegee displacement decreases (the point at which the squeegee starts to oscillate backwards, and the paste velocity goes to zero). The squeegee and the paste establish contact again during the next squeegee forwards oscillation and then move forwards synchronously.

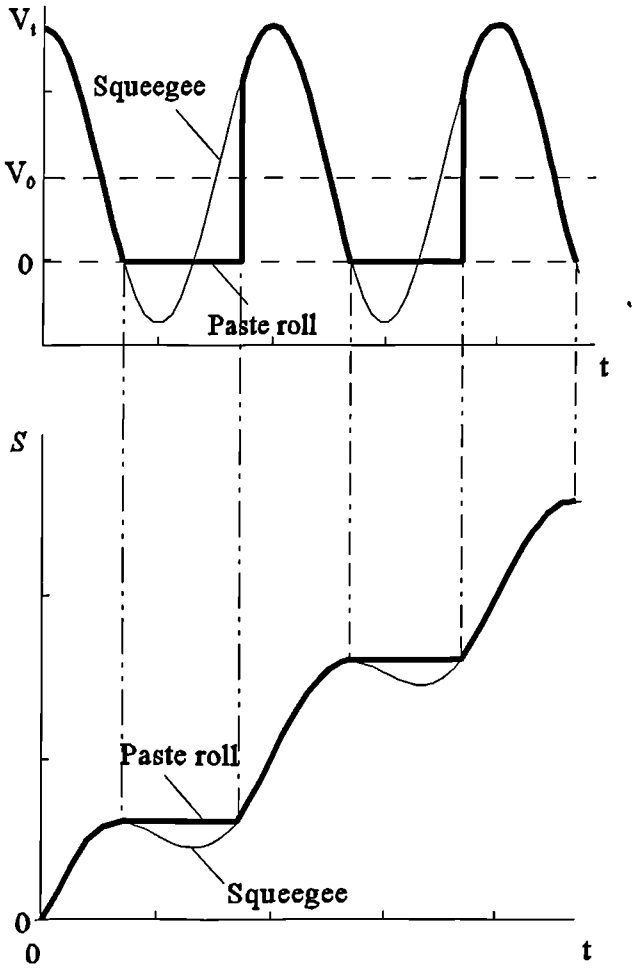

Figure 3.4 Displacement and velocity profiles of squeegee and paste roll.

In the above analysis, it is assumed that as the squeegee moves backwards, the acceleration force of the squeegee exerted on the paste is greater than the tack force between the squeegee and the paste roll, and hence the paste roll is separated from the squeegee. Therefore, it is necessary to examine the squeegee acceleration. The vibration frequency of the squeegee can be up to 200 Hz, equivalent to 400π rad/s (Anon, 1994). If the vibration frequency, for a typical application, is 150 Hz and the amplitude is 0.2 mm, then the squeegee acceleration modulus will be $A\omega^2 = 0.2\times10^{-3}\times300^2\,\pi^2 \approx 176$ m/s^2, which is about eighteen times the gravitational acceleration, g = 9.8 m/s^2. This indicates that the acceleration force would be much higher than the tack force and that the paste roll would

be separated from the squeegee as the squeegee oscillates backwards. Examining the vibration velocity amplitude, $V_s = A\omega$, it can be seen that, to keep V_s to be a constant, if A is multiplied by a factor and ω is divided by the same factor (or vice verse) the value of V_s does not change. However this will affect the value of the acceleration modulus, $A\omega^2$. This means that to enhance the paste roll separation from the squeegee, a relatively high frequency (ω) and a relatively low amplitude (A) are required as this can lead to a high acceleration modulus. It will be also seen, from the analysis of paste packing inside apertures (see **3.2**), that relatively high frequency and relatively low amplitude are required. The acceleration of the squeegee at the moment when the squeegee starts oscillating backwards can be derived from the velocity and accelerate equations as follow. At the moment when the squeegee starts to oscillate backwards, the squeegee velocity equals zero, that is:

$$V_t = 0 \quad \Rightarrow \quad \cos(\omega t) = -\frac{V_0}{A\omega} = -\alpha \tag{3.4}$$

where α is the ratio of the constant squeegee velocity to the amplitude of the vibration velocity, and $\alpha < 1$. The acceleration of the squeegee is:

$$a_t = -A\omega^2\sin(\omega t) = -A\omega^2\sqrt{1-\cos^2(\omega t)} = -\omega V_s\sqrt{1-\alpha^2} \tag{3.5}$$

For fixed values of α and V_0, Equation (3.5) indicates that the increase of the frequency, ω, will lead to an increase in the backward acceleration of the squeegee at the moment when the squeegee oscillates backwards. Equation (3.5) also indicates that, if $\alpha < 1/3$, the acceleration of the squeegee, at the moment when the squeegee oscillates backwards, is nearly equal to the acceleration modulus.

3.1.3 The paste roll in front of the squeegee and the filling of paste into the apertures

A. The forces acting on the paste roll

Recall that the paste roll in front of the squeegee is primarily generated by external forces

exerted on it by the moving squeegee. This section presents the analysis of the rolling motion of the paste in front of the squeegee and an examination of the effect of the external forces on the paste roll. Comparison shows that the paste roll diameter is much smaller than the paste roll length, which means that the forces acting on the paste roll can be taken as two dimensional case. Figure 3.5 shows a cross-sectional view of the paste roll and the forces acting on the paste roll and the paste rolling direction. Three types of forces acting on the paste roll can be identified. Firstly, there are the shear stresses (also called frictional forces), τ_1 and τ_2. τ_1 acts on the squeegee and paste roll interface and is against the paste rolling direction, while τ_2 acts on the substrate and paste roll interface and is in the paste rolling direction. Then there are the pressure forces, $\mathbf{P}_1$ and $\mathbf{P}_2$. $\mathbf{P}_1$ is perpendicular to the squeegee and paste roll interface, while $\mathbf{P}_2$ is perpendicular to the substrate and the paste roll interface. And finally there is the gravity force G.

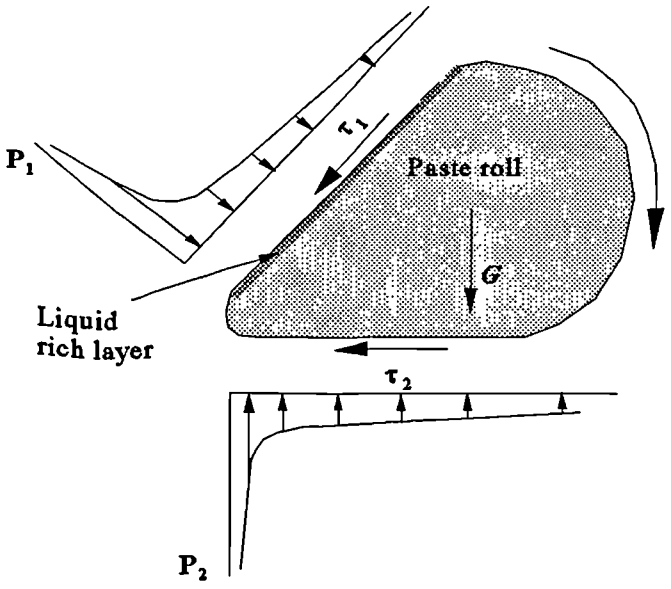

Figure 3.5 Forces acting on paste roll.

For a constant speed squeegee printing process, the forces acting on the paste roll are in a steady state, in which the shear stresses, τ_1 and τ_2, and the pressures, P_1 and P_2, are all position variables only. But in a vibrating squeegee printing process, all these forces are not only functions of position but also functions of time, that is both the shear stresses and the pressures at a given point vary with the squeegee velocity.

***B.* The paste roll in front of the squeegee**

On close observation of the forces shown in Figure 3.5, it can be seen that τ_2 generates a positive torque on the paste roll which supports the paste rolling action, while τ_1 generates a negative torque on the paste roll which opposes the paste rolling action. This means that for the stencil printing process, any changes to the printing process parameters which helps to increase τ_2 or to decrease τ_1, will also help to enhance the paste roll. A good paste roll is known to be essential for good aperture filling and for good paste deposition. The vibration of the squeegee does have the effect of reducing the resistance τ_1 by generating a liquid rich layer at the interface between the paste roll and the squeegee blade. By theoretical analysis using lubrication theory, Cox (1967, 1974) showed that, if a spherical particle moves near a flat plate with a relative speed, $V_{\parallel}$, parallel to the plate, then the plate resistant force acting on the particle is given by:

$$F = -\frac{16}{5}\pi\eta_o r V_{\parallel} \ln\left(\frac{2r}{\delta}\right) \qquad as \quad r \gg \delta \tag{3.6}$$

where η_o is the viscosity of the liquid, r is the radius of the particle and δ is the gap size between the plate and the surface of the particle. Equation (3.6) indicates that, for stencil printing of solder paste, if the gap, δ, between a solder particle and the leading edge of the squeegee increases, the resistant force of the squeegee on the particle decreases. The shear stress, τ_1 on the paste roll is the integration of F on a unit area, and the total resistance is the integration of τ_1 on the contact area between the squeegee and the solder paste. This means that the generation of a liquid rich layer at the squeegee and paste roll interface by the application of vibrating squeegee can help to enhance the rolling action of the solder paste in front of the squeegee.

As was stated earlier in **Chapter two,** solder paste is a dense suspension of spherical solder alloy particles in a flux/vehicle system. The volume fraction of solder particles is typically about 50%, and the mass density of the solder particle is about eight times higher than that of flux/vehicle (Hwang, 1989). Further analysis presented in **Chapter five** shows that the random loose packing density of equal spheres is about 60%, and for poly dispersed spheres the packing density increases with the standard deviation of particle size. Therefore, for solder paste with a solid volume fraction about 50% the solder particles within the solder paste are separated from each other and there are voids in the paste to be filled by the flux/vehicle system within the solder alloy particle matrix. The average gap between adjacent particles is about 15% to 22% of the average radius of the particles.

As was demonstrated in **3.1.2**, if $V_o / V_s < 1$, then the motion of the paste roll is not a continuous function of time. As the squeegee oscillates forwards and backwards, the leading edge of the squeegee impacts the paste roll. The frequency of this impaction is the vibration frequency of the squeegee. During the impactions, kinetic energy is transferred to the solder alloy particles located at the squeegee and the paste roll interface. As shown in Figure 3.6, with each impact, these particles are forced to move further into the bulk of the paste which leads to the formation of a liquid rich layer at the squeegee and paste roll interface as shown in Figure 3.5. The resistance force exerted on each particle by the squeegee is given by Equation (3.6). Then the total resistance force exerted on the paste roll by the squeegee can be written as:

$$R = -\frac{16}{5}\pi\eta_o \sum_{i=1}^{m} r_i V_{\parallel i} \ln\left(\frac{2r_i}{\delta_i}\right) \qquad (3.7)$$

where m is the total number of particles at the interface.

Comparing the vibrating squeegee with a constant speed squeegee, we note that the main difference is the effect of these impacts on the paste roll, and that under vibration the solder alloy particles at squeegee and paste roll interface are moved into the bulk of the paste. This leads to an increase in the gap, δ_i, between particle and squeegee leading edge. For the

case, where we assume $\delta_i = 0.2\, r_i$ for the constant speed squeegee, and $\delta = 0.3_i r$ for vibrating squeegee, then from Equation (3.7) we can estimate that the total resistance with vibration is about 20% smaller than that of no vibration. It proves that, the application of a vibrating squeegee can enhance the motion of the paste roll in front of the squeegee.

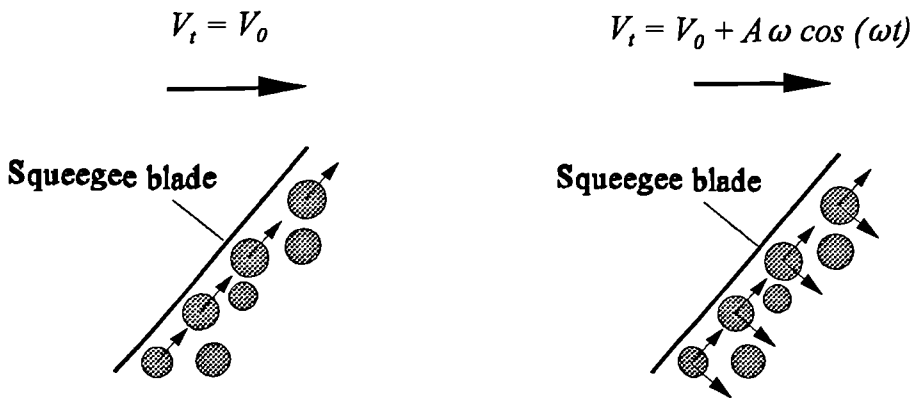

Constant speed squeegee Vibrating squeegee

Figure 3.6 Comparison of particle motion near squeegee blades.

C. The filling of solder paste into the aperture

As it has been mentioned above that, using a vibrating squeegee, the pressures, $\mathbf{P_1}$ and $\mathbf{P_2}$, exerted on the paste roll, as shown in Figure 3.5, are functions of time. As the squeegee oscillates backwards, $\mathbf{P_1}$ and $\mathbf{P_2}$ decrease below the values of $\mathbf{P_1}$ and $\mathbf{P_2}$ for the constant speed squeegee, and as the squeegee oscillates forwards, $\mathbf{P_1}$ and $\mathbf{P_2}$ will increase above the values of $\mathbf{P_1}$ and $\mathbf{P_2}$ for the constant speed squeegee. When the squeegee passes over an aperture, $\mathbf{P_2}$ decreases and the paste is forced to fill the aperture by pressure $\mathbf{P_1}$ and by the paste gravity G (G can be ignored as $\mathbf{P_1} >> G$). In experiments on the die-bounding of micro-electronic chips onto substrates with epoxy using oscillatory squeezing force (see Figure 3.7), Zwick et al (1997) found that, the application of oscillatory squeezing force significantly increases the flow rate and reduces the time required to die-bond the chip

onto the substrate. In stencil printing of solder paste using a vibrating squeegee, the effect of the oscillatory pressure P_1 is very similar to the oscillatory squeezing force in the die-bonding of micro-electronic chips. Therefore, the vibrating squeegee can enhance the speed with which the paste fills the apertures.

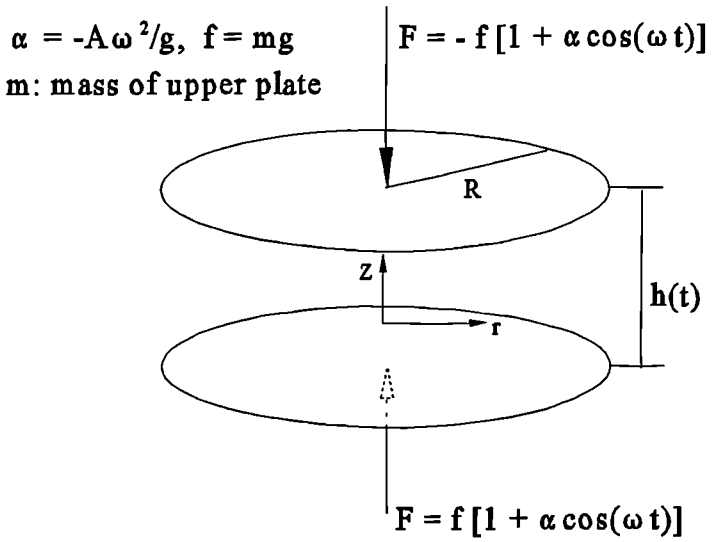

Figure 3.7 Schemetic of oscillatory squeegzing flow. (Zwick)

3.2 Packing of solder paste inside apertures

Solder paste is pushed into the apertures by the action of the moving squeegee during the printing process. The rheology of solder paste is a crucial factor which affects the paste roll and thus the quality of stencil printing. At different stages of the stencil printing process, different viscoelastic properties of the solder paste are desirable. At the aperture filling stage, a lower viscosity will make it easer for the paste to fill the apertures. But to keep the shape of the paste deposit and avoid slumping after the separation of stencil from the substrate, a relatively high viscosity is desired. The vibrating squeegee may provide the

solution to the problems caused by this contradictory processing requirements. In this section the theoretical background of oscillatory shear is introduced first. Then the viscoelastic properties of solder paste and other dense suspensions are discussed. Finally the behaviour of solder paste packing inside the apertures using a vibrating squeegee is analysed.

3.2.1 Introduction to oscillatory shear theory

One of the most common methods for testing viscoelastic materials is to measure their response (stress) to a small sinusoidally oscillating strain. Polymers show pronounced viscoelastic behaviour. As a dense suspension solder paste also shows viscoelastic behaviour. If a small strain is applied to a viscoelastic material and the shear stress generated by this strain is below the yield point of the material, then as the strain is released the microstructure of the material is able to recover to the original state and the material behaves as a solid. If a larger strain is applied to the viscoelastic material, such as solder paste, the particles are separatted and the suspension behaves like liquid. Thus oscillatory shear provides information concerning the viscoelastic properties of suspensions both below and above the yield point. Oscillatory strain is defined as (Tanner, 1985):

$$\gamma = \gamma_o \sin(\omega t) \tag{3.8}$$

and the shear rate is given by:

$$\gamma' = \gamma_o \omega \cos(\omega t) \tag{3.9}$$

where γ_0 is shear strain amplitude, and $\gamma_0\omega$ can be defined as amplitude of shear rate. Since the shear stress of a solid is a function of shear strain, and the shear stress of a liquid is a function of shear rate, then the shear stress response of a viscoelastic material as a function of time can be written as:

$$\tau(t) = \gamma_o[G'\sin(\omega t) + G''\cos(\omega t)] \tag{3.10}$$

where G' is the storage modulus and G'' is the loss modulus. Both G' and G'' are functions

of frequency ω. A complex modulus G^* is defined as :

$$G^* = G' + iG'' \tag{3.11}$$

and a complex viscosity is defined as:

$$\eta^* = \eta' - i\eta'' = \frac{G^*}{i\omega} = \frac{G''}{\omega} - i\frac{G'}{\omega} \tag{3.12}$$

η' (or G''/ω) is called dynamic viscosity and it is an indication of the flow capability of a viscoelastic material. For a Newtonian fluid η' is equal to the steady-flow Newtonian viscosity. For an ideal elastic solid, the shear stress is only the function of the shear strain. A viscoelastic material shows both liquid and solid properties. The phase shift is an important parameter and is defined as:

$$\varsigma = \text{arc tan } (\frac{\eta'}{\eta''}) = \text{arc tan } (\frac{G''}{G'}) \tag{3.13}$$

ς is an indicator, comparing the fluidity and solidity of a given viscoelastic material under a given oscillatory shear strain. Both η' and η'' are frequency-dependent variables and can be measured experimentally.

3.2.2 The viscoelastic properties of solder pastes and some dense suspensions

To examine the nature of the viscoelastic properties of solder paste, a common method is to measure its response, the storage modulus and the loss modulus, to frequency sweep. Figure 3.8 shows a plot of the storage modulus, the loss modulus and the complex viscosity of solder paste as functions of frequency (Hwang, 1989). We note that Figure 3.8 was plotted on a log-axis system. To simplify the analysis, a small section from the loss modulus curve can be taken as linear on the log-axis system. Then the relationship between the loss modulus and the frequency can be written as:

$$\log G'' + \log C_1 = b_1 \log \omega \tag{3.14a}$$

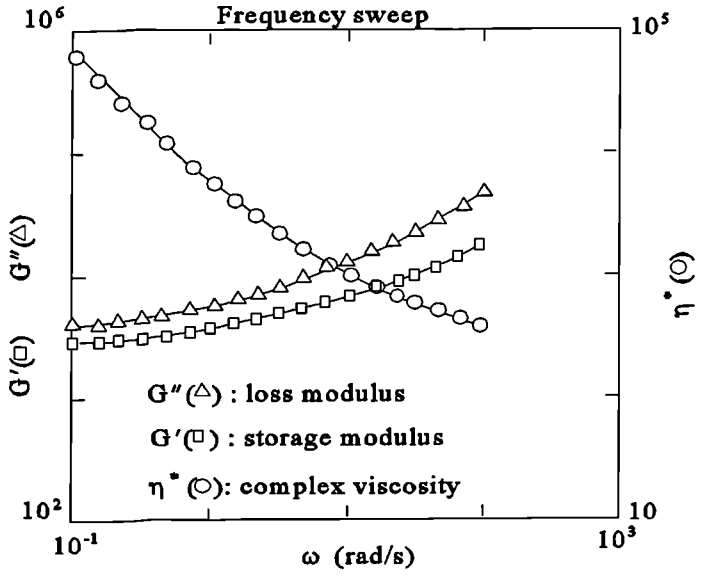

Figure 3.8 Solder paste response to frequency sweep.(Hwang)

By the same process, the relationship between the storage modulus and the frequency can be written as:

$$\log G' + \log C_2 = b_2 \log \omega \qquad (3.15a)$$

where C_1, C_2 are constants and b_1, b_2 are the slopes of the curves, G'' is loss modulus and G' is storage modulus, ω is frequency. Figure 3.8 shows that both C_1 and C_2 are positive. For convenience Equation (3.14a) and Equation (3.15a) can also be written in another form as follows:

$$C_1 G'' = \omega^{b_1} \qquad (3.14)$$

and

$$C_2 G' = \omega^{b_2} \qquad (3.15)$$

Then from the definition for η' and η'', see Equation (3.12), we have:

$$\eta' = \frac{G''}{\omega} = \frac{\omega^{b_1-1}}{C_1} \tag{3.16}$$

and

$$\eta'' = \frac{G'}{\omega} = \frac{\omega^{b_2-1}}{C_2} \tag{3.17}$$

For the case shown in Figure 3.8, the slopes of $G''(\omega)$ and $G'(\omega)$ are both less than 1 (ie. $b_1<1$ and $b_2<1$). Then it can be concluded from Equation (3.16) and Equation (3.17) that as the frequency increases both η' and η'' of the solder paste decrease.

Further insight into the effect of oscillatory shear on the rheological properties of solder paste can be provided by the results of oscillatory shear tests on other viscoelastic materials. Jomha *et al* (1990) investigated the effects of superimposing an oscillatory shear strain on a steady shear strain. The test was carried out with a shear-thinning carboxymethyl cellulose(CMC) solution, and two shear-thickening suspensions at concentration of between 40% and 60% weight solid. Solder pastes are typically used in the shear-thinning region, hence the experimental results on CMC are relevant to the case of stencil printing of solder paste. As discussed in section **3.1.1**, the velocity of vibrating squeegee is the superimposition of an oscillatory velocity on a steady velocity. Therefore, the effect of superimposing an oscillatory shear strain on a steady shear strain is very similar to the effect of the application of a vibrating squeegee in stencil printing of solder paste.

One of Jomha's experimental results is shown in Figure 3.9, which gives a comparison of steady shear stress and the mean superimposed shear stress (dyne/cm^2), with oscillatory shear strain of 0.5 and frequency of 50 rad/s. Figure 3.9 shows that for most of values of steady shear rates used in the range of experiments, the mean superimposed shear stress observed is obviously less than the steady shear stress (notice that it was plotted in a log-axis coordinate). For steady shear rate, the viscosity is the ratio of the shear stress to steady shear rate. If we define the ratio of the mean superimposed shear stress to the steady shear

rate to be the mean superimposed viscosity, then the mean superimposed viscosity is less than the viscosity measured in the steady shear rate test. This experimental result indicates that superimposing an oscillatory shear rate on a steady shear rate can enhance the fluidity of the viscoelastic material.

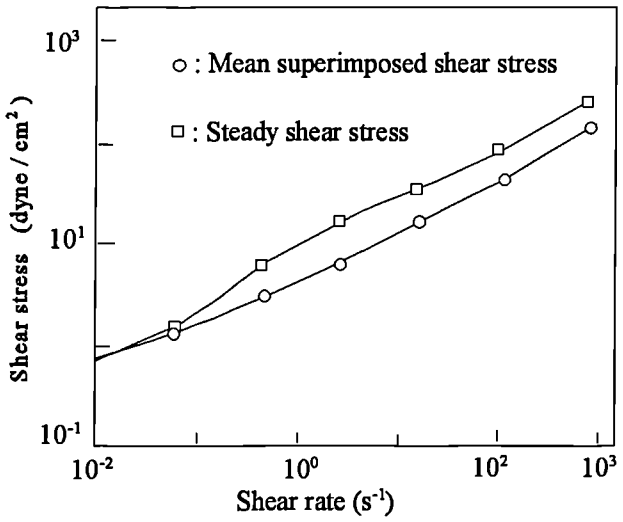

Figure 3.9 Steady shear stress and superimposed shear stress for CMC ($\omega = 50$ rad/s, $\gamma = 0.5$). (Jomha et al)

Schultz et al (1993) experimentally investigated the flow behaviour of fresh cement paste under oscillatory shear. The physical parameters of the cement paste used were as follows: mean particle size 9μm, and with 80% particles in the range 3μm to 20μm (compared to 15μm to 45μm for solder alloy particles); the pastes were prepared at water/cement levels 0.40, 0.45 and 0.5 (compared to 0.5 for solder paste). Both frequency and strain sweep experiments were carried out. Figure 3.10 shows one of the experimental results of frequency sweep test in which the strain amplitude was kept at 0.0001. Again notice that, the frequency sweep test demonstrates that as the frequency increases, dynamic viscosity of the cement paste decreases.

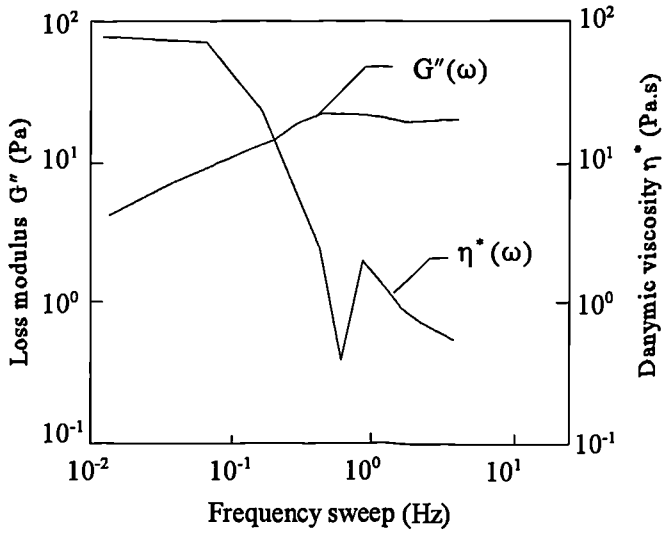

Figure 3.10 Response of fresh cement paste to frequency sweep.(Schultz)

The results of the work by Hwang, Jamha et al and Schultz et al show that the flow capability of viscoelastic materials can be enhanced by the application of oscillatory shear since the dynamic viscosity decreases. Such viscoelastic characteristics of dense suspensions have been utilized in many industrial fields. Perhaps the most familiar example of utilization of the viscoelastic properties of dense suspensions is the application of vibrators by masons to provide high and uniform packing density and a water rich surface layer when using concrete for building and road construction work.

3.2.3 Prediction of solder paste behaviour inside the aperture

In the previous section, the oscillatory shear theory and measuring method were introduced, and the responses of solder paste and some dense suspensions to oscillatory shear were examined. In this section the analysis of the effect of vibrating squeegee on the packing of solder paste particles inside the apertures is presented.

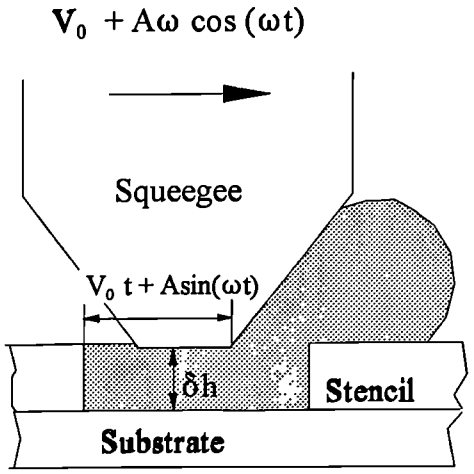

Figure 3.11 Behaviour of solder paste beneath the tip of a vibrating squeegee.

The thickness of the stencil is typically about 0.15 to 0.2 millimetre, so it is reasonable to assume that the shear strain inside the aperture is linearly distributed between the substrate and the tip of the squeegee blade. Experimental observation showed that due to the deformation of the blade tip caused by the contact pressure between the squeegee and the stencil, it is reasonable to assume the blade tip to be flat (Mannan et al, 1994). The interaction between the vibrating squeegee and the solder paste inside the stencil aperture is illustrated in Figure 3.11. Taking the aperture edge as the origin of the displacement of the vibrating squeegee, then from the displacement Equation (3.1), the shear strain in the paste beneath the squeegee can be written as:

$$\gamma = \frac{S}{\delta h} = \frac{V_0 t + A \sin(\omega t)}{\delta h} \tag{3.18}$$

And from the velocity Equation (3.2) of the vibrating squeegee the shear rate in the paste can be written as:

$$\gamma' = \frac{V}{\delta h} = V_o/\delta h + A\omega\cos(\omega t)/\delta h \tag{3.19}$$

In Equation (3.18) δh is the height from squeegee tip to the substrate, and S is the distance from the edge of the aperture to the squeegee tip. Examination of Equation (3.8) and Equation(3.18) shows that the shear strain in the paste inside the aperture is a combination of a linear strain term and an oscillatory strain term. Examination of Equation (3.9) and Equation (3.19), shows that the shear rate in the paste inside the aperture is also a superimposition of an oscillatory shear rate on a constant shear rate. If the constant shear stress and oscillatory shear stress are additive, then the total shear stress in the solder paste inside the aperture consists of two components: one is induced by the constant shear rate and the other is induced by the oscillatory shear rate.

As was noted earlier in the discussion of Figure 3.8, under oscillatory shear, the dynamic viscosity of solder paste decreases as the oscillatory frequency increases and also in the discussion of Figure 3.9, it was noted that for viscoelastic materials, the mean shear stress induced by superimposing an oscillatory shear rate on a constant shear rate is smaller than the shear stress induced by constant shear rate. Therefore, it is expected that the dynamic viscosity of the solder paste packed inside the aperture should decrease due to the application of a vibrating squeegee, and under vibration the shear stress in the paste inside the aperture should be less than that without vibration. Both the reductions of the dynamic viscosity and the shear stress could lead to a good packing of paste inside the apertures because of the enhancement of the fluidity of the solder paste by the vibrating squeegee.

In the above analysis the oscillatory shear experimental results on other viscoelastic materials (CMC and cement paste) were quoted. Of course there may be major differences between solder pastes and these materials, in particular in the microstructure, the particle size and the rheological properties of the vehicles, which means that the experimental results cannot be directly applied to solder pastes. But from these experimental results and from the viscoelastic properties of solder paste given by Hwang (1989), there is sufficient evidence to predict that the use of vibrating squeegee in the stencil printing of solder pastes can improve the printing process. The prediction is based on the fact that the application of oscillatory shear will reduce the dynamic viscosity of the solder paste.

3.2.4 Effect of the vibration parameters

In the previous section the effect of the vibrating squeegee on the packing of solder paste inside the apertures was analysed using the oscillatory shearing theory of viscoelastic materials. It is necessary to examine the effect of the vibration parameters, frequency and amplitude, further.

In section **3.1** it was postulated that if $V_o < V_s$ the squeegee has a backward oscillation during each vibration cycle, $T = 2\pi/\omega$, see Figure 3.3. This backward oscillation may further enhance the packing of solder paste particles into the stencil apertures. The following is the analysis of the effect of these parameters.

Examination of the external forces exerted on the paste roll, Figure 3.5, shows that in the stencil printing process, high static pressures $\mathbf{P}_1$ and $\mathbf{P}_2$ are generated near the squeegee tip which causes a backward solder paste flow beneath the squeegee as the squeegee passes over the apertures. This phenomenon was analysed by Mannan et al (1994) and by Ocwzarek et al (1990). Ocwzarek et al estimated that the average velocity of paste beneath the squeegee tip is about 10% of the paste velocity in front of the squeegee. Mannan et al (1994) also studied the deformation of squeegee caused by the pressure between stencil and squeegee. They concluded that, during stencil printing, as the squeegee passes over the apertures the tip of the squeegee blade will dip into the aperture which may cause scooping. Both the backward flow of solder paste beneath the squeegee tip and the dipping of squeegee blade tip imply that inside the apertures the surface of solder paste behind the squeegee is higher than the squeegee tip, as shown Figure 3.11. So with a vibrating squeegee, as the squeegee oscillates backward, the rear edge of the squeegee tip will push more paste into the apertures leading to further compaction and a better filling. This effect can compensate for poor filling of solder paste that may occur in the printing process using a constant speed squeegee. With a vibrating squeegee, its backward motion may lead to higher packing density of solder paste particles. The action of the vibrating squeegee on the solder paste has often been likened to the way "a mason oscillates a float to level and pack

his mortar" (Anon, 1994). This analogy is important, in that it provides a useful visualisation of the nature of the printing process with a vibrating squeegee and the condition in which improved printing can be achieved.

To examine Equation (3.1) again, which gives the squeegee displacement:

$$S = V_o\, t + A \sin(\omega t) \tag{3.1}$$

Notice that V_o is the printing speed and for a typical stencil printing process its value is in the range of 15 mm/s to 40 mm/s. If the value of V_o is preset, then the actual squeegee displacement is primarily determined by the vibration parameters (amplitude A, and the frequency ω). To quantitatively examine the effects of A and ω, a constant printing speed of 20 mm/s is assigned to V_o. Figure 3.12 and Figure 3.13 illustrate the effects of A and ω on the squeegee displacement, S, respectively.

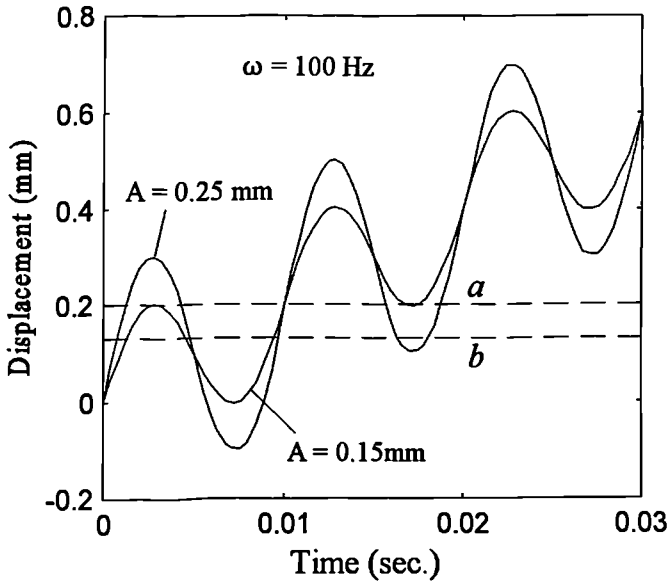

Figure 3.12 Effect of amplitude on squeegee displacement.

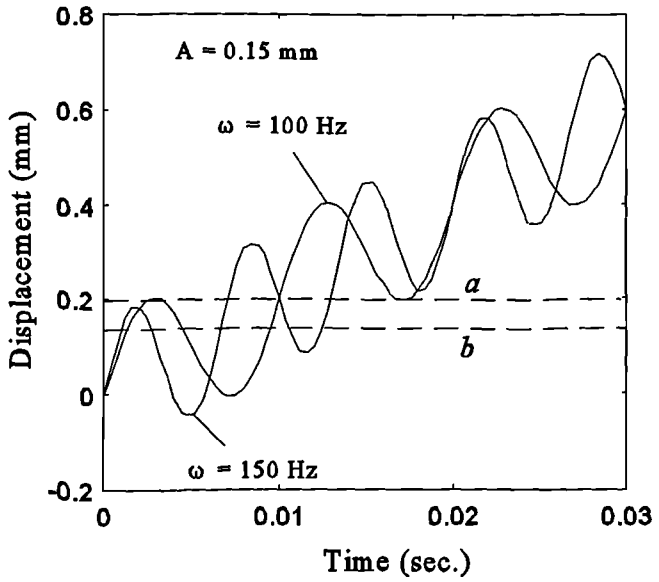

Figure 3.13 Effect of frequency on squeegee displacement.

In Figure 3.12 the vibration frequency ω is fixed to 100Hz, and the amplitudes are 0.15 mm and 0.25 mm respectively. To compare the effect of amplitude, two horizontal lines, *a* and *b*, can be drawn in this figure as two reference positions in an aperture. Then it is seen that the squeegee displacement curve for $A = 0.15$ mm intersects the horizontal line *a* at one time only, and intersects the horizontal line *b* 3 times. Whilst the displacement curve for $A = 0.25$ mm has three intersections with line *a* and 5 intersections with line *b*. This means that as the amplitude increases, the distance of the backward stroke of the squeegee increases. So the duration over which the squeegee impacts on the paste inside the aperture increases.

In Figure 3.13 the vibration amplitude is fixed to 0.15 mm, and the frequencies are 100 Hz and 150 Hz respectively. Again two horizontal lines, *a* and *b*, are drawn to represent two reference points in an aperture. Figure 3.13 shows that the displacement curve for $\omega = 100$ Hz intersects line *a* one time only, and intersects line *b* three times. While the displacement

curve for $\omega = 150$ Hz has three intersections with horizontal line *a* and five intersections with horizontal line *b*. This means that, at a given interval of time, as the frequency increases, the number of the backward strokes of the squeegee increases. So the duration over which the squeegee impacts on the paste inside the aperture increases.

To visualise the impaction effects as a vibrating squeegee passes over an aperture described above, Figure 3.14 illustrates the forwards/backwards motion of the vibrating squeegee, with the same parameters used in Figure 3.12. The displacements of the vibrating squeegee over a typical stencil aperture for two different vibration amplitudes are shown by S_1 and S_2. The arrows indicate the direction of motion of the vibrating squeegee. To compare the effect of amplitude, two reference positions in the aperture are represented by *a* and *b*. Then it is seen that for the squeegee displacement S_1 the paste at position *a* is levelled by the squeegee only once and that at position *b* is levelled three times (two forward and one backward). For displacement S_2 the pastes at position *a* and at position *b* are both levelled five times (three forward and two backward). A similar illustration with the values of parameters of Figure 3.13 is shown in Figure 3.15. The space between two arrows represents half of the vibration period. Figure 3.15 shows that the increasing of frequency can also enhance the impaction effects.

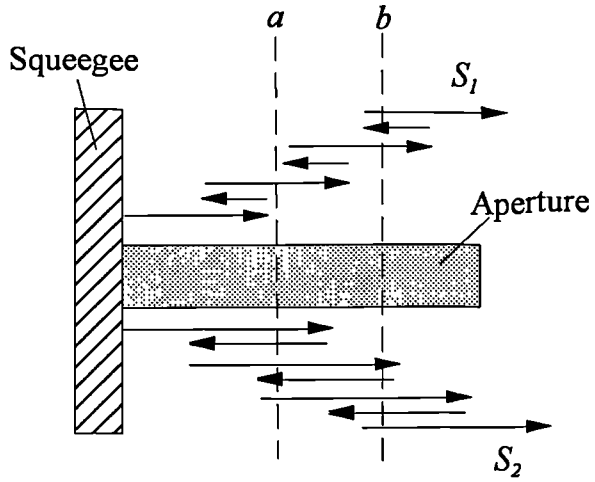

Figure 3.14 Schematic of squeegee displacements for different amplitudes.

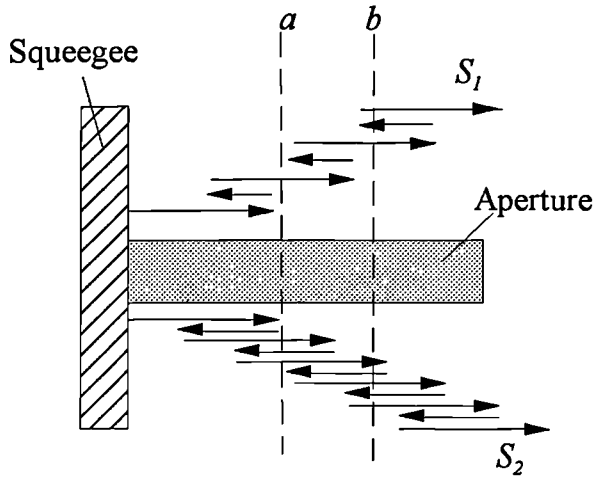

Figure 3.15 Schematic of squeegee displacements for different frequencies.

The above analysis demonstrates that, because of the application of vibrating squeegee, under the condition $A\omega > V_0$, the squeegee works on the paste inside the aperture in its forward and backward motions, thus providing better packing. The condition for ensuring that the entire paste inside the aperture experiences a needed number of squeegee backward strokes can be derived. Again consider the squeegee displacement as shown in Figure 3.16, a horizontal line is drawn from the first peak of the displacement. The sequence of the backward strokes are represented by 0, 1, 2, ..., n. Then there is:

$$S(t_0) = S(t_1) = S(t_2) \ldots = S(t_n) \tag{3.20}$$

Figure 3.16 shows that, if V_0 is much smaller than $A\omega$, then at the first peak there is $t_0 \approx \pi/(2\omega)$, and the displacement is:

$$S(t_0) = \frac{V_0\pi}{2\omega} + A \tag{3.21}$$

It is also seen from Figure 3.16 that at the $(n+1)th$ trough $t' = (2n+1.5)\pi/\omega$, and the

displacement at t' is:

$$S(t') = V_0\frac{\pi(2n+1.5)}{\omega} + A\sin[\pi(2n+1.5)] = V_0\frac{\pi(2n+1.5)}{\omega} - A \qquad (3.22)$$

To ensure the paste inside the aperture experiences n backward strokes in the same position, the following inequality must stand up:

$$S(t') < S(t_0) \qquad (3.23)$$

Substitution of the values of $S(t_0)$ and $S(t')$ to Equation (3.23) and re-arrangement lead to:

$$\frac{A\omega}{V_0\pi} > n + \frac{1}{2} \qquad (3.24)$$

Equation (3.24) indicates that if the constant speed, V_0, and the needed number of backward strokes, n, have been given, the condition can be fulfilled by an increase in either the frequency, ω, or the amplitude, A. As was noted earlier in section **3.2.2**, the frequency

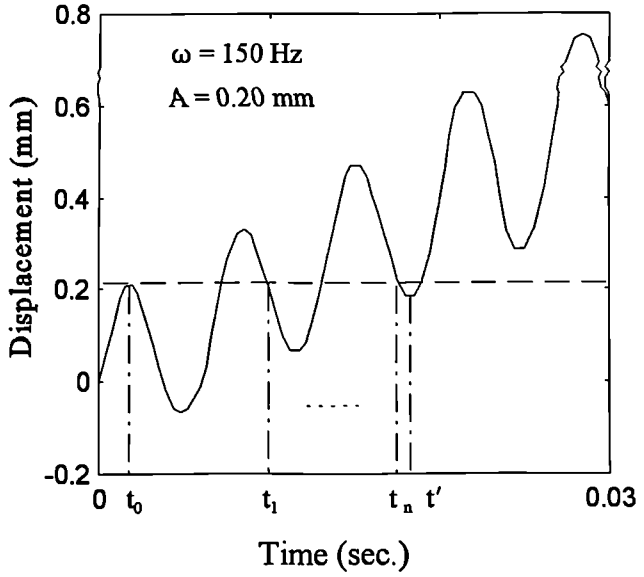

Figure 3.16 The backward oscillation of vibrating squeegee.

sweep measurement indicated that the dynamic viscosity of solder paste, η', decreases as the oscillatory frequency increases (No reports were found on the response of solder paste to the strain sweep). It is therefore better to select a relatively high frequency and a small amplitude rather than a relatively low frequency and large amplitude.

The parameter combination of high frequency and small amplitude is also better for the paste roll in front of the squeegee and for the reduction of the amount of paste sticking to the squeegee blade as the squeegee is lifted at the end of a printing stroke. Recall that the squeegee oscillatory amplitude of velocity is $A\omega$ and acceleration modulus is $A\omega^2$. To see the effects of A and ω on the acceleration modulus, two cases are examined. In the first case A is taken be 0.3 mm and ω is taken be 100 Hz (about 628.3 rad/s), and in the second case A is taken be 0.2 mm, ω is taken be 150 Hz (about 942.5 rad/s). For both cases the oscillatory amplitudes of velocity are the same, which is 0.1884 m/s, but the acceleration modulus for the first case is 118.4 m/s^2, while for the second case it is 177.5 m/s^2 which is 1.5 times that of the first case ie a relatively high frequency, ω, and a small amplitude, A, leads to a relatively high acceleration modulus, which can enhance the separation of solder paste from the squeegee.

3.3. Summary of Chapter three

In this chapter the behaviour of solder pastes in stencil printing use a vibrating squeegee has been theoretically analysed. The idea for the use of the vibrating squeegee is taken directly from that of a mason oscillating a float to level and pack the mortar. The vibrating squeegee utilises the same effect.

The effect of the vibration on the paste roll in front of the squeegee was analysed in section **3.1**. This analysis showed that the vibrating squeegee impacts the paste roll and produces a liquid rich layer at the interface between the squeegee leading edge and the paste roll. Models based on lubrication theory were used to predict that this liquid rich layer could

reduce the squeegee resistance on the paste and enhance the rolling of the paste.

In section **3.2**, the oscillatory shear theory of viscoelastic materials was introduced. Under oscillatory shear, the dynamic viscosity of solder paste decreases as the oscillatory frequency increases. Compared with constant shear rate, the superimposition of a oscillatory shear rate on a constant shear rate can reduce the shear stress in a dense suspension. Under the action of the vibrating squeegee, the solder paste packed inside the apertures experiences oscillatory shearing and the dynamic viscosity decreases. The fluidity increases which will lead to good paste packing quality inside the apertures.

The effect of the vibration parameters, frequency ω and amplitude A, on the printing process were also discussed in section **3.2**. It was concluded that if the vibration velocity amplitude, $A\omega$, is kept constant, then using a combination of a relatively high frequency, ω, and a small amplitude, A, will enhance the rolling action of the paste in front of the squeegee, enhance the packing of paste particles inside the apertures and also help to reduce the amount of paste sticking on the squeegee as it is lifted at the end of the printing stroke.

Chapter Four

Experiments on Solder Paste Response to Vibration

The theoretical analysis of the behaviour of solder pastes under the action of a vibrating squeegee was presented in **Chapter three**. The analysis showed that the use of the vibrating squeegee for stencil printing offers a number of advantages over the conventional high speed squeegee system. **Chapter four** presents results of the experiments designed to verify and validate the analytical predictions. Three different sets of experiment were conducted. The first set was for oscillatory shear measurements on solder paste samples. In the second set of tests, printing tests were carried out with a prototype of a vibrating squeegee to investigate the effect of process parameters such as the vibration frequency and the vibration amplitude. In the final set of experiments, vibration tests were carried out on paste samples to investigate the effect of vibration on solder powder particle re-arrangement and the changes in the paste microstructure.

4.1 High frequency oscillatory shear measurement on solder paste

As was stated earlier in **Chapter three**, solder paste is a viscoelastic materials, and the viscoelastic properties of a viscoelastic material under oscillatory shear can be characterised by its loss modulus, G'' (or by its dynamic viscosity, $\eta' = G''/\omega$) and by its storage modulus, G'. Figure 3.8 shows a typical response of solder paste to oscillatory shear and it shows that as the frequency increases the dynamic viscosity of solder paste decreases which means the fluidity of solder paste can be enhanced by oscillatory shear. Notice that the upper range of the frequency in Figure 3.8 is 100 rad/s, equivalent to about 16 Hz. However, the applied frequency of the vibrating squeegee is expected to be about 50 ~ 200 Hz. Therefore, it is necessary to examine the viscoelastic properties of solder paste under high frequency oscillatory shear.

4.1.1 Instrumentation and shearing methods

The loss modulus and storage modulus of the solder paste were measured on a StressTech Rheometer, (see Figure 4.1), in which the sample can be sandwiched either between two parallel discs or between two coupled cone plates. The upper disc is driven at a controlled rate to shear the samples. In this experiment the parallel disc geometry was used.

In oscillatory shear measurement, there are two types of shearing methods. The first uses strain control and frequency sweep, and in this method the shear strain amplitude is kept constant at a given value and the frequency is varied over a given range. Then the shear stress in the sample is measured and converted to storage modulus and loss modulus as functions of frequency. The second uses shear stress control and frequency sweep, and in contrast, the shear stress amplitude in the paste is kept constant and the frequency is varied over a given range. Then the shear strain is measured and converted to storage modulus and loss modulus as functions of frequency. Figure 4.2 shows the strain control and the shear stress control methods.

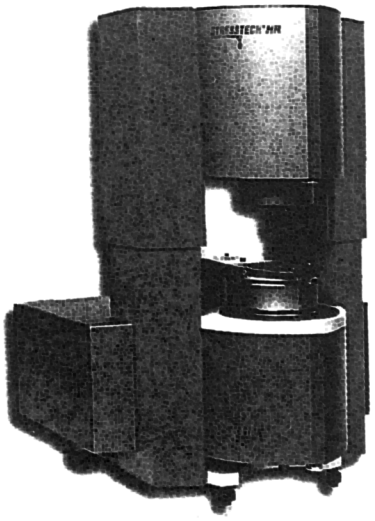

Figure 4.1 Picture of StressTech Rheometer.

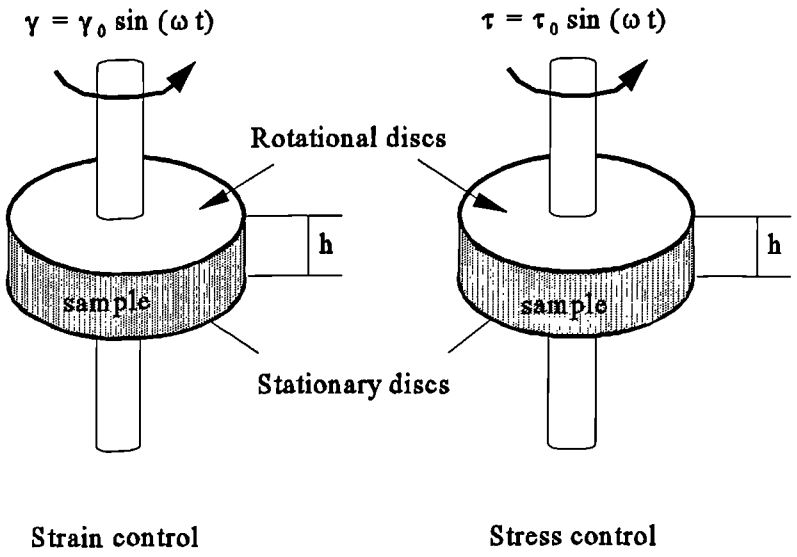

Figure 4.2 Methods of oscillatory measurement.

It is known that the rheological properties of solder paste and most, if not all, dense suspensions are sensitive to temperature change. Therefore, temperature control is essential for accurate measurement. In the measurements carried out on the StessTech Rheometer, the temperature was kept at a constant value, 25° C.

4.1.2 Experimental procedure

The experimental procedure used can be split into three steps, the equipment setup, sample preparation and the measurement.

The equipment setup included the followings: setting the temperature, the height of the gap between the two parallel discs, the amplitude of the shear strain if strain control, (or the shear stress if stress control), the range of frequency and the measuring points, and the experiment duration.

The sample was gently stirred to ensure the solder particles and the flux/vehicle were well mixed. Then a sufficient sample was placed on the bottom disc. After the top disc was lowered to the preset position for the gap width between the two discs, the excess paste sample was squeezed out the gap and was cleaned away otherwise it would affect the measuring accuracy.

Once the equipment setup and sample preparation was completed, the measurement was started. The frequency sweep could be either from low value to high value or from high value to low value. At the end of the test, the equipment was automatically stopped.

4.1.3 Oscillatory parameters and solder paste samples

Following the above procedure three sets of measurements were carried out. The experimental conditions are given in Table 4.1. The first measurement was shear strain control and the other two were stress control. In order to comparing with Hwang's result, Figure 3.8, the range of frequency of the first measurement was from 0.1 Hz to 20 Hz, about 0.63 to 125 rad/s. The shear stresses in the second and third tests were set to different values. High shear stress corresponded to large shear strain. The purpose of using different shear stresses was to examine the effect of shear strain on the viscoelastic properties of the paste sample.

Table 4.1 Experiment condition

Experiment	control method	frequency (Hz)	measuring points	disc gap (mm)	temperature
First	strain 5×10^{-3}	0.1 ~ 20	23	0.5	25°C
Second	stress 500 Pa	50 ~ 90	9	0.5	25°C
Third	stress 1000 Pa	50 ~ 90	9	0.5	25°C

The samples were taken from two fresh solder pastes. One sample was used in the first experiment, and the other one was used in the second and third experiments. The volume fractions of solder particles for both samples are about 50%. The range of the particle size is from 20 μm to 45 μm and both pastes contain rosin-based mildly activated (RMA) flux.

4.1.4 Oscillatory shear measurement results and discussion

A. Controlled strain frequency sweep

Figure 4.3 shows the result of strain control measurement from which it can be seen that at lower frequencies, the loss modulus and the storage modulus are about the same magnitude, about 0.6 kPa to 0.7 kPa, and the phase shift is around 45° to 50°. Notice that the phase shift is defined as ζ = arc tan (η'/η'') = arc tan (G″/G′). As the frequency increases both loss modulus and storage modulus increase, but the rate of increase of the loss modulus is much higher than that of storage modulus. The phase increases up to 80°, and the behaviour of the solder paste is more like a viscous liquid than an elastic solid.

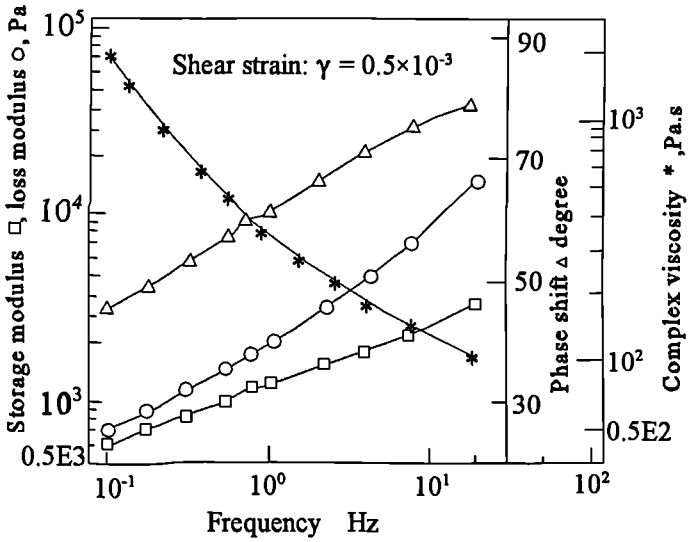

Figure 4.3 Strain control oscillatory measurement of solder paste.

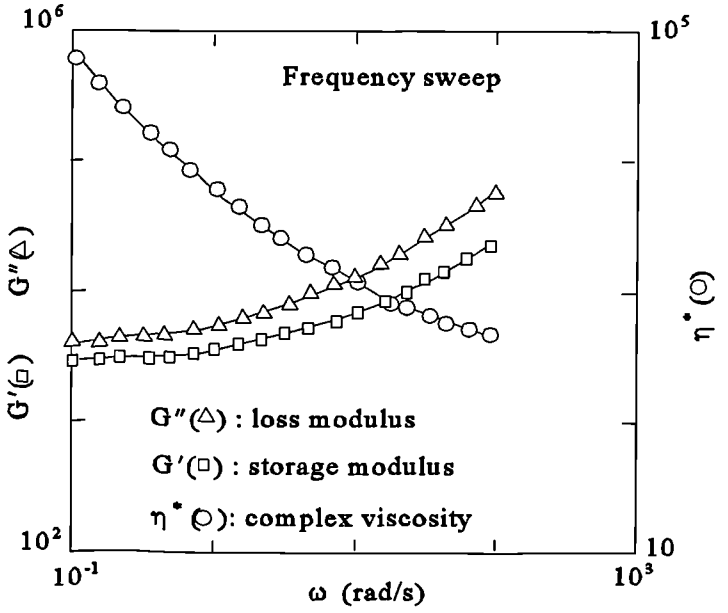

Figure 3.8 Oscillatory measurement of solder paste. (Whang)

Figure 4.3 also shows that the modulus of the complex viscosity, $\eta^* = (\eta'^2 + \eta''^2)^{1/2}$, decreases as the frequency increases. The dynamic viscosity, $\eta' = \eta^* \sin \zeta$, and the parameter, $\eta'' = \eta^* \cos \zeta$ both decrease as the frequency increases. For convenience Figure 3.8 is reproduced alongside Figure 4.3. Comparing Figure 4.3 with Figure 3.8 it is easy to observe that η^*, G″ and G′ have similar trends. There are, however, significant differences between the two figures, this may be attributed to the different samples used and different experimental conditions. Nevertheless it can be concluded that, the dynamic viscosity decreases as the oscillatory frequency increases; the loss modulus is higher than the storage modulus anywhere in the range; the gap between the loss modulus and the storage modulus increases with the frequency that leads the increase of phase shift with frequency.

B. Stress control frequency sweep

The second and third experiment were shear stress control measurements. For each shear stress value the measurement was repeated three times. Comparison of results of the same

shear stress shows high repeatability. Figure 4.4 and Figure 4.5 show two typical measurement results of 500 Pa and 1000 Pa shear stresses respectively.

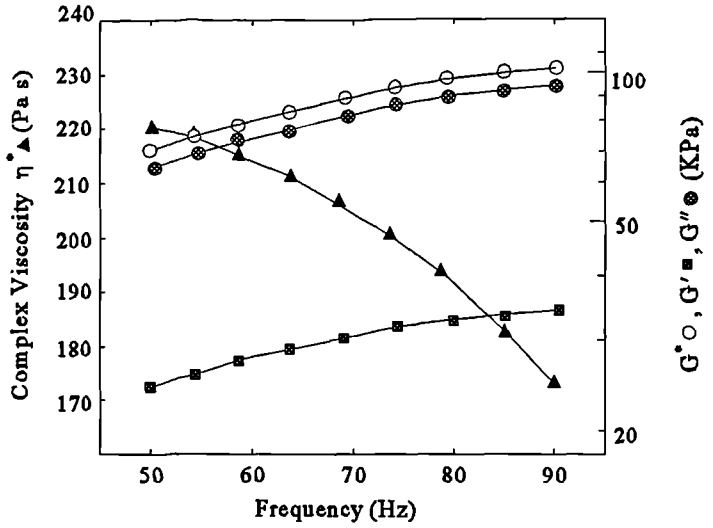

Figure 4.4 Shear stress control oscillatory measurement of solder paste, stress = 500 Pa, gap = 0.5 mm.

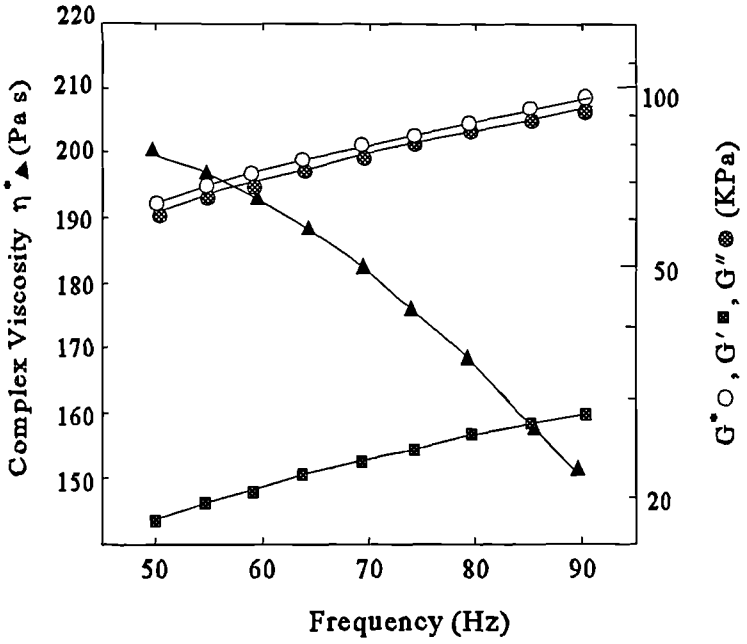

Figure 4.5 Shear stress control oscillatory measurement of solder paste, stress = 1000 Pa, gap = 0.5 mm.

Observation of Figure 3.8, Figure 4.3, Figure 4.4 and Figure 3.5, the following common characteristics can be identified. As the frequency increases the complex viscosity decreases, for example at shear stress of 500 Pa, as the frequency increases from 50 Hz to 90 Hz, the complex viscosity decreases from 220 Pa.s to about 170 Pa.s, and at shear stress of 1000 Pa it decreases from about 200 Pa.s to about 150 Pa.s. The dynamic viscosity, $\eta' = \eta^* \sin \zeta$, also decreases as the frequency increases. Comparing of Figure 4.4, Figure 4.5 with Figure 4.3, the difference of phase shift can also be observed, that is at low frequency, (0.1 to 20 Hz, see Figure 4.3) the phase shift significantly increases with frequency, while at high frequency, 50 to 90 Hz, the phase shift is nearly a constant, which is about 70° ($G''/G' \approx 2.7$) at a shear stress of 500 Pa and is about 75° ($G''/G' \approx 3.7$) at a shear stress of 1000 Pa. This may imply that under high frequency oscillatory shear, the ratio of loss modulus to storage modulus is a constant. As stated earlier in **Chapter three**, the phase shift is an indicator of the fluidity of a viscoelastic material, that is, the higher the phase shift, the more the behaviour of the viscoelastic material is like that of a liquid. Therefore, the vibrating squeegee with high frequency can help the packing of paste inside stencil apertures.

On further comparison of Figure 4.4 with Figure 4.5, it can be seen that the shear stress does not affect the loss modulus of solder paste, but it affects the storage modulus. As the frequency increases from 50 Hz to 90 Hz the loss modulus of both figures increases from about 63 kPa to about 95 kPa, while the storage modulus increases from about 23 kPa to about 34 kPa, see Figure 4.4 (shear stress of 500 Pa), and from about 17 kPa to about 26 kPa, see Figure 4.5 (shear stress of 1000 Pa). This observation can be explained as following. Rheological theory (Tanner, 1985) suggests that if a very small shear strain is applied to a viscoelastic material, it will induce a small deformation in the material; then as the strain is released the deformation is partially recoverable, and the smaller the shear strain the higher the recovering ratio. If the shear stress generated by the shear strain is below the yield point of the material, then the deformation is completely recoverable. For controlled shear stress oscillatory measurement, the shear strain can be calculated by $\gamma_o = \tau_o/G^*$, where γ_o is the shear strain, τ_o is the controlled shear stress and G^* is the complex modulus.

For $\tau_0 = 500$ Pa, the shear strain at frequency of 50 Hz can be estimated, from Figure 4.4, to be $\gamma_0 = 500/67000 \approx 7.5\times10^{-3}$. For $\tau_0 = 1000$ Pa the shear strain can be estimated, from Figure 4.5, to be $\gamma_0 = 1000/65000 \approx 1.5\times10^{-2}$ that is about twice of the shear strain at shear stress of 500 Pa. Therefore the recoverability of deformation at lower shear stress is higher than that at higher shear stress. The storage modulus at lower shear stress is higher than the storage modulus at higher shear stress.

Hwang (1989) pointed that a high level of thixotropy in solder paste, (the time dependent flow behaviour), may lead to deposit slumping on the pad of PCB's resulting in bridge defects. To examine the thixotropic characteristics of the paste sample and to examine the effect of changing direction of frequency on the experimental results, two frequency reverse loop measurements were conducted at a shear stress of 1000 Pa. In the two measurements, the frequency was decreased from 90 Hz to 50 Hz, and then was continuously increased to 90 Hz. Figure 4.6 shows one of the reverse loop measurement results. It is seen that the ramping-down curve nearly overlaps the ramping-up curve. This demonstrates that, first the extent of thixotropy of the paste sample is very small, and second, changing direction of the frequency does not affect the experimental results. These characteristics of the paste can help to maintain deposit resolution on the PCB's, hence reducing bridge defects.

4.1.5 Summary of the oscillatory shear measurements

a. Under oscillatory shear the dynamic viscosity of solder paste decreases as the oscillatory frequency increases. Therefore, oscillation can help to enhance the fluidity of solder paste.

b. At high oscillatory frequency the loss modulus of solder paste is much higher than its storage modulus. With shear stress of 500 Pa, the phase shift, ζ, is around 70° and with shear stress of 1000 Pa it is around 75°. So the behaviour of solder paste under oscillatory shear is more like that of a viscous liquid than that of solid.

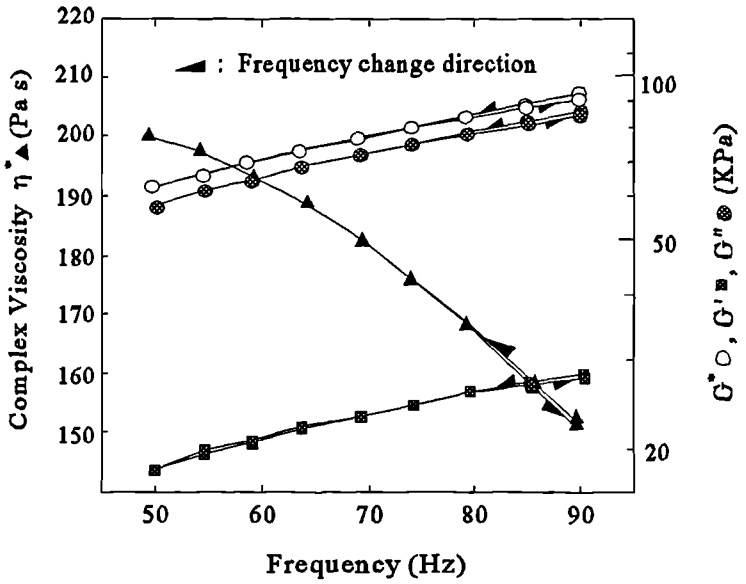

Figure 4.6 Frequency reverse loop measurement results.

c. The storage modulus with low shear stress, corresponding to small shear strain, is higher than that with high shear stress, corresponding to large shear strain. This means that the storage modulus of solder paste is not only dependent on frequency but also dependent on shear strain. The increase of oscillatory shear strain can reduce the deformation recoverability of solder paste.

4.2 Experimental study of paste roll in front of a vibrating squeegee

It was predicted in **Chapter three** that the use of a vibrating squeegee can generate a liquid rich layer between squeegee and paste roll interface. This liquid rich layer can help to enhance the paste roll and can also help to reduce the amount of paste that sticks on the squeegee as the squeegee is lifted at the end of printing stroke. To validate the above predictions, experiments were carried out using a prototype experimental rig. These experiments were designed to simulate printing using the vibrating squeegee system. This

section presents the experiments.

4.2.1 Experimental setup and paste samples

The experiments were performed using two different prototype setups. The first apparatus, as shown in Figure 4.7, was used to perform the experiments in which the frequency range was from 30 Hz to 120 Hz. The second apparatus, as shown in Figure 4.8, was used to perform the experiments in which the frequency range was from 100 Hz to 300 Hz. The reason for the use of two apparatuses was that when the frequency was higher than 100 Hz the vibration amplitude was too small to obtain optimal frequency and amplitude combination in the first apparatus. As illustrated in Figure 4.9, the first apparatus consisted of the following equipment:

a. A vibration system, which included a V401 Vibrator and a Power Amplifier, was used as the vibration source. The vibrator could only bear axial load. The frequency and amplitude of the vibrator were controlled by the Power Amplifier. The frequency range was from 0 to 25 kHz, and the amplitude range was from level one to level nine. The amplitude value at each level was dependent on the load and frequency in that the heavier the load the smaller the amplitude and the higher the frequency the smaller the amplitude. A Wayne Kerr Vibration Meter was used to calibrate the amplitude. The vibrator was fixed on the head of a milling machine.

b. One squeegee stand and four aluminum squeegee blades, 120 mm in width, with different printing angles (the angle between the squeegee blade and the horizontal plane), 45°, 55°, 60° and 70°, and two auxiliary supporting shafts were designed. The supporting shafts were fixed on the head of the milling machine through a stand. Two axial ball bearings were used to support the squeegee to slide on the supporting shafts. The squeegee was connected to the vibrator shaft, and was driven to vibrate along and against the feeding direction of the milling machine.

c. Due to the difficulties encountered in making a special stencil, a steel plate, (4 mm thick × 300 mm length), was used as the stencil. The plate was fixed on the machine table and moved synchronously with the machine table at constant feeding speed towards the squeegee. The maximum feeding speed of the machine table was 25.4 mm/s. As the plate passed beneath the squeegee, the paste sample on the plate was pushed by the squeegee blade. A ruler was placed beside the plate to measure the paste roll formation distance, which was the distance travelled by the squeegee from the point of its initial contact with the paste to the point where the paste started rolling.

In the second setup, illustrated in Figure 4.8, a small blade, 40 mm in width, was directly fixed on the shaft of a V201 Vibrator. The effective testing distance was only about 50 mm and the printing speed had to be controlled manually by pushing the plate towards the vibrating blade.

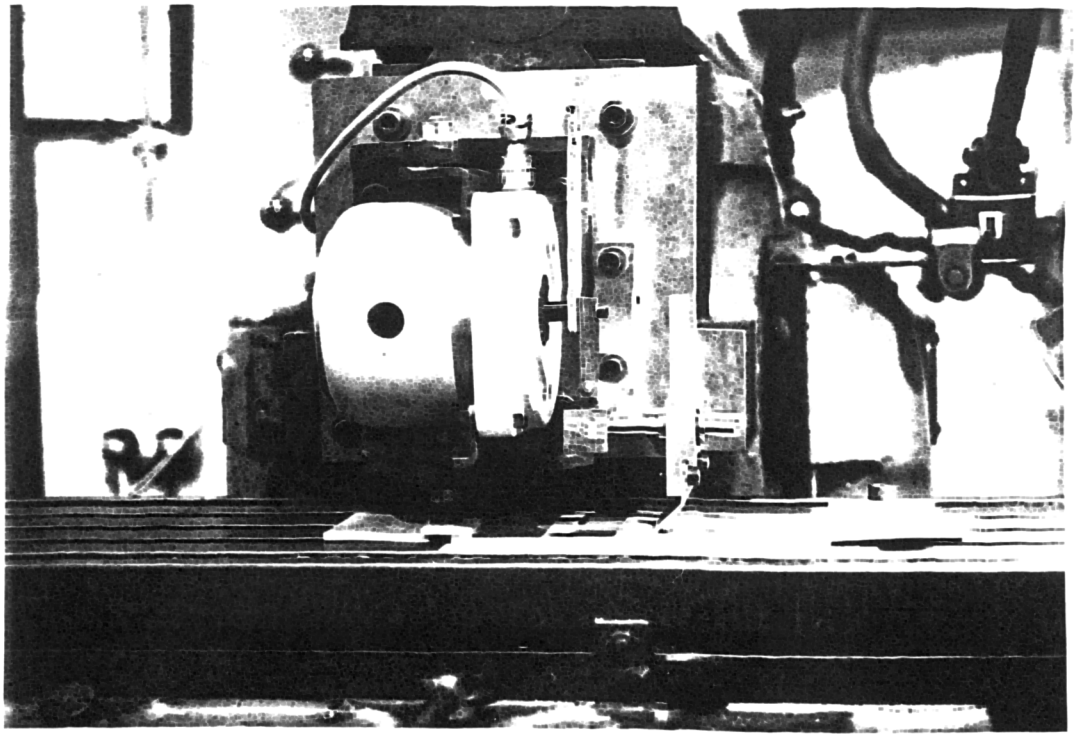

Figure 4.7 Apparatus I of vibrating squeegee system.

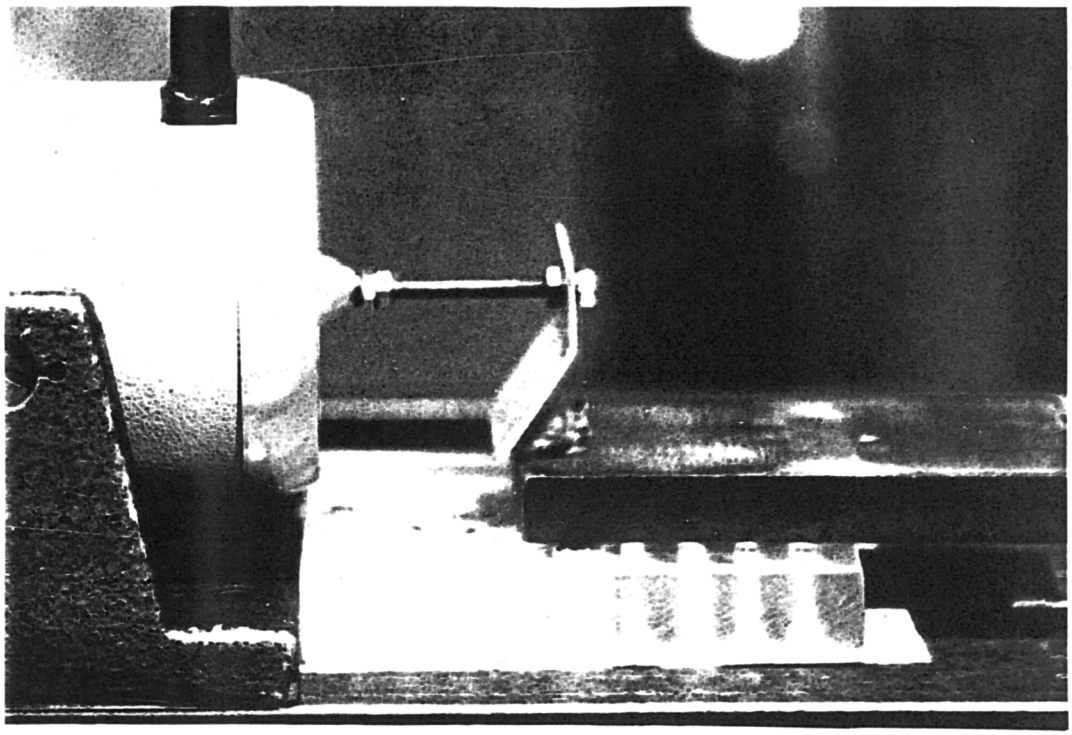

Figure 4.8 Apparatus II of vibrating squeegee system.

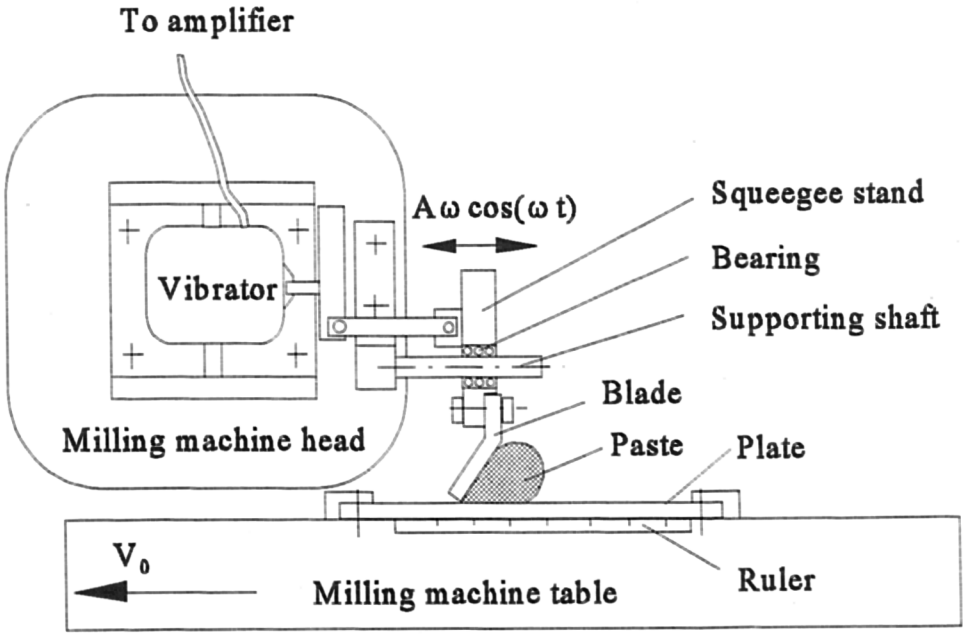

Figure 4.9 Illustration of experimental setup for vibrating squeegee system.

The same paste sample as used in the oscillatory shear measurement was used in the experiments performed using both apparatuses. To examine the possibility of use of high metal load solder paste, another paste sample was also tested in the second setup. The second paste sample has the same composition as the first one but its shelf life has already expired two years ago and was apparently drier than the first one. Because of flux/vehicle evaporation the metal load of this sample should be higher than that of the first one although the exact value was not measured.

4.2.2 The experimental procedure

A. Process parameters selection

The main aim of the experiment was to examine the effects of vibration frequency and amplitude of the squeegee on the paste behaviour in the printing process. Preliminary tests showed that the change of the constant printing speed (V_o), from 10 to 20 mm/s, did not affect the paste behaviour as the squeegee was vibrated. This is because the vibration speed, $A\omega$, used in the experiment was more than ten times the constant speed. Therefore, only the frequency and amplitude of the vibrating squeegee were chosen as the main parameters. The constant printing speed in the first apparatus was 20 mm/s, (a common printing speed), and in the second apparatus was about 10 mm/s. The reason for choosing 10 mm/s as the constant speed in the second apparatus was to allow the manual control to be easy and accurate. The squeegee blade with a contact angle of 60°, (a commonly applied printing angle), was intensively studied; other angle blades were not systematically tested. The vibration frequency was from 30 Hz to 300 Hz and the vibration amplitude was from 0.1 mm to 1.1 mm. The test sequence of frequency was randomised. After each test, the sample was replaced by new one. Table 4.2 shows the test sequence and parameters. Observation on the experiments showed that the amplitude, smaller than 0.1 mm or larger than 1.5 mm, was out of the optimal range. Therefore, some marked (**) amplitudes in Table 4.2 were not calibrated.

B. Testing procedure

For each process parameter combination, the sample was placed on the plate; and the machine table was raised to allow the plate to touch with the squeegee blade. After the vibrator was switched on at selected frequency and amplitude, the machine table was then started to allow the stencil to pass beneath the vibrating squeegee; and at the end of the test stroke, both the machine table and the vibrator were stopped.

Table 4.2 Test sequence and parameters (Temperature: 22°C~23°C, Relative humidity: 35~39)

Sequence	Freq. (Hz)	Amplitude (mm)			Vibrator
1	80	0.13	0.24	0.31	V401
2	100	0.07	0.15	0.21	V401
3	0				V401
4	50	0.35	1.10	**	V401
5	120	**	**	**	V401
6	30	**	**	**	V401
7	100	0.24	0.40	0.62	V201
8	80	0.23	0.38	0.60	V201
9	120	0.18	0.30	0.49	V201
10	200	0.15	0.19	0.24	V201
11	300	**	**	**	V201
12	150	0.23	0.38	0.51	V201

(** : Not calibrated)

4.2.3 Results of vibrating blade experiment and discussion

Figures 4.10 to Figure 4.19 show the photographs of the paste sample for different vibrating squeegee printing conditions to demonstrate the typical response of the paste. The effects of the squeegee vibration parameters on the paste behaviour are discussed here.

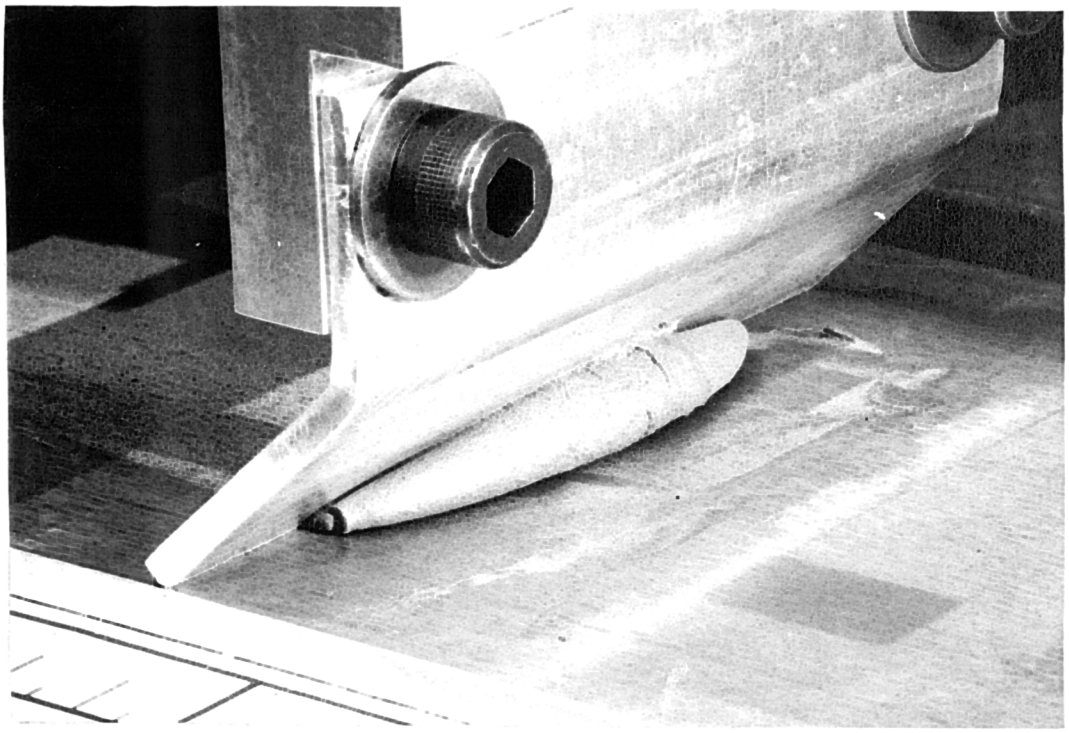

Figure 4.10 Solder paste response to constant speed squeegee (no vibration).

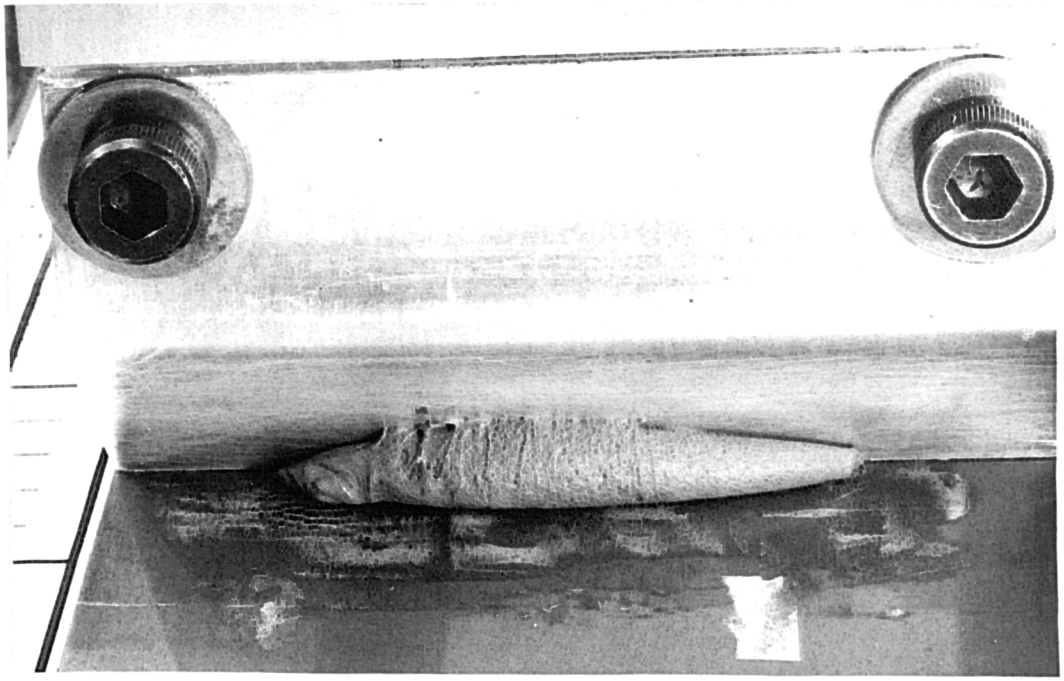

Figure 4.11 Solder paste response to vibrating squeegee (ω = 50 Hz, A = 0.35 mm).

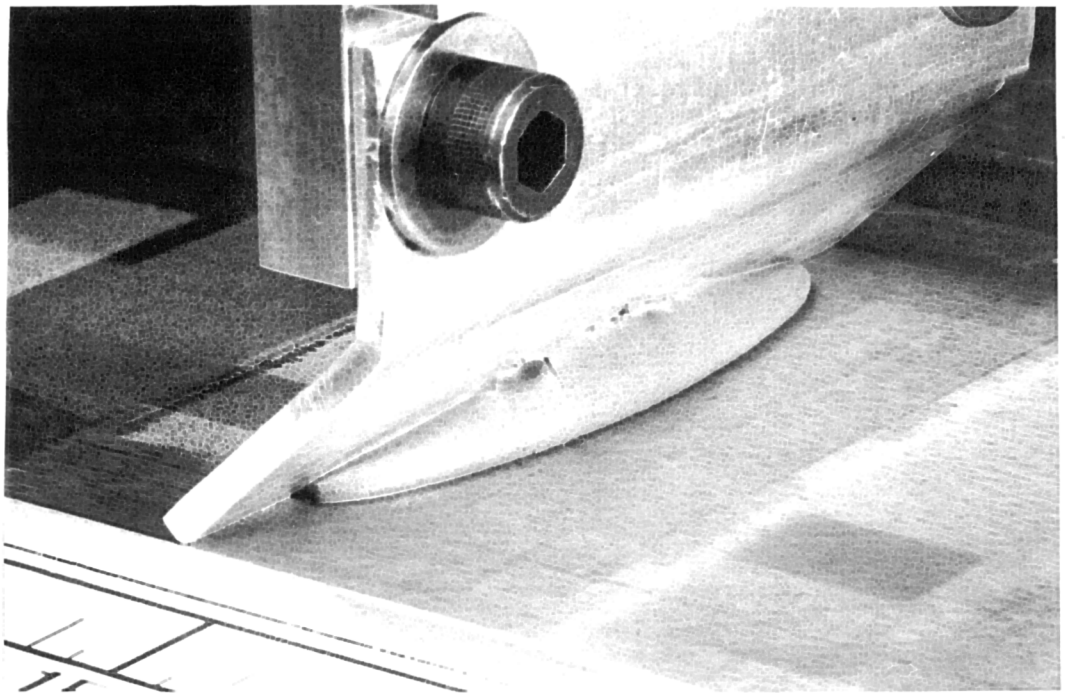

Figure 4.12 Solder paste response to vibrating squeegee (ω = 80 Hz, A = 0.31 mm).

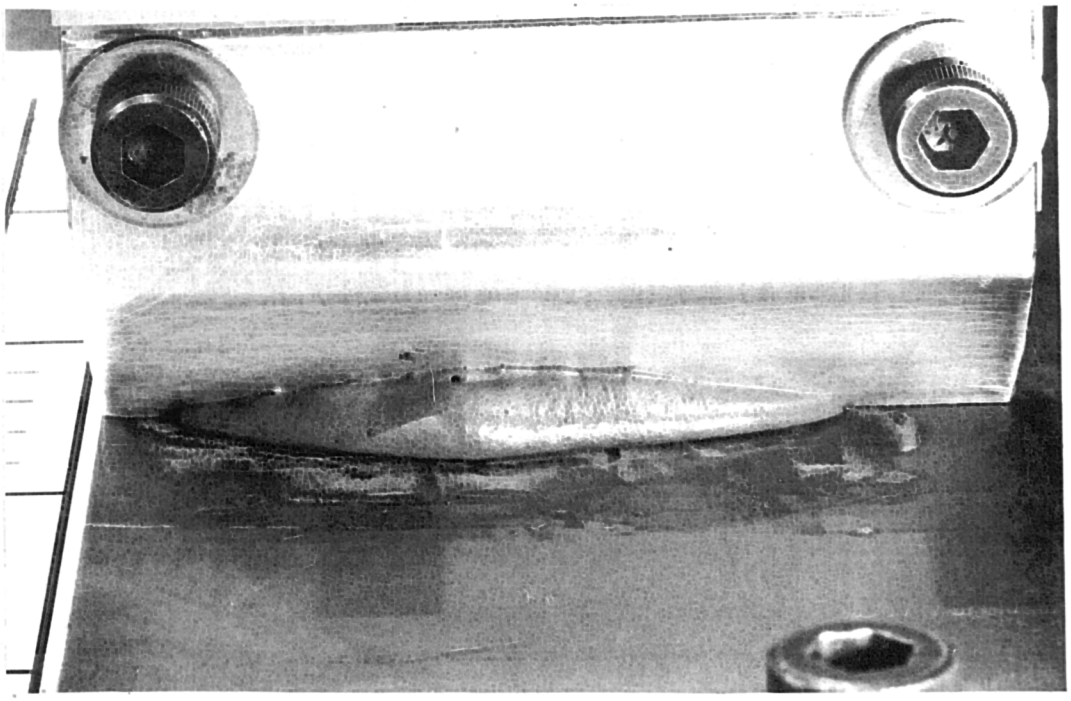

Figure 4.13 Solder paste response to vibrating squeegee (ω = 100 Hz, A = 0.21 mm).

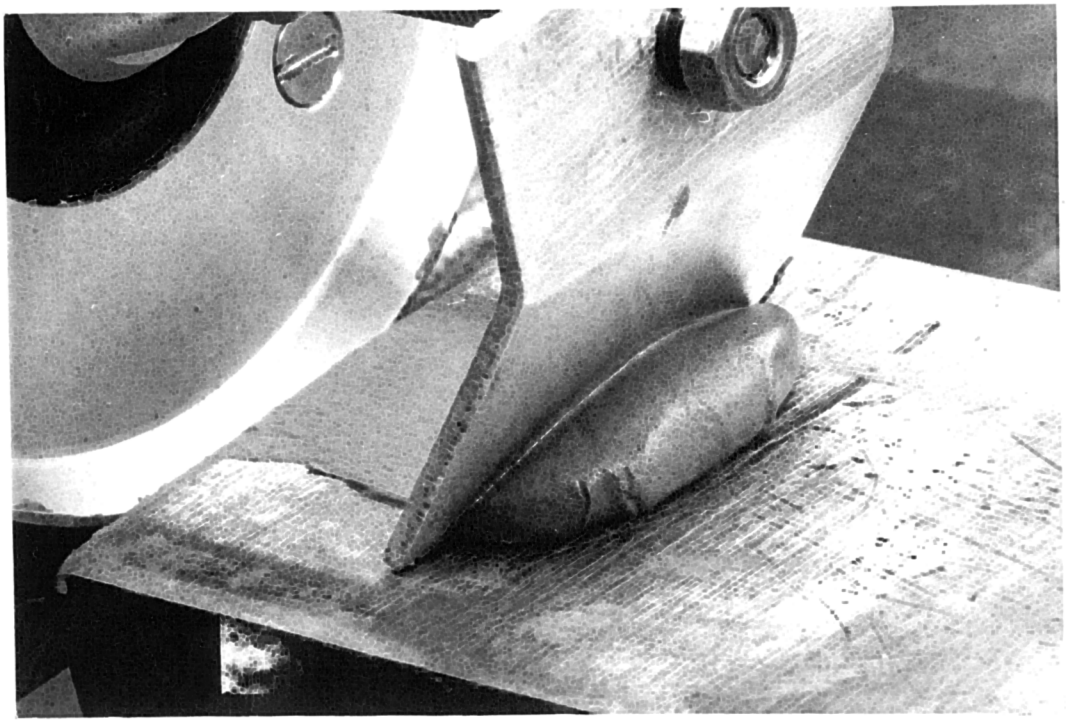

Figure 4.14 Solder paste response to vibrating squeegee (ω = 100 Hz, A = 0.26 mm).

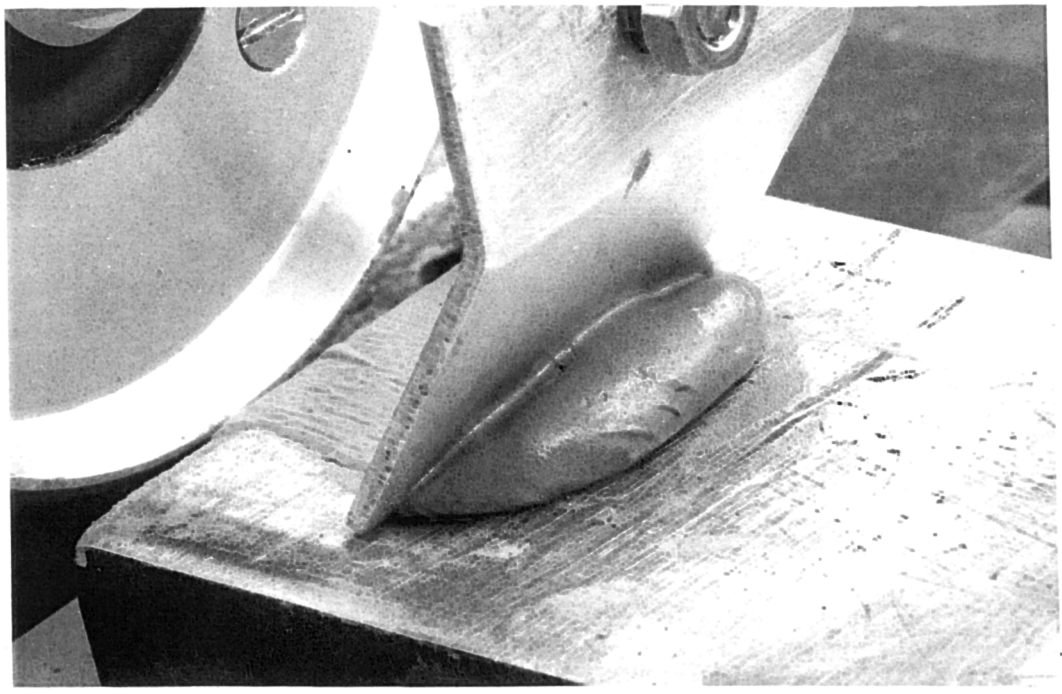

Figure 4.15 Solder paste response to vibrating squeegee (ω = 120 Hz, A = 0.30 mm).

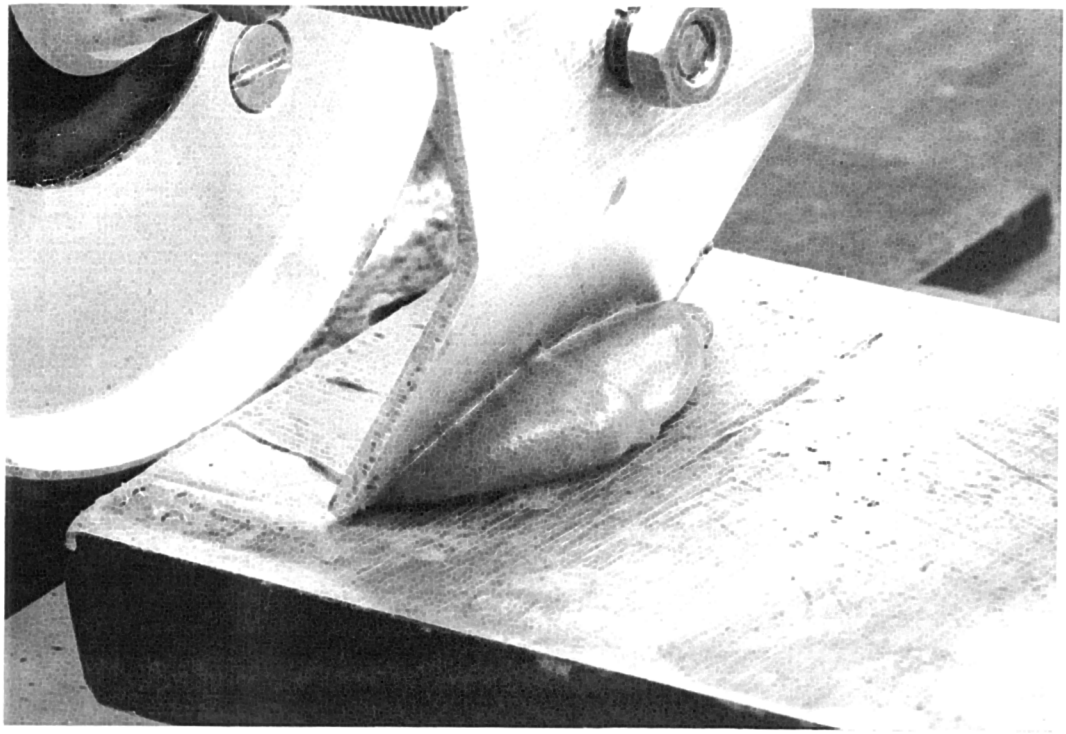

Figure 4.16 Solder paste response to vibrating squeegee (ω = 150 Hz, A = 0.23 mm).

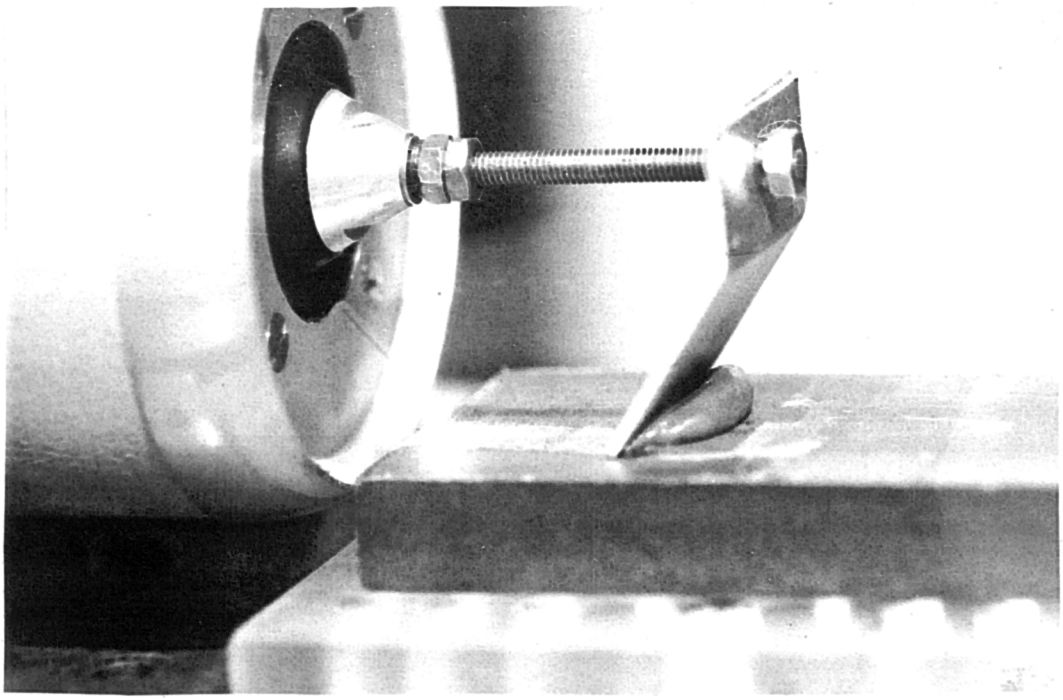

Figure 4.17 Solder paste response to vibrating squeegee (ω = 200 Hz, A = 0.15 mm).

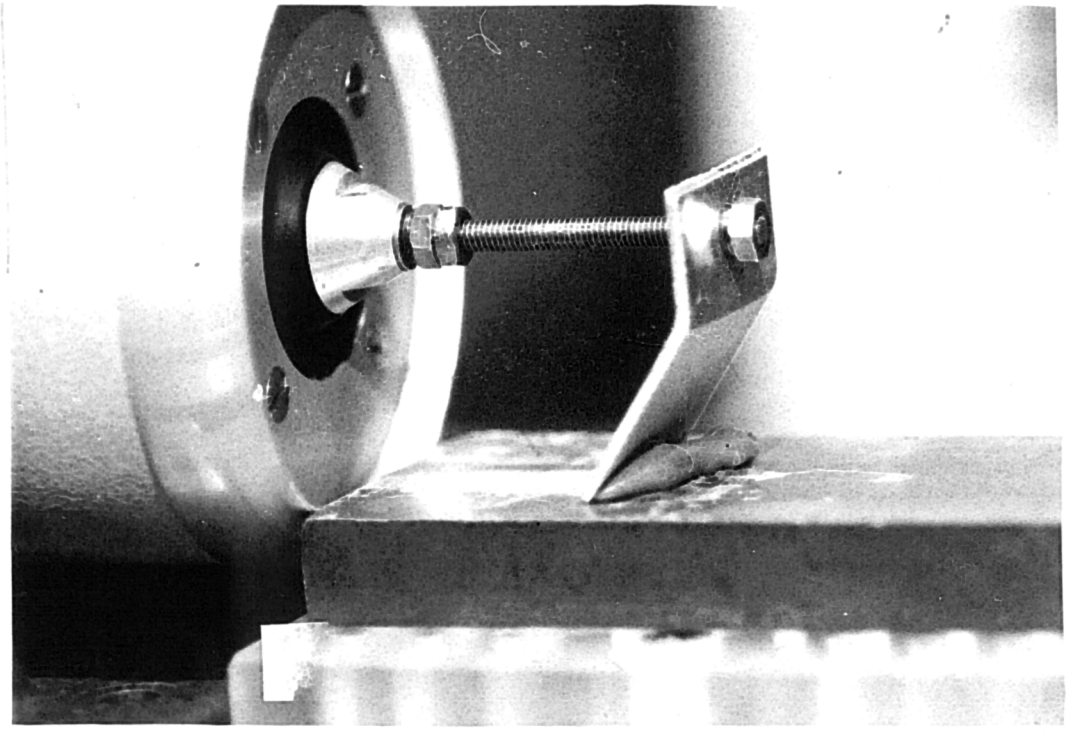

Figure 4.18 Solder paste response to vibrating squeegee (ω = 150 Hz, A = 0.38 mm).

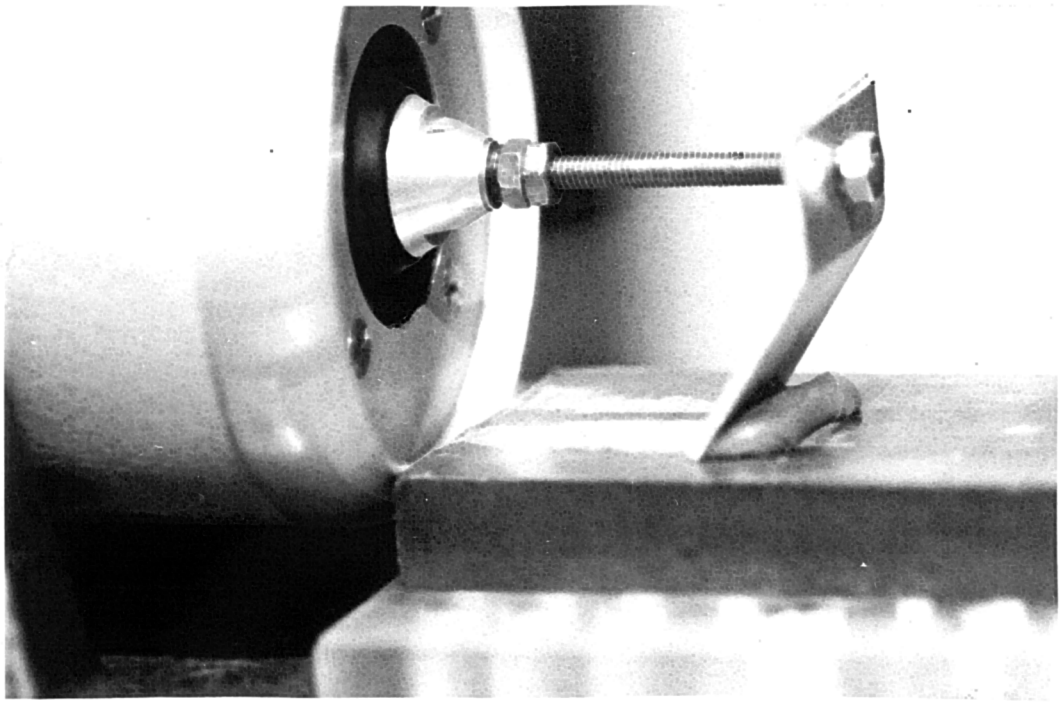

Figure 4.19 Solder paste response to vibrating squeegee (ω = 200 Hz, A = 0.24 mm).

A. The optimal parameters

It was observed in the experiments that (see Figure 4.13 to Figure 4.17), by the impaction of the vibrating squeegee a liquid rich layer was generated at the paste roll and squeegee blade interface. This liquid rich layer acted as a lubricating agent that could reduce the resistance of the squeegee blade on the paste roll. Comparison of the above pictures showed that the surface of the paste roll with vibration was much smoother than that without vibration. A smooth paste roll surface may lead to better packing of paste inside stencil apertures. This can be explained as that, during the aperture filling stage, a rough paste roll surface may wrap air bubbles into the apertures that leads to insufficient paste deposits on the substrate. It was also observed in the experiments that with suitable vibration parameters the paste rolls in front of the squeegee without sliding. The experiments showed that to obtain a good paste roll the squeegee vibration frequency and amplitude should fall into specific ranges. For the paste tested the suitable range of vibration frequency was from around 80 Hz to around 200 Hz and the suitable range of vibration amplitude was from around 0.1 mm to around 0.37 mm. The correlation between suitable frequency and amplitude is shown by the shadowed area of Figure 4.20. This figure can be used as a reference for the selection of the vibration parameters. Oscillatory shear experiments, section **4.1**, has shown that the dynamic viscosity of solder paste decreases as the oscillatory frequency increases. Therefore the application of a vibrating squeegee with high frequency and small amplitude is expected to obtain better paste packing inside stencil apertures than that with low frequency and large amplitude. At frequency of 80 Hz and amplitude of 0.37 mm, the vibration speed, $A\omega$, is about 0.185 m/s and the accelerate, $A\omega^2$, is about 93.5 m/s^2, while at frequency of 200 Hz and amplitude of 0.10 mm, the vibration speed is about 0.126 m/s and the accelerate is about 158 m/s^2. The vibration speed is five to ten times higher than the constant printing speed, 10~20 mm/s, and the accelerate is above ten times higher than the gravitational accelerate, $g = 9.8\ m/s^2$. It is recommended to select relative high frequency and small amplitude from Figure 4.20. Such selection is beneficial to the reduction of the volume of paste sticking on the squeegee as it is lifted at the end of a printing stroke as shown in Figure 4.21.

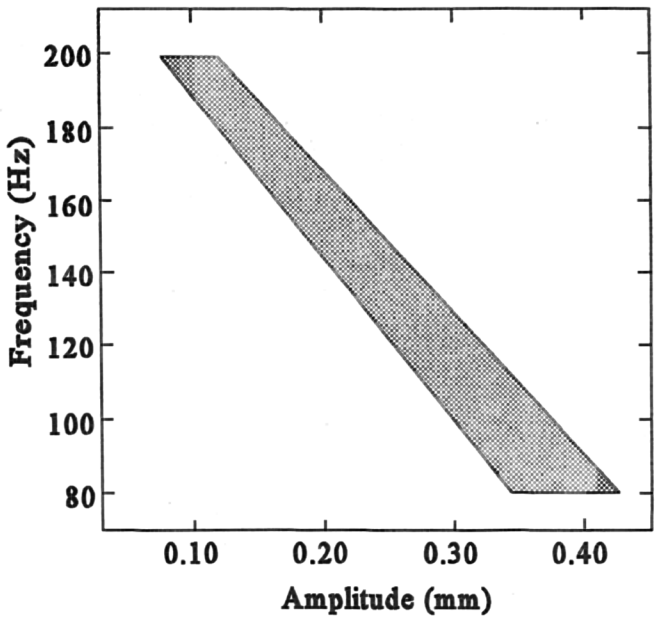

Figure 4.20 Correlation between suitable frequency and amplitude.

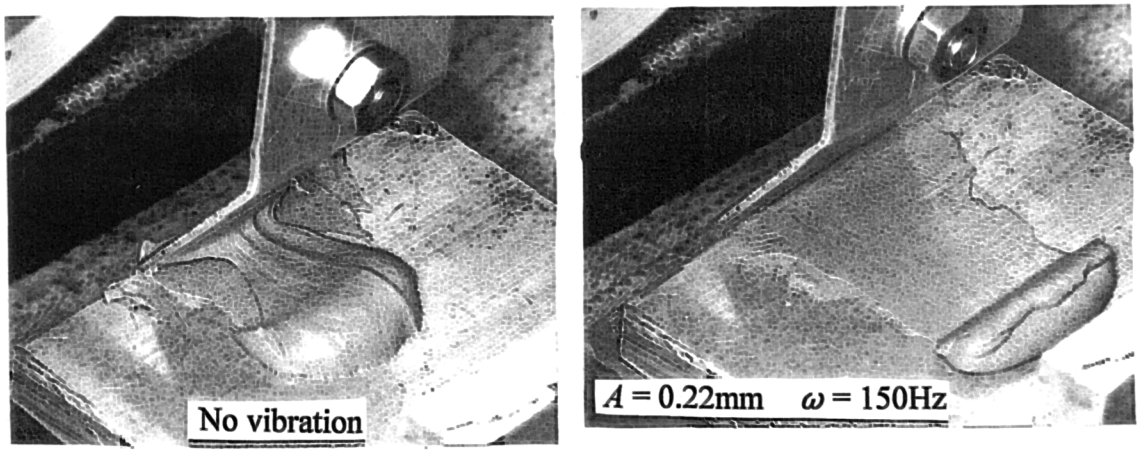

Figure 4.21 Effect of vibration on the reduction of paste sticking on the blade.

The experiments also showed that, with suitable vibration parameters, the distance from the start position of the printing stroke to the position where the paste roll was formed was much shorter than that without vibration. With vibrating parameters selected from the shadow area of Figure 4.20, this distance was less than 50 mm, and it was around 130 mm without vibration. This effect is very important for the increase of productivity. In practice, to ensure the printing quality, an extra distance has to be set for the printing stroke to allow the formation of paste roll. The application of a vibrating squeegee can reduce the distance of the printing stroke. For example, for a printing speed of 20 mm/s, above three seconds can be saved in each printing stroke due to the quick formation of paste roll.

B. Low frequency

Experimental results showed that the use of a vibrating squeegee with low frequency, below 50 Hz, and small amplitude, blow 0.2 mm, could also help the paste roll and ease paste sliding compared with no vibration. Nevertheless, this effect was not significant. As analysed in **Chapter three**, see Figure 3.2 and Figure 3.3, with low frequency and small amplitude the squeegee cannot effectively impact the paste roll to generate a liquid rich layer. Under such condition it was observed that, as the squeegee was lifted, the effect of vibration on the reduction of paste sticking to the squeegee was also not significant. This is because that the inertial force of the paste ($mA\omega^2$, where m is the mass of the paste) generated by vibration is not sufficient to overcome the paste adhesion to the squeegee. While, with low frequency, below 50 Hz, and large amplitude, above 0.8 mm, it was observed that, the vibrating squeegee could eliminate the sliding of paste on the plate, under such condition the surface of the paste roll was found to be rougher than that with small amplitude, as shown in Figure 4.11. This phenomenon may be attributed to the generation of air bubbles at the blade and paste roll interface, as sketched in Figure 4.22. With low frequency and large amplitude, as the squeegee oscillates backwards, the paste may only be partially separated from the paste, and the region of paste roll surface near the squeegee is not smooth. Again this is because of insufficient inertial force (for example with a frequency of 100 Hz and an amplitude of 0.35 mm the acceleration, $A\omega^2$, is 138 m/s^2, while

with 50 Hz and 0.8 mm the acceleration is only about 79 m/s^2). Then as the squeegee oscillates forward and touches the paste roll it will wrap the air at the interface to form bubbles that lead to a rough surface.

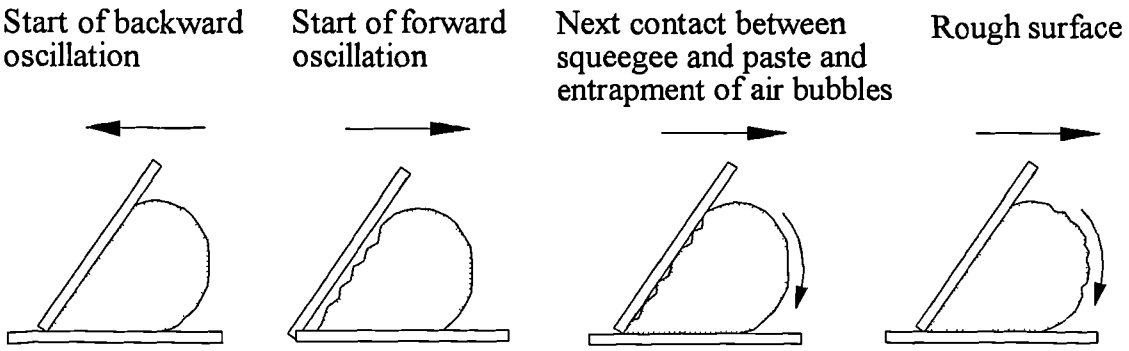

Figure 4.22 Generation of air bubbles and roughness of paste roll surface.

C. High frequency

Observation of the experiment with high frequency and large amplitude, see Figure 4.19, showed that the paste was pushed to flow away from the squeegee and could not form a paste roll. Under such condition, the appearance of the paste was very thinning was like a liquid. This phenomenon is consistent with the oscillatory shear measurement that is the storage modulus decreases as the shear strain increases. Although a vibrating squeegee pushing the paste in front of it is not as the same as oscillatory shearing, the effects of the two processes on the storage modulus of the solder paste are similar. To obtain a good paste roll and to maintain the resolution of the deposits on the PCB's, for storage modulus it is not a case of the smaller the better, but an optimum, i.e. high frequency and large amplitude are not suitable for the vibrating squeegee.

D. High metal load paste response

Figure 4.23 shows the response of the expired paste sample to the vibrating squeegee. For

this paste sample, without vibration the paste was only pushed by the squeegee to slide on the plate, no rolling was observed. In contrast, with vibration, both good paste roll and liquid rich layer were observed in the experiments. This was because that the dynamic viscosity of the paste was effectively reduced by using the vibrating squeegee. This suggests that a high metal load paste can be used in stencil printing with a vibrating squeegee which is appealing because it reduces bridging defects and voids after reflow soldering, and sometimes, helps residue cleaning. However, the hurdle is that, with high metal load, maintaining the paste with workable rheology is difficult, such as the applicable viscosity (Hwang, 1989). The vibrating squeegee may be one of the potential solutions to tackle this difficulty.

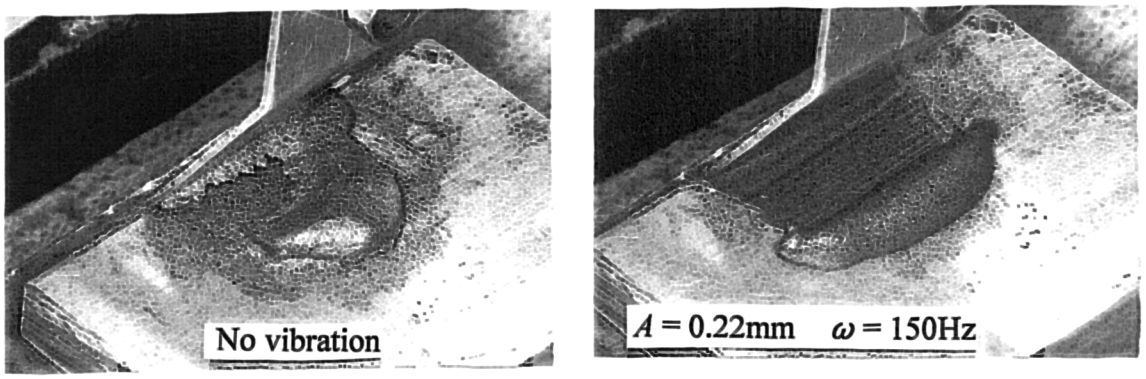

no vibration vibration (ω=150 Hz, A = 0.35 mm)

Figure 4.23 Response of high metal load paste to vibrating squeegee.

4.2.4 Main conclusion of vibrating squeegee experiments

In this section the experiments of the response of solder pastes to a vibrating squeegee were presented. Experimental results validated the theoretical prediction of **chapter three**. The

followings are the main conclusions:

i. The application of a vibrating squeegee can generate a liquid rich layer at the squeegee blade and paste roll interface. This liquid rich layer can reduce the squeegee blade resistance on the paste, so enhances the paste roll;

ii. For printing speed of 10 to 20 mm/s, the suitable range of frequency is from 80 to 200 Hz, and the suitable range of amplitude is from 0.1 to 0.37 mm, the high frequency should have small amplitude and the low frequency should have large amplitude. Below the ranges, the effect of vibration on paste roll is not significant, while, above the ranges, the paste will be pushed to flow away from the squeegee;

iii. The application of vibrating squeegee can also help to reduce the amount of solder paste that would stick on the squeegee blade as the squeegee is lifted at the end of a printing stroke;

iv. Using a vibrating squeegee, solder pastes with high metal loads may be applicable to stencil printing.

4.2.5 Further improvements on the experiment

As sketched in Figure 4.9, in this experimental apparatus, because of the geometrical restriction of the vibrator, the squeegee was supported by two shafts, which were not in the same horizontal level as the vibrator. If the squeegee was rigidly connected to the vibrator shaft there would be had a bending load on both the vibrator shaft and the squeegee supporting shafts. To reduce this load, a connecting bar was used to connect the squeegee and the vibrator by revolution joints. Such structure reduced but did not eliminate the bending load on the vibrator shaft and on the supporting shafts. The bending load and the connecting joints would generate noises, such as low frequency and variable large amplitude. Such noises were observed during experiment that could weaken the effect of

the vibrating squeegee on the paste roll. Therefore it is suggested that improvements on the experimental system should be made to eliminate such noises in further studies.

Another shortcoming of the experimental system was that the vibrator was directly fixed to the milling machine head. The heavy machine body would damp the vibration. So it is suggested that some measures should be taken to isolate the vibrator from the machine.

After above improvements were made, it could be expected that experimental results would be better than those achieved in this work.

4.3 The behaviour of solder paste inside a vibrating container

The effect of the vibrating squeegee on the packing of solder paste inside stencil apertures was theoretically predicted in **Chapter three**. Owing to the difficulty in manufacturing a special stencil for the experiment, the effect of the vibrating squeegee on the packing of solder paste inside apertures could not be investigated directly. Instead, paste samples were vibrated inside a cylindrical container that could reflect, to some extent, the behaviour of solder paste inside apertures during stencil printing using a vibrating squeegee. This section presents the experiments

4.3.1 The experimental procedure

Figure 4.24 shows a picture of the equipment for this experiment. A cylindrical aluminum container (18 mm inside diameter and 10 mm heigh) was fixed on the shaft of a V201 vibrator. The same samples as used in the vibrating squeegee experiment were used here. First a sample was put into the container after gently stirring. Then the container was subjected to a sinusoidal vibration on the horizontal plane for a period of 10 seconds. Pictures and microscope photographs of the samples were taken before and after vibration.

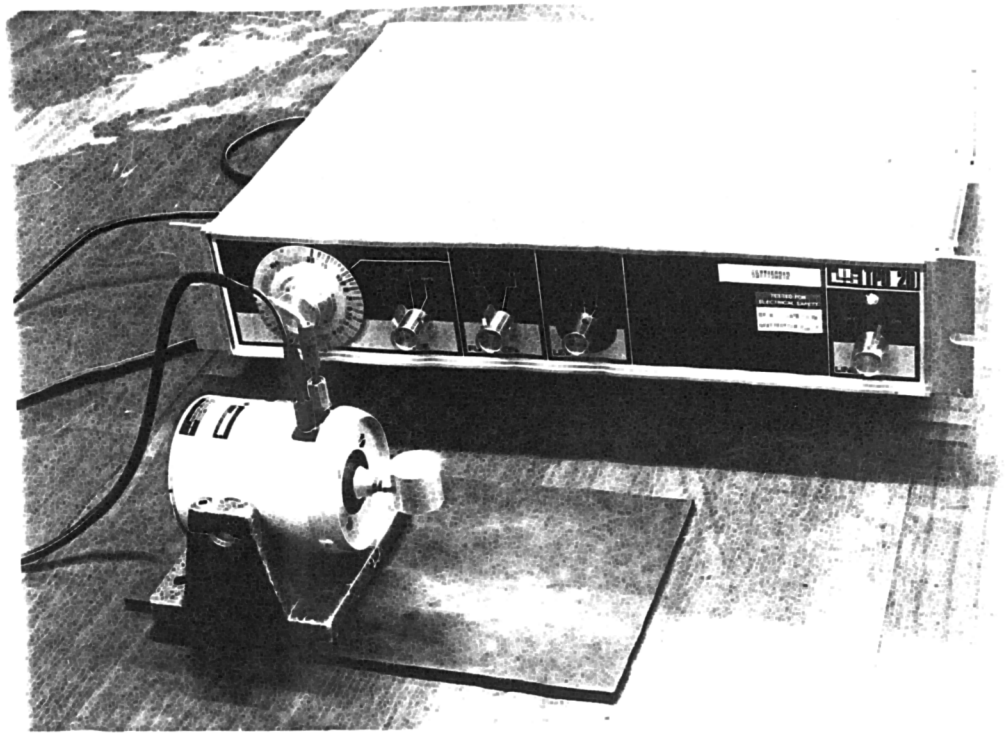

Figure 4.24 Picture of vibrating container.

The vibration frequency was ranged from 60 Hz to 150 Hz. For each frequency three levels of amplitude were tested. Calibrations showed that the amplitude was ranged from 0.2 to 0.7 mm.

4.3.2 Results and discussion of vibrating container

Figure 4.25 to Figure 4.28 are the pictures taken before and after vibration with different vibration parameters on the solder paste sample. Figure 4.29 is the microscope photograph, which shows the effect of the vibration on the paste microstructure. The followings can be observed from these pictures:

i. After vibration, a liquid rich layer was found generated at the interface between the

container wall and the paste sample. A liquid rich layer could be observed at the surface of the sample. The principle of the generation of the liquid rich layer at the container and sample interface is the same as the generation of liquid rich layer by a vibrating squeegee. As the container was vibrating, the particles near the container wall were caused by contacts the wall to move inwards onto the sample leaving a liquid rich layer at the interface. The surface liquid rich layer was the result of the particle subsidence. The mass density of 63Sn/37Pb solder particles is 8.3 g/cm^3, which is about nine times of the mass density of the flux/vehicle, 0.9 g/cm^3 (Hwang, 1989), and even in the static the particles tend to fall under the gravitational force. Application of vibration can accelerate the falling process. This is because during vibration, neighbouring particles collide with each other and this may break the bridges between them and lead particles filling the voids. The formation of both liquid rich layers can be beneficial to the printing quality. First the liquid rich layer near the aperture wall can help the paste to withdraw from the aperture and reduce the number of particles that stick on the aperture wall. Second the liquid rich layer at the paste surface can lubricate the squeegee tip that makes the packing surface smooth and a smooth surface can prevent the deposit from slumping in the component placement stage. The surface liquid rich layer can also effectively wet the leads of components that results in durable metallic inter-joints after reflow soldering. The subsidence of particles can also enhance the adhesive force between solder paste and the substrate that may reduce tamping of the apertures.

ii. Careful comparison of the sample surface levels before and after vibration showed that, after vibration, the sample surface inside the container was lower than that before vibration. This may suggest that the application of vibration can help to reduce the voids occupied by air and obtain high paste packing density inside the apertures.

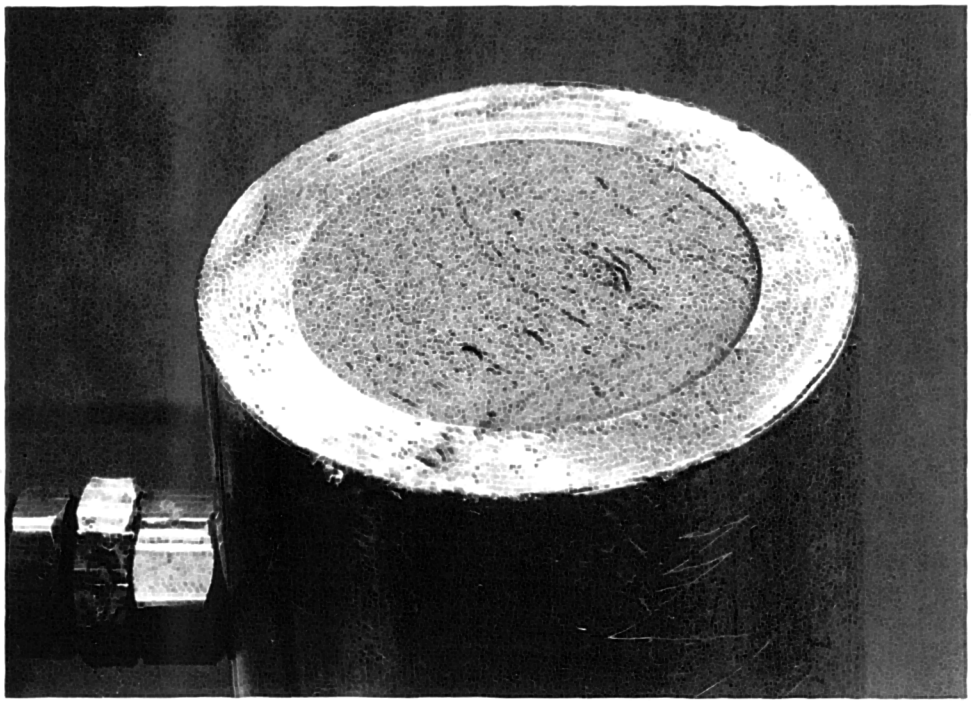

Figure 4.25 The packing of paste sample inside the container before vibration.

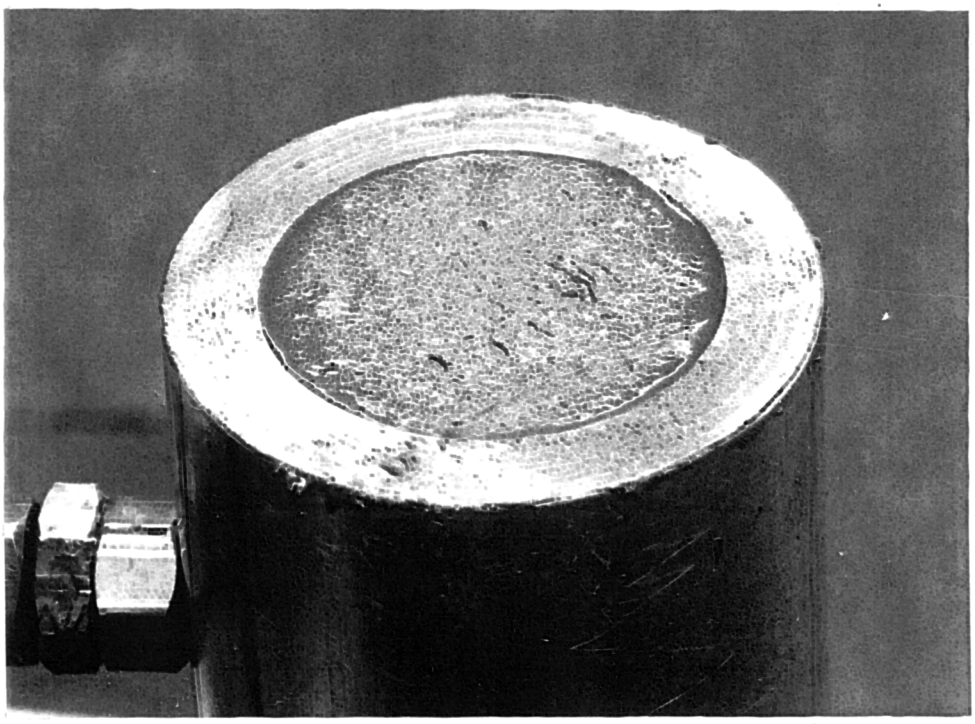

Figure 4.26 The packing of paste sample inside the container after vibration.

(ω = 80 Hz, A = 0.42 mm)

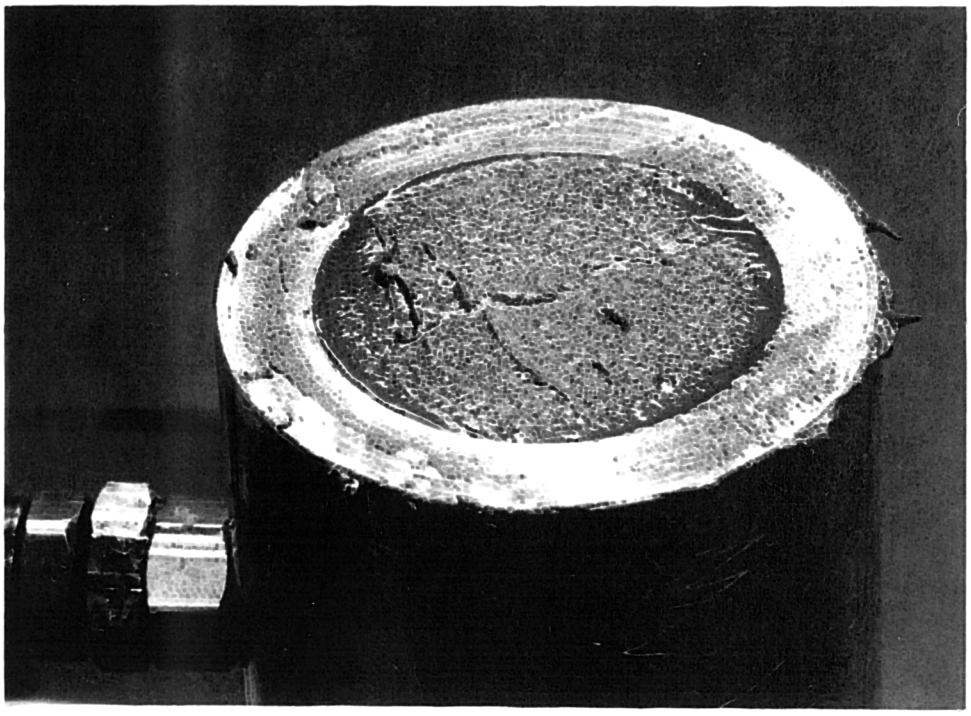

Figure 4.27 The packing of paste sample inside the container after vibration.
(ω = 120 Hz, A = 0.35 mm)

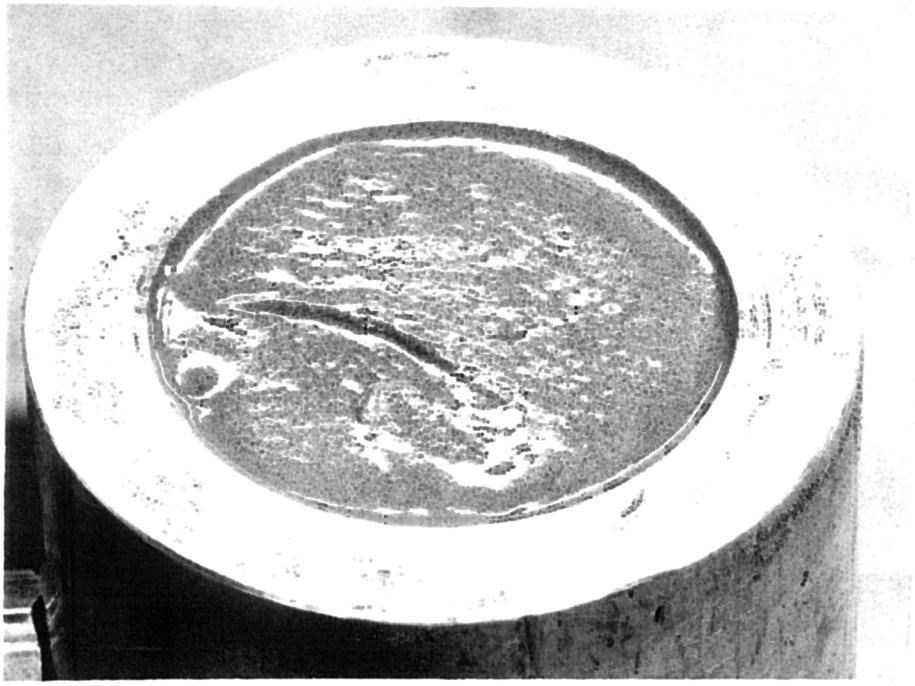

Figure 4.28 The packing of paste sample inside the container after vibration.
(ω = 150 Hz, A = 0.30 mm)

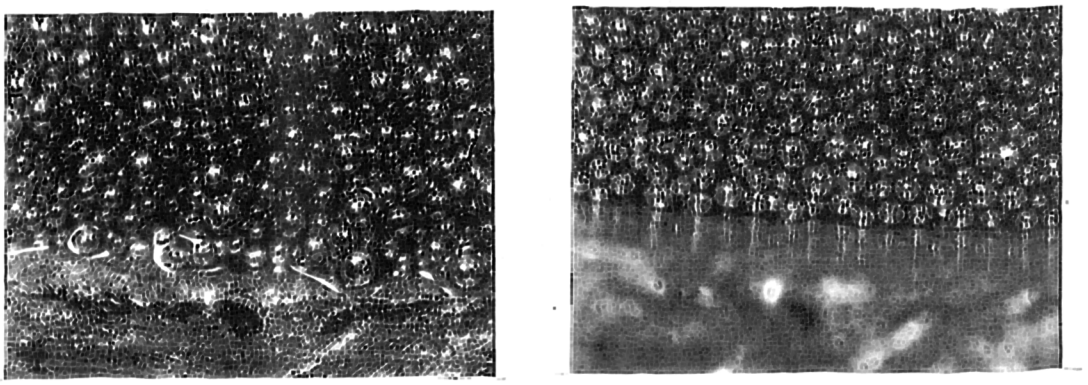

Before vibration After vibration

Figure 4.29 Particle re-arrangement by vibration (ω =150 Hz, A =0.30mm).

iii. Comparing the micro-photos taken before and after vibration, Figure 4.29, shows that after vibration the arrangement of solder particles, beside the boundary liquid rich layer, was more uniform than that before vibration. To discuss the effect of vibration on particle rearrangement, take three equal particles that are randomly placed on a horizontal line with unequal distance, as shown in Figure 4.30. The gap between particle *1* and *2* is assumed originally lager than that between particle *1* and *3*, the relative position of particle *2* and *3* is assumed unchanged and the particles are separated by a high viscous liquid medium. If the system of the three particles is vibrated, then as the vibration is from right to left particle *3* transfers energy to particle *1*, which will move towards particle *2*; as the vibration is from left to right, particle *2* transfers energy to particle *1*, which will move towards particle *3*. Because the gap between particle *1* and *3* is smaller than that between particle *1* and *2*, the energy transferred to particle *1* by particle *3* is higher than that by particle *2*. So the trend of the motion of particle *1* is from right to left. Finally particle *1* vibrates in a balance point

where is in the middle between particle *2* and *3*.

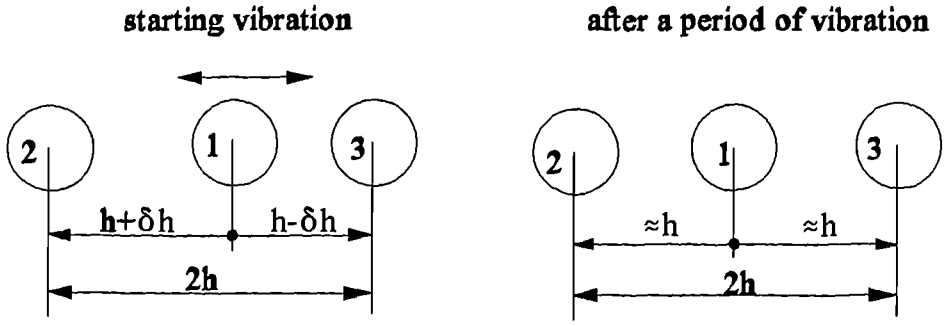

Figure 4.30 The effect of vibration on particle arrangement

The uniform rearrangement of particles by vibration may lead to the reduction of the viscosity of the solder paste. For a dense suspension, such as solder paste, the gaps between near-neighbour particles are much smaller than the particle radii. Therefore, the particle movement will be dominated by lubrication forces. If the radii of three particles are the same (r), the relative velocities of particle *2* and *3* to particle *1* are the same (u). The gaps between particle *1* and particle *2* and between particle *1* and particle *3* are $h+\delta h$ and $h-\delta h$, then the lubrication force acting on particle *1* by particle *2* and *3* is (detail see **Chapter 6**):

$$F = \pi \eta_o ur \left[\ln\left(1+\frac{r}{(h+\delta h)}\right)+\ln\left(1+\frac{r}{(h-\delta h)}\right)\right] = \pi \eta ur \ln\left[1+\frac{r(2h+r)}{h^2-\delta h^2}\right] \quad (4.1)$$

where η_o is the viscosity of the vehicle. If $\delta h = 0$, then the force F is minimized. So uniform arrangement of particles may lead to the viscosity reduction of the solder paste. The reduction of viscosity is also beneficial to the withdrawing of paste from the apertures. Again it shows the potential of the use of high metal load paste. Uniform arrangement of particles can also help to improve reflow soldering quality.

4.3.3 Main conclusion of the vibration experiment of solder paste inside a container

The vibration experiment of solder paste inside a container showed that (1) vibration can generate liquid rich layers at solder paste and container wall interface and at the sample surface; (2) vibration leads to high packing density; (3) after vibration the arrangement of particles is more uniform than before vibration. The liquid rich layers and the uniform arrangement of solder particles can help to improve the printing quality of solder paste.

4.4 Summary of Chapter four

To validate the theoretical prediction of the behaviour of solder paste in stencil printing using a vibrating squeegee, three experiments were conducted. This chapter reports the experimental results. The followings are the main conclusions of this chapter.

The viscoelastic properties of solder paste were studied by frequency sweep oscillatory shear measurement. The experimental result on solder paste showed that the dynamic viscosity of solder paste decreases as the oscillatory frequency increases; at high frequency (50 to 90 Hz) the storage modulus of solder paste is much smaller than the loss modulus. Therefore under oscillatory shear the behaviour of solder paste is more like that of a viscous liquid than an elastic solid. The result also showed that the storage modulus of solder paste under high shear stress (large shear strain) is smaller than that under low shear stress (small shear strain).

The second experiment was the vibrating squeegee. Experimental results of the vibrating squeegee proved the application of a vibrating squeegee can generate a liquid rich layer at the squeegee blade and paste roll interface. This liquid rich layer acts as a lubricating agent between the squeegee blade and the paste that could reduce the squeegee resistance on the paste roll, There is empirical evidence to show that a good paste roll is essential for the proper filling the apertures, for achieving good paste withdrawal, and thus more consistent deposits on a substrate. The formation of a liquid rich layer can also help to reduce the

potential for the paste roll to stick on the squeegee blade at the end of the printing stroke. This experiment also showed that the vibrating squeegee can reduce the distance needed for the formation of a paste roll at the start of the printing stroke. The quick formation of a paste roll can help to reduce the length of printing strokes, so saving time. The effect of the vibration parameters on the stencil printing quality was investigated in this experiment. Results analysis shows that the suitable range of frequency is from 80 Hz to 200 Hz, and the suitable range of amplitude is from 0.10 mm to 0.37 mm.

In the third experiment the paste sample was vibrated in a cylindrical container. Experiment results showed that under vibration liquid rich layers can be generated at container wall and sample interface and at the sample surface. The liquid rich layer at the interface can help the withdrawal of solder paste from the aperture and the liquid rich layer at the surface can help to achieve level paste deposit on the substrate. Microscope photos showed that under vibration the particle arrangement is more uniform than without vibration. This uniform arrangement may reduce the viscosity of solder paste. Uniform arrangement of particles can also help to improve the soldering quality and obtain reliable connection between components and substrate. It is necessary to point that the third experiment may, only to some extent, reflects the response of the paste packed inside an aperture to the action of a vibrating squeegee. Therefore, a real stencil printing test using a vibrating squeegee is needed to examine the above behaviours observed in the vibrating container tests.

Chapter Five

Numerical Simulation of the Maximum Solid Concentration and the Micro-structure of Solder Paste

5.1 Highlight of Chapter five

Solder pastes are dense suspensions of spherical solder alloy particles embedded in a flux/vehicle system. The rheological characteristics, such as the viscosity, pseudo-plasticity and yield point, of a dense suspension are significantly affected by the solid concentration, usually represented by solid volume fraction of particles suspended in it. The particle size distribution also significantly affects the rheological characteristics of dense suspensions. In industrial application, the rheological characteristics of the dense suspensions should be under control to achieve the good application results. As was stated earlier in **Chapter two** the stencil printing quality of solder pastes for SMT is directly affected by the rheological properties of the pastes.

Among the rheological characteristics of a solder paste, viscosity is the most important one. It may affect every sub-stages of the stencil printing process, hence the final quality of the assembly. The flux/vehicle system, by itself, is a non-Newtonian fluid. The addition of solder powder to the flux/vehicle system makes the viscosity of solder paste an even more complex parameter. It is convenient to represent the viscous property of a dense suspension by the relative viscosity, the ratio of the viscosity of the dense suspension to that of the liquid medium. Studies demonstrate that, under high shear rate, the relative viscosity is only a function of the ratio of solid volume fraction presents in the suspension to the maximum solid volume fraction (Gadal et al, 1980). This is based on the fact that, under high shear rate, the flow of a dense suspension is dominated by the hydrodynamic interactions between neighbouring particles. Generally, the relative viscosity of a dense suspension can expressed as:

$$\eta_r = \frac{\eta_s}{\eta_o} \propto \left(\frac{\phi}{\phi_m}\right) \tag{5.1}$$

where η_s is the viscosity of the suspension; η_o is viscosity of the liquid medium; ϕ is the real solid volume fraction of suspended particles and ϕ_m is the maximum solid volume fraction. Equation (5.1) shows that η_r increases with increase of ϕ and decreases with increase of ϕ_m.

For a dense suspension of known particle size distribution, ϕ_m should be a constant. Although there is divergence in the literature on the definition of ϕ_m, the random loose packing density is widely accepted as the maximum solid volume fraction of the dense suspensions of monosized spherical particles. In industrial applications, most dense suspensions, such as solder paste, are of spherical particles with size dispersions. However, data on random loose packing of particles with size distributions are very scarce, and hence the lack of viscosity models of dense suspensions of distributed particles.

As was stated earlier, under high shear rate, the flow of a dense suspension is dominated by the hydrodynamic interactions between neighbouring particles. Computer simulation models have been developed to study the flow of dense suspensions. These models treated a dense suspension as a two phase material (ie. the liquid medium and the solid particles), rather than a continuous liquid. Flow properties have been obtained by simulating the interactions among individual particles. In such simulations, the initial positions of each particle should be known first and an understanding the micro-structure of a dense suspension is needed. Here the micro-structure of a dense suspension infers the suspended position of each individual particle in the liquid medium and its relation to its neighbours, such as the number of neighbour particles, and the gaps between it and its neighbours. Such an understanding may help to reveal the effects of particle size distributions and solid volume fractions on the viscosity of dense suspensions.

In this chapter, novel computer simulation algorithms of the random loose packing and the

micro-structure of solder pastes are presented. As solder pastes are dense suspensions and share the same characteristics with other dense suspensions of spherical particles, the term "dense suspensions" will often be used interchangeably with the term "solder pastes" in this chapter. In fact, the simulation algorithms are applicable to the random loose packing of any spherical particles and the micro-structures of any dense suspensions. Section **5.2** gives a brief review of the methodology used in the study of random packing of hard spherical particles. Section **5.3** presents the new simulation algorithms developed in this study while section **5.4** discusses the simulation results.

5.2 Study of the random packing of hard spherical particles

The random packings of hard spheres have long been of interest and have been studied for many years because they serve as useful models for many physical systems and for industrial practice. They are found in, for example, powder metallurgy, ceramics, soil science, biology, physics, chemistry. The random packings of particles are normally characterised by two parameters, the packing density and the average contact number (also called the coordinate number). The packing density is the ratio of the total particle volume to the volume of the space occupied by the particles, and the average contact number is the mean value of the number of particles that contact a particular particle. There is proportional relationship between packing density and contact number, that is the higher the packing density the higher the average contact number. Three methods are used in the study of random packing of particles, the experimental method, the analysis method and the numerical simulation method.

5.2.1 Experiment and analysis methods

A. Experimental method

In the early years, experimentation was the main method used in the study of the random packing of hard spheres (Scott, 1960; Bernal et al, 1960).

Scott (1960) investigated the random packing of hard spheres intensively by experiments. In the experiments, between two and twenty thousand steel balls of equal size were poured into a rigid container, and then the packing density was measured. The random packing achieved by this method was defined as "loose random packing". The lower limit of the packing density was measured to be 0.59. It was also found that, after pouring the balls into the container and then shaking or tapping the container could increase the packing density. The packing achieved by this method was defined as the "dense random packing", or "close random packing". The upper limit of the close random packing density was 0.63. Experimental results showed that, for both loose and close random packings, the packing densities were highly dependent on the number of the balls used in the experiments. Figure 5.1 shows the effect of number of balls on the packing densities. As the number of balls increases both the random loose and close packing densities increase. This indicates that with fewer balls the rigid container wall has a strong effect on the packing density. To eliminate the effect of the rigid wall of the container, an experiment was conducted using an unextended balloon as the container.

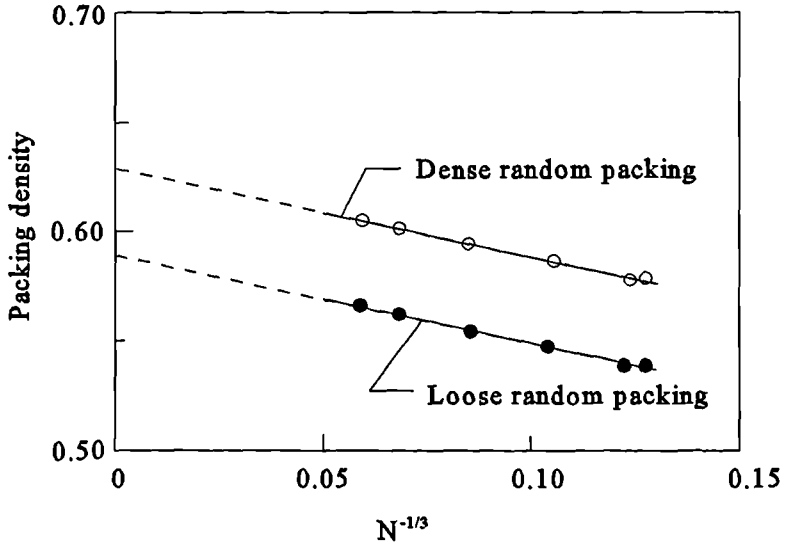

Figure 5.1 Packing density versus number of balls, N. (Scott)

Bernal and Mason (1960) studied the contacts among equal spheres by experiments. In the experiments, the balls were shaken down and compressed first, then the packing was soaked in black paint. After thoroughly drying, the mass of the balls was unwrapped, and the contact marks on the surface of each sphere were counted. There were two types of contact, close contact and near contact, as shown in Figure 5.2. At the packing density of 0.62 the total average contact number was found to be 8.5 and the close contact number was found to be 6.4. Bernal and Mason suggested that the packing density, 0.62, obtained in their experiment was a reasonable approximation to Scott's close random packing density. The number of balls used in their experiments was between 1000 and 5000, which was less than that used by Scott. The packing density was lower than that obtained by Scott. This result confirmed that the packing density was affected by the number of balls. By the method similar to Scott's, Bernal and Mason obtained the result that the loose random packing density was 0.6, the average total contact number was 7.1 and the average close contact number was 5.5. The histograms of close contact and total contact number of the close random packing obtained by Bernal and Mason are shown in Figure 5.3.

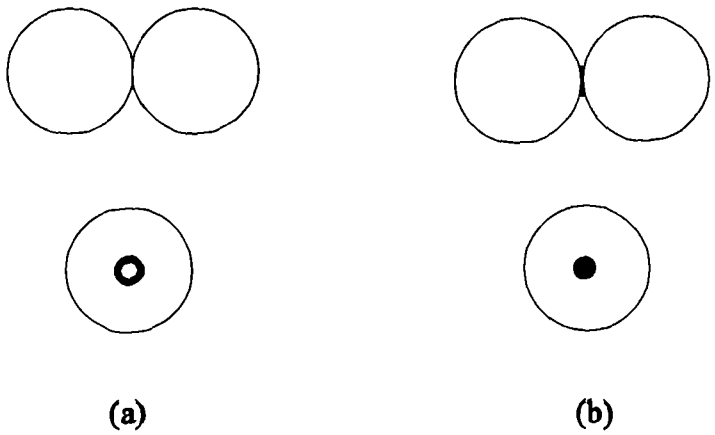

Figure 5.2 Contact between balls: (a) close contact, (b) near contact. (Bernal et al)

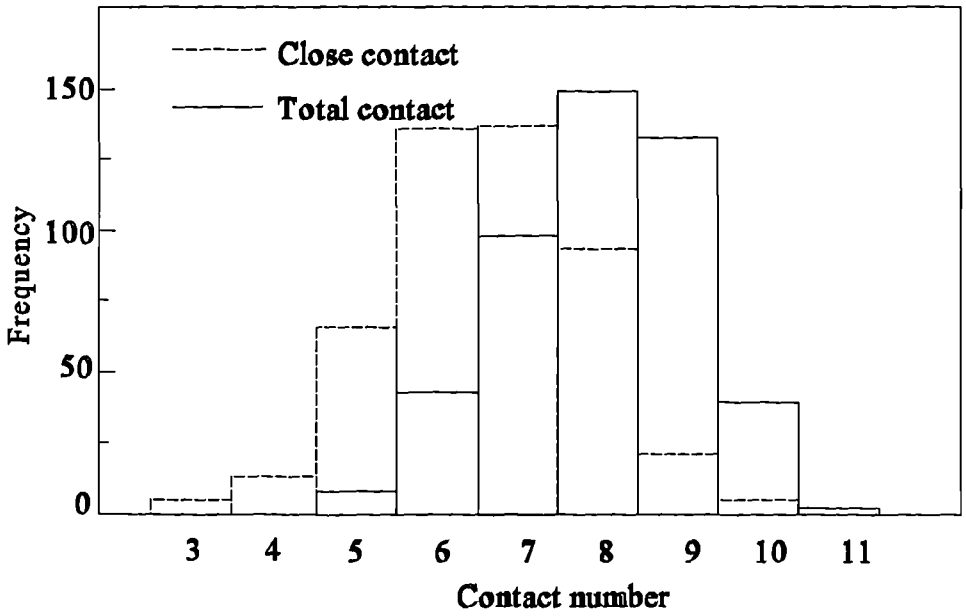

Figure 5.3 Histogram of contact number. (Bernal et al)

These experiments were conducted under the effect of gravity. To minimize the gravity effect Onoda and Liniger (1990) conducted a random loose packing experiment in a liquid. The specific gravities of the particles and the liquid were the same. By extrapolating experimental data, they estimated the loose packing density without the gravity effect to be 0.555±0.005.

B. Analysis method

Gotoh and Finney (1974) applied a statistical geometrical approach to predict the random packing density of equal spheres. They approach made the following assumption; " For a given sphere to be stable against displacement in a given direction, it must be supported by three spheres in that direction, the group of four spheres forming a tetrahedron. The same stability criterion must also apply for the opposite direction". Then the statistic method was applied to establish the probable density function of the arbitrary relative positions of the

four spheres. The packing density was calculated from the most probable tetrahedron. Their results suggested that the lower and upper limits of the random packing density were 0.6099 and 0.6472 respectively. Comparing with experimental results, it is seen that both the lower and upper limits of packing density achieved by this method were higher than that obtained by experiments. This could be attributed to the assumption that the displacement of one sphere must be confined by three spheres in one direction and by three other in the opposite direction. In fact, in a random loose packing situation, the minimal close contact number may be less than five, (see Figure 5.3 in which the contact number was composed of close contact and near contact). It is also true that bridges between neighbouring spheres could occur in the packing.

Gamba (1975) studied the packing of spheres by means of integral geometry. First he calculated the packing density of equal discs in a two dimensional situation. Then this approach was extended to the case of three dimensional geometry. For two dimensional geometry case, shown in Figure 5.4, the centres of four contacting discs define a parallelogram, and the relative positions of the four discs can be defined by angle α. At a given angle, the area of the parallelogram is given by $4r^2 \sin\alpha$. The packing density is the ratio of the area of one disc to the area of the parallelogram. Assuming that angle α obeys uniform distribution over $[\pi/3, \pi/2]$, then the average area of the parallelogram was calculated as:

$$A = \frac{\int_{\pi/3}^{\pi/2} 4r^2 \sin a \, da}{\int_{\pi/3}^{\pi/2} da} = \frac{12r^2}{\pi} \qquad (5.2)$$

and the average packing density is calculated to be:

$$\rho_2 = \frac{\pi r^2}{A} = \frac{\pi^2}{12} \cong 0.8225 \qquad (5.3)$$

Gamba extended this approach to the case of three dimensional geometry and calculated the random packing density of equal spheres to be:

$$\rho_3 = \frac{4}{3}\pi \int_0^{\frac{1}{2}} \int_0^{\frac{1}{2}} \int_0^{\frac{1}{2}} (1-x^2-y^2-z^2+2xyx)^{\frac{1}{2}} dxdydz \qquad (5.4)$$

Numerical integration solution of Eq. (5.4) is 0.596, which is in good agreement with experimental results.

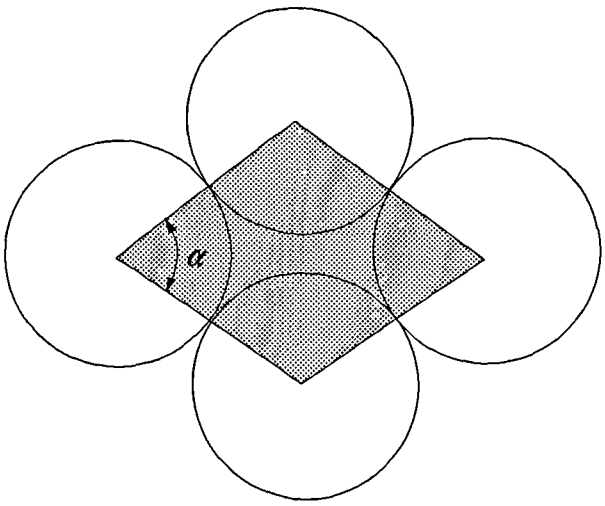

Figure 5.4 Integral geometry of random packing of equal discs. (Gamba)

Gotoh and Finney (1975) pointed out the dangers of using direct two dimensional analogues, developed by Gamba, because the geometries of two and three dimensions are essentially different. For example, it is difficult to define states in two dimensions that could be equivalent to random packing in three dimensions. They also pointed that the assumption of uniform distribution of angle α took no account of the local geometrical restrictions.

Further theoretical analysis carried out by Finney (1976) gave a packing density of 0.665, that by Woodcock and Angell (1981) gave a packing density of 0.654 and that by Berryman (1983) gave a packing density of 0.64±0.02. Comparison of experimental results with

analytical results shows that the random packing density obtained by theory is higher than that obtained by experiment. Perhaps this is because in all of the analytical methods the packing densities were derived from the possible relative positions of only a couple of particles. In contrast, in real random packing situation the positions of particles are always restricted relative to each other.

Both experimental and analytical methods played important roles in the study of random packing of spherical particles in the early years. However, the disadvantages of these two methods are obvious. By experiment, a very large number of particles are required to reduce the boundary effect of the container wall. Measurement of the contact number and the accurate positions of particles is also very difficult. The analytical method could not give detailed information, such as the relative positions between neighbouring particles. Besides, as pointed out above, the packing density obtained by analytical methods is always higher than that obtained by experiments.

5.2.2 Computer simulation methods

Since the late sixties, as computers became more powerful, computer simulation methods have been introduced to the study of the random packing of particles. Comparing with experimental method, computer simulation saves the experiment costs. The geometric characteristics of the packings, such as the accurate position and the contact number of each particle, are attainable by computer simulation.

Although a lot of random packing simulation models have been developed, they may be classified into two categories according to the generation sequence of particles. The first is the sequential generation model and the second is the collective generation and relocation model.

A. Sequential generation models

By an sequential generation model, only one particle is randomly added to the surface of an existing cluster at a time until a packing of many particles is formed. According to the criterion of adding particles to the cluster surface, the sequential generation models can be further classified into two groups, the "gravitational dropping model" and the "centre growing model".

As shown in Figure 5.5, using the "gravitational dropping model" (Tory et al 1968; Visscher and Bolsterli, 1972; Finney, 1976; Woodcock and Angell, 1981), the physical process of sequentially dropping balls into a bin by gravitational force is simulated by the Monte Carlo method. The balls are sequentially dropped from random positions above the bin. Once a new ball makes contact with three balls (already inside the bin) and its position is gravitational stable, then it stops moving. If the contact is not stable, the ball rolls down further under gravitational force until it reaches a stable position. Afterwards the position of the ball does not change. By repeating the dropping process, the cluster of many balls eventually grows upwards from the bottom of the bin. Until the desired number of balls have all been dropped into the bin, the simulation is stopped. The packing properties, such as the packing density and the contact number, are counted.

Figure 5.6 shows the addition of a new particle to the packing surface using the "centre growing model" (Bennett, 1972; Berryman, 1983; Konakawa et al, 1990; Lu et al, 1994). A seed particle is initially placed at the origin. The second particle is generated in a random position and is moved towards the first one until the two particles contact each other. Then the third one is generated and moved to contact both the first and the second particles. An additional particle beyond the third one is placed from a random direction to the surface of the centre cluster. The addition of a new particle to the cluster obeys a similar rule to that used by the "gravitational dropping model"; that is the new particle makes contact with three particles (on the cluster surface) and its position does not change afterwards. By such a method, a large cluster of many particles that grows outwards from the packing centre is

eventually generated.

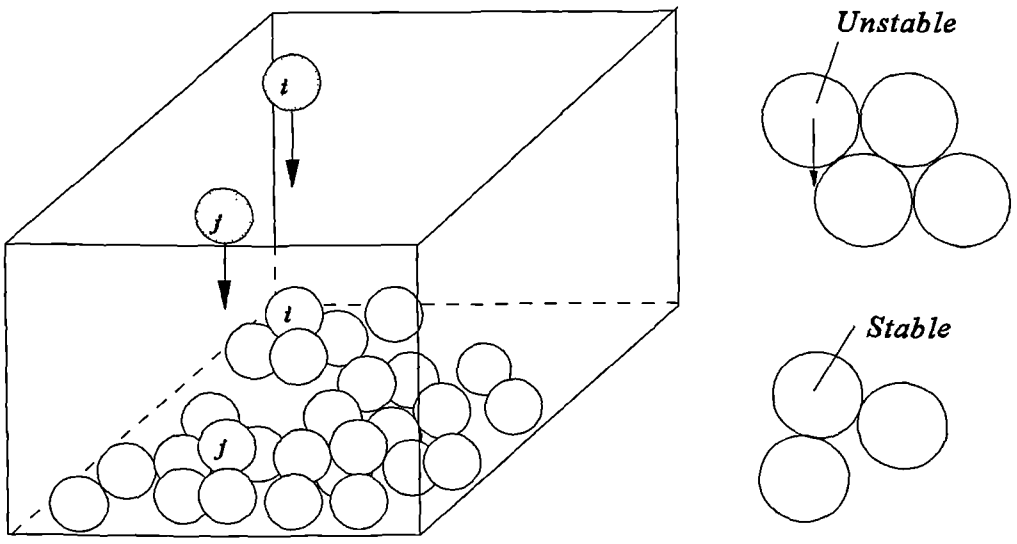

Figure 5.5 Gravitational dropping model.

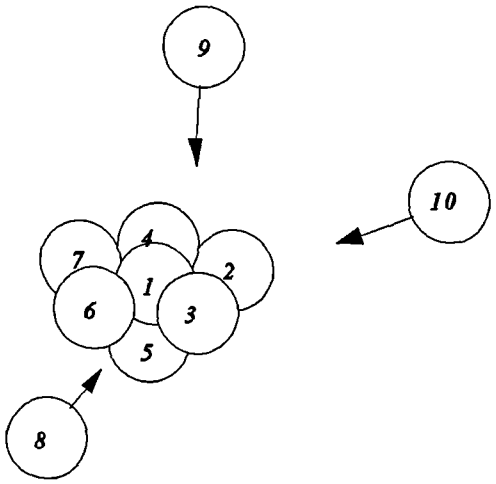

Figure 5.6 Centre growing model.

Both the "gravitaional dropping model" and the "centre growing model" are applicable for random loose packing and random close packing. For random loose packing, a new particle is added to the surface of the cluster from only one position above the bin by the "gravitational dropping model", or from only one random direction by the "centre growing model". This method of adding a new particle to the cluster is called the local rule. In contrast, for random close packing, the method of adding a new particle to the cluster surface is different from the local rule. On the cluster surface many sites are available to place a new particle. By the gravitational dropping model, a new particle can be tried to drop into the bin from ten or more random positions above it. Therefore, ten or more sites on the cluster surface can be identified as the candidate. Then only the lowest site is chosen to place the new particles. A similar method is applied for the centre growing model, by which, among ten or more possible sites, the nearest one to the cluster centre is chosen to place the new particle. This method of adding new particles is called the global rule. The packing density and contact number obtained by global rule are higher than that obtained by local rule.

The typical average contact number obtained by the sequential generation model is from 6.0 to 7.0 and this agrees with experimental results. However, the range of the packing density is from 0.51 to 0.61 and this is lower than experimental results. Comparing the sequential generation model with a real packing process shows that, in the simulation, once a particle is placed to the cluster surface its position does not change afterwards, while in reality the new added particles will interact with the already packed particles whose positions will be changed by the interactions until a system balance state is reached. The sequential generation models cannot simulate the interactions between particles. Simulation results obtained by the centre growing model showed that both the average contact number and the packing density decrease as the packing dimension increases (Bennett, 1972; Lu et al, 1994). In contrast, experimental results showed that the packing density increases with the number of particles and gradually approaches a stable value, for example, 0.6 for random loose packing. Therefore, the centre growing model may have some inherent disadvantages.

The advantage of the sequential generation models is the saving of computer time, this is because after a particle is added to the cluster it does not move again. However, these models are not applicable for poly-dispersed spherical particles. This is because once a particle is added to the cluster, the sites available for the subsequent particle must be recalculated again which is difficult for unequal spheres.

B. Collective generation and relocation models

With the collective generation and relocation model, the initial positions of all particles are randomly generated simultaneously within a defined space. For example if the packing is within a cubic box of size L, then the initial positions can be generated by:

$$\begin{aligned} x_i &= L\, R_{ix} \\ y_i &= L\, R_{iy} \qquad i=1,2,\ldots,N \\ z_i &= L\, R_{iz} \end{aligned} \tag{5.5}$$

where R_{ix}, R_{iy}, R_{iz} are random numbers which are uniformly distributed over (0, 1),and N is the simulation number of particles. For equal particles, the initial packing density, ρ_I, is:

$$\rho_I = N \frac{4\pi r^3}{3\, L^3} \tag{5.6}$$

where r is particle radius. The initial packing density should be higher than the maximum packing density and in the initial state there are obviously many overlaps between neighbouring particles. Overlap occurs when the distance between the centres of two particles is smaller than the particle's diameter; then the two particles overlap each other. The overlap level between two particles is represented by the relative overlap value which is defined as:

$$\delta_{ij} = \frac{2r - l_{ij}}{r} \tag{5.7}$$

where l_{ij} is centre to centre distance between two particles and is smaller than a particle diameter.

The second step of the collective generation approach is the relocation, or the overlap relaxation, which is applied repeatedly to reduce the overlaps until an overlap free packing is obtained. Different overlap relaxation techniques have been developed. In Jodrey and Tory's model (1985) the particles are arranged in the order of their overlap values. The pair of particles with the maximum overlap value are first separated by moving the same distance along the centre to centre line to eliminate this overlap. Then the second pair and so on, as shown in Figure 5.7, until all the overlap pairs are moved. It is not difficult to see from the above description that, as two overlapped particles are separated, new overlaps could be generated. The criterion is that, the new generated overlap values should not be greater than the old one. Then the particles are arranged again in the order of the new overlap values, and the moving process is repeated until the overlap value stops decreasing.

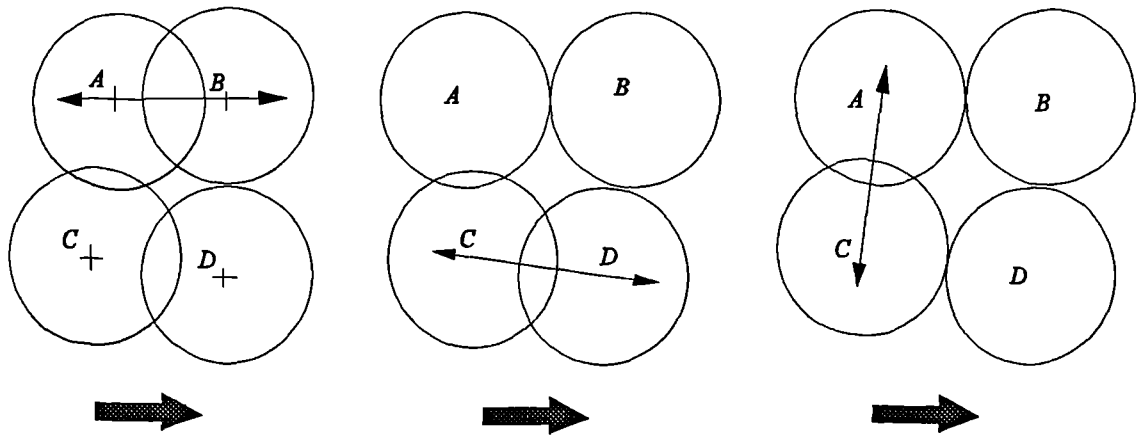

Figure 5.7 Jodrey's separation sequence of overlap particles.

In Clarke and Wiley's model (1987) one particle is moved in the direction of the vector sum of the overlaps at each time, as shown in Figure 5.8. This moving could reduce some overlaps but create or increase others. To counteract this tendency, the moving of a particle obeys the similar condition to that of Jodrey and Tory's model, that is after each moving the new generated overlap values should not exceed the maximum overlap value. This leads to the maximum overlap value decreasing to a stable point as motion continues. The third step is shrinking the particle size. The shrinking scale is dependent on the average overlap value obtained in the second step. Then the simulation goes back to the second step. By repeating the second and third steps, the overlap value is gradually reduced and when it falls below a specified value the simulation is stopped.

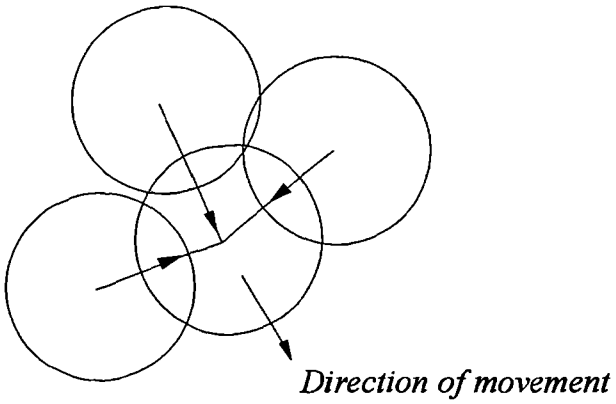

Figure 5.8 the moving of a particle by Clarke's model.

In Nolan and Kavanagh's model (1993), to release the overlaps, an artificial repulsive force between overlap particles is defined which is changed from a high order polynomial to a linear function. This repulsive force enables particles to move more freely relative to each other while in an overlap state. Weak repulsive forces allow the particles with a lager overlap number the possibility of travelling through an overlap and entering new configurations. Strong repulsive forces would tend to lock the particles into their initial

configurations. In this model, the particles are initially randomly positioned in a centre region instead of the entire dimension of the packing space. As the particles are subsequently moved to reduce the overlap, the packing explodes into the unoccupied regions. This moving process of particles is repeated and is terminated when the overlap value drops below a specified value.

The packing density obtained by collective generation and relocation models is highly dependent on the iteration times and the shrinking scale at each time. A packing density of 0.64 of equal spheres was obtained by Clarke and Wiley, 0.642 by Jodrey and Tory and 0.509 to 0.638 by Nolan and Kavanagh. It is a characteristic of these models that the contact number between particles is very small. Most adjacent particles are separated or overlapped slightly (third or forth of the magnitude of a particle radius). Therefore in the counting of contact number a small tolerance is given, and if the gap between two adjacent particles is less than this tolerance, they are taken as contact pair. By such definition, the average contact number was 6 by Jodrey and Tory, and 4.4 to 5.9 by Nolan and Kavanagh.

In comparison with sequential packing models, collective models cost more computer time due to the large number of iterations. As the computer process speed is continuously increasing, the cost of computer time is not an very important factor to be considered. In sequential packing models, both the particle positions and all the possible sites that a new particle could be added to should be stored each time. When a new particle is added to the cluster, the sites that overlap with the new particle should be deleted and the new sites should be calculated and stored again and these models take more computer memories. In the collective generation models, only the particle positions are memorised by the computer.

In practice the particle sizes are distributed, (such as the particles of the solder powder and the ceramic powder). However, most of the models of both sequential and collective models are only applicable for the random packing of equal particles. Very few models (Konakava *et al,* 1990; Nolan *et al,* 1993) have been applied for the random packing of particles with

log-normal distributions. A novel computer simulation model for the random packing of distributed particles has been developed in this work. The following section presents this simulation model.

5.3 A new simulation model for the random packing of solder particles and the micro-structure of solder paste

Using the model developed as part of this work, the random packing of spherical particles with any size distributions can be simulated. Then the particles are separated to simulate the micro-structure of dense suspensions of different solid volume fraction. The algorithm of this model is composed of three main elementss: particle size and initial position generation, overlap relaxation, and particle separation.

5.3.1 The generation of the particle sizes and their initial positions

Different methods can be applied for particle size generation. The following three methods are applicable for generation of particles with unknown theoretical distribution, normal distribution and log-normal distribution respectively.

A. Generation of particles without theoretical distribution function

The particle size distribution of solder powder has been introduced in *Chapter two*. Solder pastes made by different manufacturers have different particle size distributions (Mannan et al, 1995). In some cases, no suitable theoretical density functions can be used to represent the particle size distributions. The following technique can be used on the computer to generate the particle sizes. First linear and/or polynomial functions are employed to represent the probability accumulation function of the particle size, as shown in Figure 5.9. Then a series of random numbers (x_1, x_2, ..., x_N) which obey the uniform distribution over (0, 1) are generated by the random function. For each of these random numbers, say x_i,, a corresponding particle size, r_i, can be obtained from the probability

accumulation function, see Figure 5.9. The particle sizes (r_1, r_2, ..., r_N) generated by this method will obey the real particle size distribution.

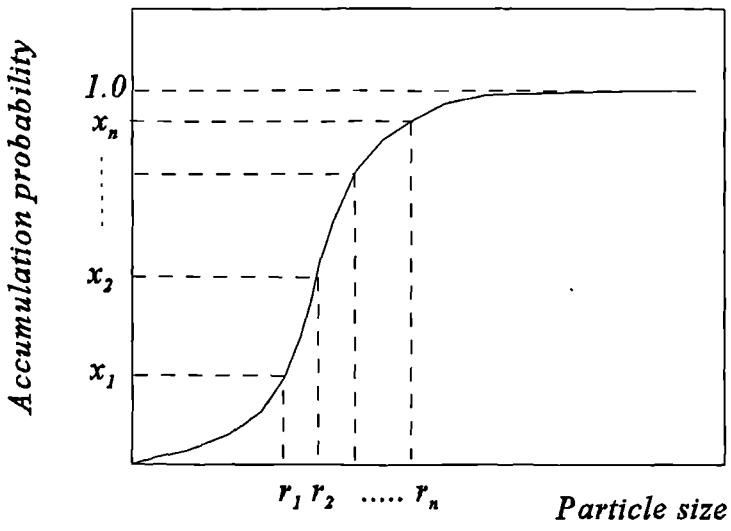

Figure 5.9 The generation of particle size from the accumulation probability.

B. Generation of particles with normal distributions

In nature and industries, normal distributions are frequently used to represent the distribution of many random variables. For example, if solder powders, coming from the same bath, are processed by two sieves of different sizes, then the particles remained between the two sieves could be approximated to a normal distribution. If a random variable, *s*, follows a normal distribution, then the probability density function is represented by:

$$f(s) = \frac{1}{\sqrt{2\pi}\ \sigma} e^{\frac{-(s-\bar{s})^2}{2\sigma^2}} \qquad (5.8)$$

where $\bar{s}$ is the mathematic expectation and σ is the standard deviation of variable s. The following equations can be employed to convert random numbers, x_{01} and x_{02}, that obey uniform distribution over (0, 1) to random number, x_1 and x_2, that obey standard normal distribution:

$$\begin{aligned} x_1 &= \sin(2\pi x_{01}) \left(-2\ln x_{02} \right)^{\frac{1}{2}} \\ x_2 &= \cos(2\pi x_{02}) \left(-2\ln x_{01} \right)^{\frac{1}{2}} \end{aligned} \tag{5.9}$$

Then x_1 and x_2 can be transferred to r_1 and r_2 which obey the ($E(r)$, σ^2) normal distribution by the equations:

$$\begin{aligned} r_1 &= E(r) + \sigma x_1 \\ r_2 &= E(r) + \sigma x_2 \end{aligned} \tag{5.10}$$

where $E(r)$ is mean value and σ is the standard deviation of the random variable r. By the above method three thousand random numbers are generated which obey the $(1, 0.2^2)$ normal distribution. Figure 5.10 is the comparison of the theoretical density function, Eq. (5.8), with that generated by the above method. It can be seen that the particle size distribution generated by computer simulation agrees with the theoretical distribution.Tests also show that the minimal random number is 0.226 and the maximum one is 1.760.

C. Generation of particles with log-normal distributions

The log-normal distribution is another important function to approximate the particle size distributions, such as ceramic and metal powders, paint material and soil particles (Rumpf, 1990). A log-normal distribution is defined as: if r is a random variable and its natural logarithm, $t = ln(r)$, obeys normal distribution, then r obeys log-normal distribution. The density function of log-normal distribution can be derived as following. If t obeys the ($\bar{t}$, σ_t^2) normal distribution and its density function is:

$$f(t) = \frac{1}{\sqrt{2\pi}\ \sigma_t} e^{\frac{-(t-\bar{t})^2}{2\sigma_t^2}} \tag{5.11}$$

t is a function of r, here $t = \ln(r)$, then the density function of r is:

$$f(r) = f(t)\frac{dt}{dr} = \frac{1}{\sqrt{2\pi}\sigma_t\, r} e^{\frac{-(\ln r-\bar{t})^2}{2\sigma_t^2}} \tag{5.12}$$

It is noted that $\bar{t}$ and σ_t are the mean value and standard deviation respectively of t not of r. The mean value and the standard deviation of r can be calculated from the following equations:

$$\bar{r} = \int_0^\infty r\, f(r)\, dr \tag{5.13}$$

and

$$\sigma_r = \sqrt{\int_0^\infty r^2 f(r)\, dr - \bar{r}^2} \tag{5.14}$$

Konakava et al (1990) defined the log-normal density function of particle radius, r, as:

$$f(r) = \frac{1}{\ln(\sigma_g)\sqrt{2\pi}} e^{\frac{-(\ln r-\ln \bar{r})^2}{2\ln^2(\sigma_g)}} \tag{5.15}$$

where σ_g is the standard deviation and $\bar{r}$ is the mean value of the particle radii. It is known that for a random variable, the integral of its density function over its definition interval should be equal to one. Tests of numerical integral of Eq. (5.15) from 0 to ∞ found that the result is not equal to one but is varied depending on the values of σ_g and $\ln\bar{r}$. Therefore, Eq. (5.15) is not the correct density function of r. Tests were also conducted on Eq. (5.12) and the result shows that the integral is equal to one no matter how the values of σ_t and $\bar{t}$

are changed. So it is believed that Eq. (5.12) is the correct form of the density function of log-normal distribution. The random numbers that obey a log-normal distribution can generated by the following steps. First Eq. (5.9) and Eq. (5.10) are employed to generate two random numbers, t_1 and t_2, which obey ($\bar{t}$, σ_t^2) normal distribution. Then t_1 and t_2 are converted to random numbers, r_1 and r_2 that obey log-normal distribution, by following equation:

$$\begin{aligned} r_1 &= e^{t_1} \\ r_2 &= e^{t_2} \end{aligned} \tag{5.16}$$

By this method three thousand random numbers were generated with mean value of one and standard deviation of 0.25. Figure 5.11 is the comparison of theoretical log-normal density function with that generated by the above method. It can be seen that the frequency density of the generated random numbers agrees well with the log-normal density function.

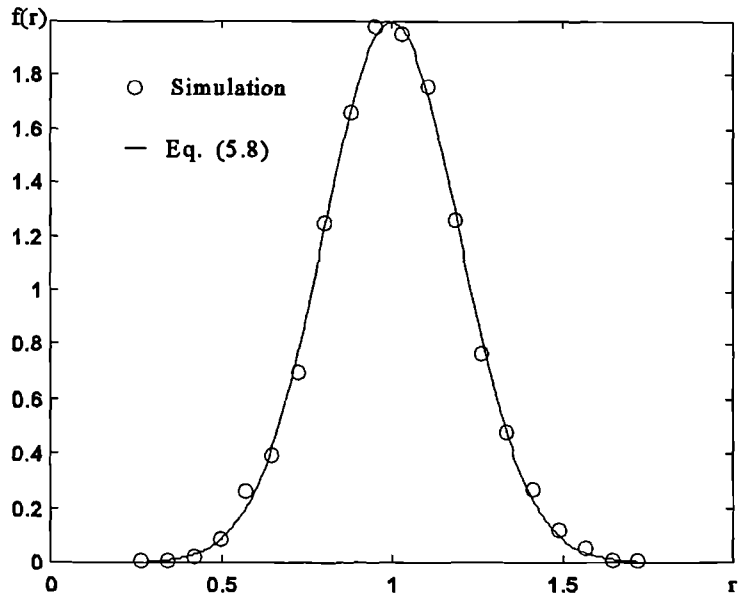

Figure 5.10 Comparison of simulation result with theoretical normal distribution.

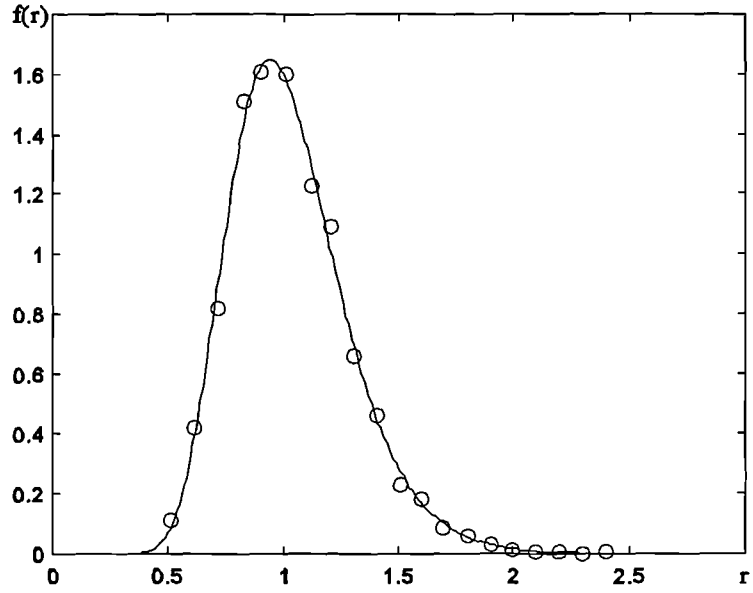

Figure 5.11 Comparison of simulation result with theoretical log-normal distribution.

Three methods for the generation of random numbers have been introduced above. Once the density function or the measured accumulation probability of particle sizes of a solder paste is known, one of the three methods can be used to generate the particle radii (r_1, r_2, r_3, ..., r_i, ..., r_N) on the computer. The subscript N is the total number of particles.

The initial particle positions can be generated by random numbers with uniform distributions. For example, if the particles are packed inside a cuboidal container with length L, width W and height H, then the initial particle positions are decided by the following equations:

$$\begin{aligned} x_i &= L\, R_{x,i} \\ y_i &= W\, R_{y,i} \qquad\qquad i = 1, 2, \ldots, N \\ Z_i &= H\, R_{z,i} \end{aligned} \tag{5.17}$$

where $R_{x,i}$, $R_{y,i}$ and $R_{z,i}$ are random numbers obeying uniform distribution over (0, 1). If

the particles are randomly packed inside a cubical container then $L = W = H$. The initial packing density is:

$$\rho_I = \frac{1}{L\ W\ H} \sum_{i=1}^{N} \frac{4}{3}\ \pi\ r_i^3 \tag{5.18}$$

In this work, the value of 0.8 is accepted as the initial packing density.

5.3.2 The relocation of particle positions - the relaxation algorithm

After the generation of particles and their initial positions, there are many overlaps between neighbour particles. The following unique relaxation methods are used to reduce or eliminate the overlaps.

A. Particle relocation

For each particle, particle i for example, first the judgement is made that if the distance between particle i and one of its adjacent particles, particle j, is smaller than the sum of the radii of the two particles that is if $l_{ij} < r_i + r_j$, where l_{ij} is centre to centre distance between particle i and j, then particle j overlaps particle i. The ratio, $(l_{ij} - r_i - r_j)/r_i$, is defined as the relative overlap value. By such judgements all the particles that overlap particle i can be identified. Second, if particle i is overlapped by n_i neighbouring particles, then from the centre of one of these particles, a new position can be decided by following equations:

$$\begin{aligned} x_{ij} &= x_j + (r_i + r_j)*\cos\ \phi_{ij}\ \cos\ \theta_{ij} \\ y_{ij} &= y_j + (r_i + r_j)*\cos\ \phi_{ij}\ \sin\ \theta_{ij} \\ z_{ij} &= z_j + (r_i + r_j)*\sin\ \phi_{ij} \end{aligned} \tag{5.19}$$

ϕ_{ij} and θ_{ij} are shown in Figure 5.12. Then if particle i is placed on this position, the overlap between particle i and particle j will be deleted. Finally the average coordinates of the n_i

new positions are taken as the new position of particle i, that is:

$$x_{i'} = \frac{1}{n_i} \sum_{j=1}^{n_i} x_{ij}$$
$$y_{i'} = \frac{1}{n_i} \sum_{j=1}^{n_i} y_{ij} \qquad (5.20)$$
$$z_{i'} = \frac{1}{n_i} \sum_{j=1}^{n_i} z_{ij}$$

Figure 5.13 shows the two dimensional case of the relocation of particle i.

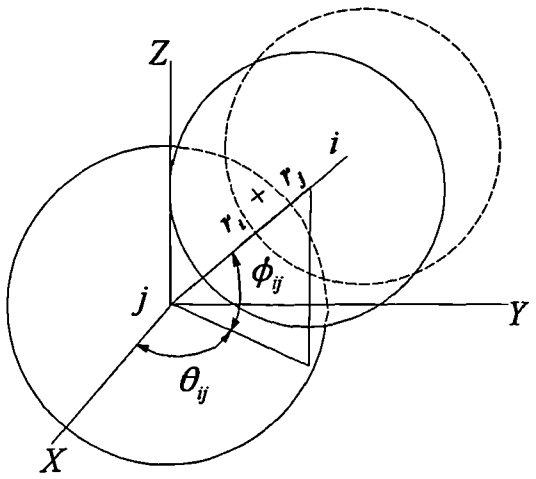

Figure 5.12 The new position of particle i respect to particle j.

This relaxation is applied to all of the particles. After one iteration each particle has been relocated once by the above relocation rule and the overlap rate decreases. This relocation step is repeatedly executed. Figure 5.14 shows a two dimensional case, in which ***a*** is the initially generated positions of three hundred particles and ***b*** is the relocation after fifty iterations. The mean radius of the particles is 1.0 and the standard deviation is 0.2. Comparison of Figure 5.14 ***a*** with ***b*** shows that the initially generated particles are highly overlapped with each other, and after fifty iterations the overlaps are significantly reduced.

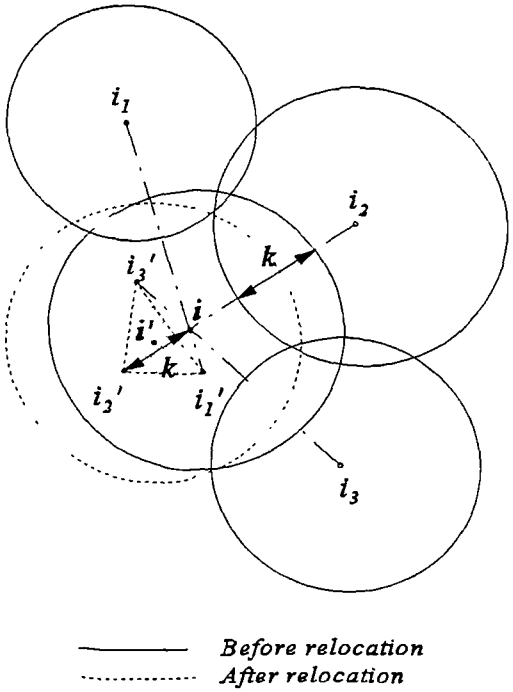

Figure 5.13 The relocation of particle *i*.

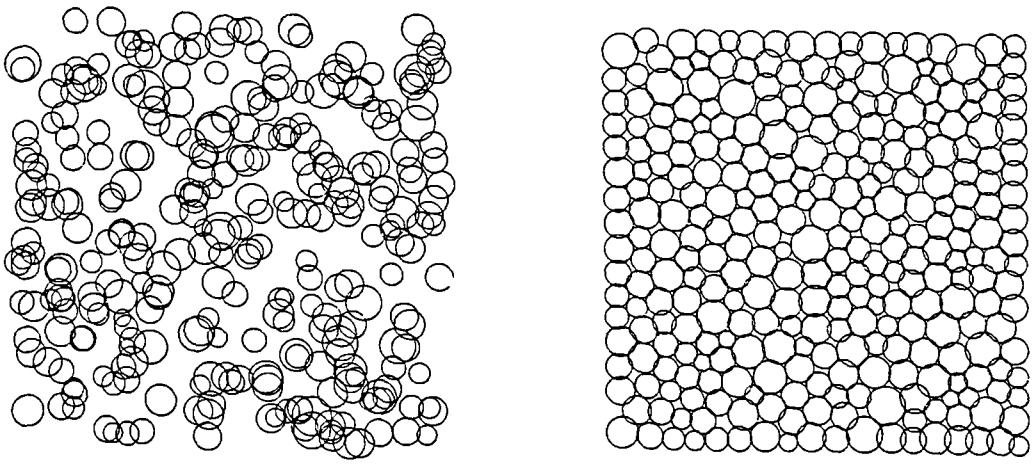

Initially generated positions — New positions after 50 iterations

a — ***b***

Figure 5.14 Relocation of particles and overlap relaxations.

To accelerate the reduction of the overlap rate and to avoid the formation of bridges between neighbour particles in the packing, the following two methods are used. The first one is the disturbance of particles. After a few given interactions, each particle is 'vibrated' around its present position by giving a very small disturbance. The disturbance is generated by the following equations:

$$\begin{aligned} x_{i'} &= x_i \pm dx\ R_{xi} \\ y_{i'} &= y_i \pm dy\ R_{yi} \\ z_{i'} &= z_i \pm dz\ R_{zi} \end{aligned} \qquad i = 1,2,\ldots, N \qquad (5.21)$$

where R_{xi}, R_{yi} and R_{zi} are random numbers that obey uniform distribution over (0, 1); dx, dy and dz are the disturbing moduli which gradually decreases as the simulation progresses; the sign, ±, indicates that the disturbance takes 0.5 probability to be positive and 0.5 probability to be negative. By Eq. (5.21) each particle has the equal opportunity to be disturbed in any direction from its present position.

The second method is the random sequential process. The above relocation process is carried out from particle i through particle n. If this relocation process is always in the same sequence, the random characteristics of the packing may be affected. Therefore, after the vibration of particles, the sequence of a new iteration is randomly rearranged by the following method. If the total number of particles is N, first N random numbers, q_1, q_2, ..., q_N, which obey uniform distribution over (0, 1) can be generated. Then comparison of the values of these numbers. If the value of the *ith* random number, q_i, is the minimum one, then particle i is placed in the first position in the new queue. If the q_j is the second minimum one, then particle j is placed in the second position in the new queue. By this comparison each particle is placed in a position according to the value of q. This new queue is taken as the relaxation sequence of the new iteration. For example, if there are ten particles, and the present sequence is (p_1, p_2, ..., p_{10}). Ten random numbers are sequentially generated as (0.32, 0.79, 0.21, 0.85, 0.03, 0.67, 0.28, 0.92, 0.13, 0.42). By the above method, the sequence of a new iteration can be rearranged as (p_5, p_9, p_3, p_7, p_1, p_{10}, p_6, p_2, p_8).

***B.* Examination of the relative overlap value**

After a number of iterations, the average relative overlap value and the overlap number gradually reduced to stable values and more relaxation interactions do not reduce the two values further. Then the average relative overlap value is compared with a threshold, $d\epsilon$. If the average relative overlap value falls bellow $d\epsilon$, then the data of particle radii and positions are saved to a data file, the contact number and the packing density are counted and the simulation is stopped. If the average relative overlap value is higher than $d\epsilon$, the simulation goes to the next step. In this work, 10^{-4} is accepted as the threshold, $d\epsilon$, which means that the average overlap value of the final random packing of particles is less than $10^{-4}r$.

***C.* Expansion of the packing space**

After the examination, if the average relative overlap value is still higher than the threshold, the random packing cannot be accepted as overlap free. See Figure 5.14 ***b***, a lot of particles are still overlap with each other at this stage. Then the packing space is expanded in three dimensions by the same expansion factor. For example, if the packing is within a cubic space, and its present size is L, then after expansion its new size will be $L' = \alpha_l L$. α_l is the expansion factor that is larger than one and its value is dependent on the present average relative overlap value. Then the simulation goes back to the particle relocation step. By repeating step ***A*** through step ***C***. An overlap free particle random packing can be finally obtained. It is found that by this simulation algorithm, if the initial packing density is taken to be 0.8, then after ten to twelve expansions the overlap free random packing can be achieved.

5.3.3 Generation of micro-structure of solder paste - particle separation

For a solder powder, the above simulation algorithm can be employed to obtain the random packing of drying solder particles. The following method is applied to separate the particles

from the random packing to simulate the micro-structure, the suspended positions of solder particles within the flux/vehicle system, of a solder paste of a given solid volume fraction.

If the random packing of N solder particles is generated within a cubic space, and the final size of the packing space is L, then the final packing density can be obtained by:

$$\rho = \frac{1}{L^3} \sum_{i=1}^{N} \frac{4}{3} \pi r_i^3 \tag{5.22}$$

If the solid volume fraction of a solder paste is known to be ϕ, which is smaller than the random packing density, ρ, then the size of the cubic space, L_s, occupied by the solder paste should be:

$$L_s = \left(\frac{1}{\phi} \sum_{i=1}^{N} \frac{4}{3} r_i^3 \right)^{\frac{1}{3}} \tag{5.23}$$

From Eq. (5.22) and Eq. (5.23) the ratio, S, of the size of the space occupied by the solder paste, L_s, to the size of the random packing space of drying solder particles, L, can be derived as:

$$S = \frac{L_s}{L} = \left(\frac{\rho}{\phi} \right)^{\frac{1}{3}} \tag{5.24}$$

This ratio, S, is defined as the separation factor. The solder particles of the random packing can be separated from each other by two steps. The first one is the separation step, which separates the particles by the following equations:

$$\begin{aligned} x_{si} &= S\, x_i \\ y_{si} &= S\, y_i \qquad i = 1,2,\ldots, N \\ z_{si} &= S\, z_i \end{aligned} \tag{5.25}$$

where $(x_i\ y_i\ z_i)$ are the centre coordinates of particle i in the random packing, and $(x_{si}\ y_{si}\ z_{si})$ are the coordinates of particle i after separation. The second one is the disturbing step,

by which each separated particle is disturbed a random distance in a random direction. As shown in Figure 5.15, the disturbing equations are:

$$\begin{aligned} \delta x_i &= \delta l_i \cos \theta_{i2} \cos \theta_{i1} \\ \delta y_i &= \delta l_i \cos \theta_{i2} \sin \theta_{i1} \qquad i = 1, 2, \ldots, N \\ \delta z_i &= \delta l_i \sin \theta_{i2} \end{aligned} \tag{5.26}$$

where δl_i is the disturbing distance and θ_{1i} and θ_{2i} determine the disturbing direction. δl_i is given by:

$$\delta l_i = \beta_i r_i (S - 1) \qquad i = 1, 2, \ldots, N \tag{5.27}$$

where β_i obeys uniform distribution over (0, 0.9). The selection of 0.9 as the upper terminal of β_i ensures that, after disturbance, the particles are still separated from each other without contact or overlap. In Eq. (5.26) θ_{1i} obeys uniform distribution over (0, 2π), and θ_{2i} is determined by:

$$\theta_{2i} = \pm \frac{\pi}{2} \gamma_i^{\sqrt{3}} \qquad i = 1, 2, \ldots, N \tag{5.28}$$

where γ_i obeys uniform distribution over (0, 1), and the sign, ±, gives θ_{2i} the probability of 0.5 to be positive or negative. Therefore, the distribution interval of θ_{2i} is ($-\pi/2$, $\pi/2$). θ_{1i} and θ_{2i} give particle i the equal opportunity to be disturbed in any direction. After the disturbing step the micro-structure of a solder paste is finally obtained.

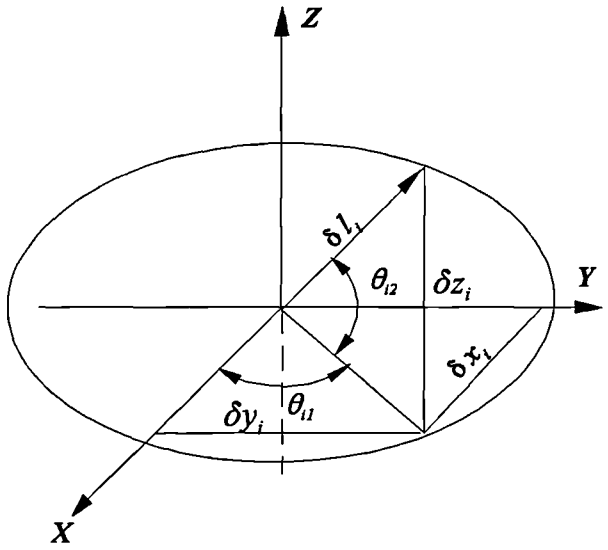

Figure 5.15 The disturbing distance and direction of particle *i*.

5.3.4 Effect of particle number on packing density and the isostatic packing test

Simulation results show that the packing density is affected by the number of particles, that is the fewer the particles the lower the packing density. As the number of particles increases to a sufficiently large value, the packing density approaches a stable value. Taking equal particles for example, Figure 5.16 shows the relationship of the packing density and the particle number, from which it is seen that as the particles are more than two thousands the packing density approaches a stable value. Because the particles at the packing surface have fewer neighbours than those particles inside the packing bulk, when counting the average contact number, the particles at the packing surface should not be taken into account. In this work, to obtain reliable statistical results, three thousand particles are employed in each simulation.

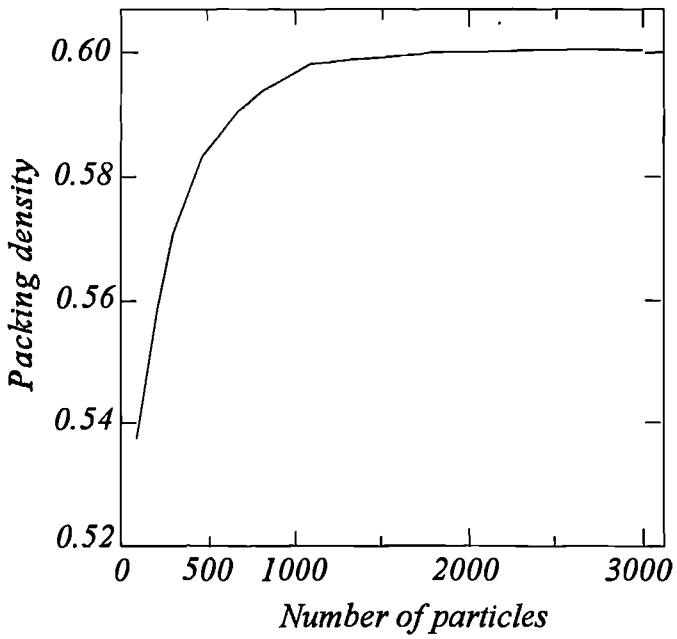

Figure 5.16 The influence of particle number on the packing density.

The distribution of particle positions can be examined by a hypothetic test, which shows that the random packing obtained by this algorithm is highly isostatic. The following example shows the steps of the hypothetic test. For the random packing of three thousand particles within a cubic space, first the central region of the packing space was divided into eight sub-cubic spaces with equal volume. Then the number of particles in each sub-cubic space was counted which gave the results as (246, 241, 259, 243, 247, 253, 243, 252). The hypothesis of uniform distribution of particle positions was examined by the χ^2 hypothetic test method. The test result showed that, with 95% confidence, the hypothesis was true. This hypothetic test confirmed that the random packing obtained by the above simulation algorithm is isostatic.

5.4 The simulation results and discussion

The simulation algorithm developed in this study was used for investigating the random packing of solder particles and the micro-structure of solder pastes. Each simulation involved three thousand particles, and for convenience, and to allow for comparison, the mean particle radius was taken as 1.0 in all of the simulation. With the normal distribution, the standard deviation of the particle radii was taken to be between 0.0 and 0.25, and for the log-normal distribution, the standard deviation was chosen to be between 0.15 and 0.45.

5.4.1 The random packing of solder particles

Figure 5.17 shows the three-dimensional view and the two dimensional cross-sectional view of a typical random packing of three thousand particles within a cubic space obtained by this simulation algorithm. The particle sizes obey a normal distribution, the mean radius is 1.0 and the standard deviation is 0.15. Table 5.1 gives the statistical data generated from one simulation.

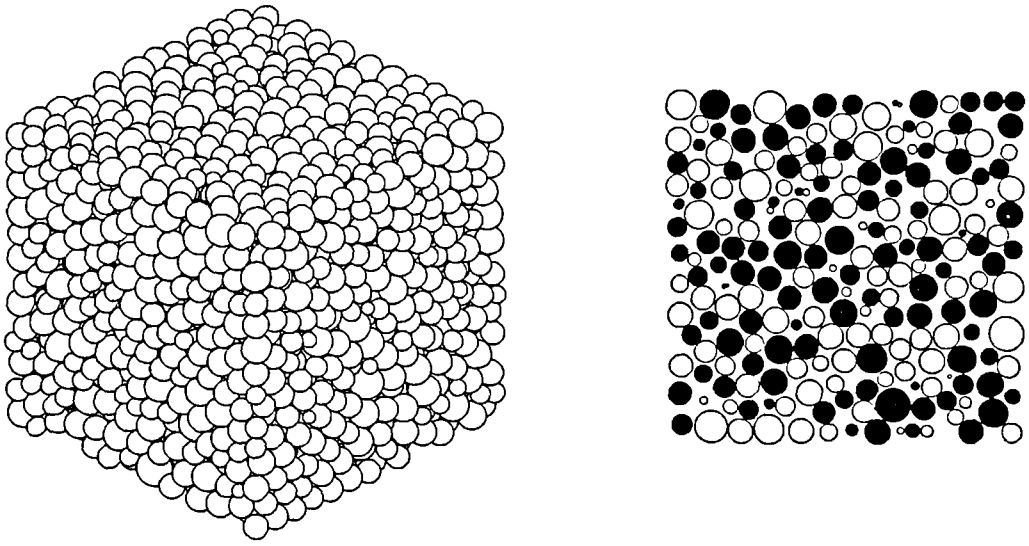

Figure 5.17 Two and three-dimensional views of particle random packing.

Table 5.1 Statistical data of simulation results.

Particle Number = 3000 Mean radius = 1.000 Standard deviation = 0.15 Packing density = 0.6093 Mean contact number = 5.9333			
Particle size	Frequency	Contact number	Frequency
0.51556 ~ 0.60657	10	3	80
0.60657 ~ 0.69759	55	4	176
0.69759 ~ 0.78860	161	5	311
0.78860 ~ 0.87962	446	6	279
0.87962 ~ 0.97064	667	7	233
0.97064 ~ 1.06165	711	8	129
1.06165 ~ 1.15267	513	9	62
1.15267 ~ 1.24368	291	10	21
1.24368 ~ 1.33470	105	11	13
1.33470 ~ 1.42572	33	12	1
1.42572 ~ 1.51673	8	13	1

A. The packing density

The packing density, defined by Eq. (5.22) for a cubic container, is one of the most important characteristics of random packing. As was introduced in section **5.1**, there are two types of random packing of particles: the random loose packing and the random close packing. The packing density of equal particles obtained by this simulation algorithm is 0.602 which is in excellent agreement with the widely accepted random loose packing density, 0.60. Therefore, we can say that this simulation algorithm is applicable for the random loose packing of spherical particles.

It has been demonstrated in many studies (Konakava and Ishizaki, 1990; Shapiro and Probstein, 1992; Nolan and Kavanagh, 1994) that the random packing density increases

with the dispersion (the standard deviation) of particle sizes. Figure 5.18 shows the relationship between the packing density and the standard deviation of particle radii obtained in this work. The main reason why the packing density increases with the standard deviation of particle radii is because, with high standard deviation, the small particles can fill the voids between the larger particles. Figure 5.18 also suggests that, with the same standard deviation, the packing density of log-normal distributed particles is slightly higher than that of normally distributed particles. For a random number that obeys the normal distribution (E(r), σ^2), the probability that it is greater than E(r)+3σ or it is smaller than E(r)-3σ is only about 0.0014. Therefore, for the three thousand particles used in the simulation, it is expected that more than 2990 particles should fall into the interval between E(r) - 3σ and E(r) + 3σ. In contrast, for log-normal distribution, the probability that a random number is greater than E(r) + 3σ is about 0.009, which means that about 30 particles are expected to be greater than E(r) + 3σ. The existence of certain large particles may induces the increase of the random packing density. The existence of large particles can be seen from the density function of the log-normal distribution (Figure 5.11).

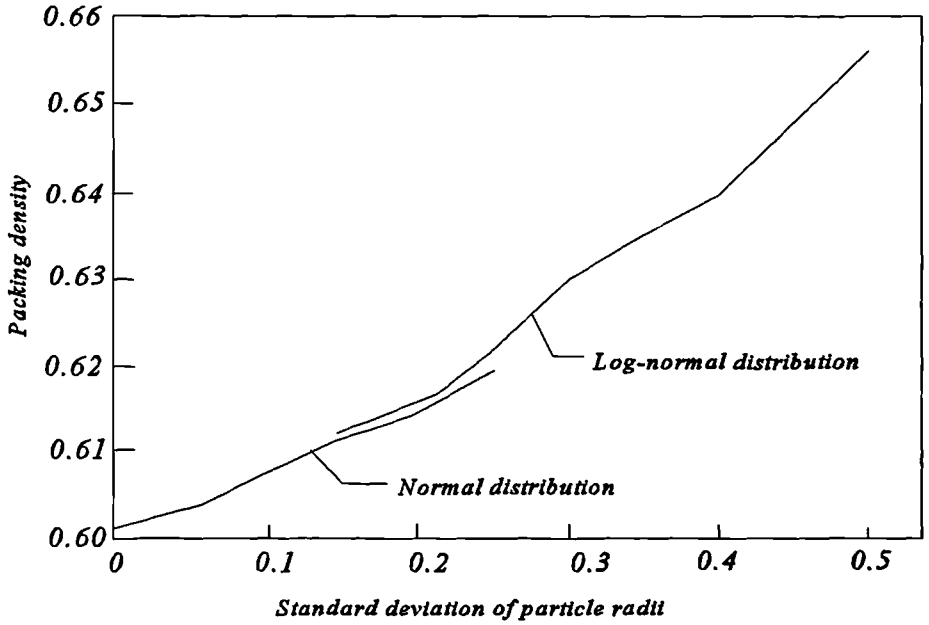

Figure 5.18 The relationship between packing density and particle size dispersion.

B. The contact number

As was stated previously in section **5.3**, in the random packing obtained by the new simulation algorithm, the neighbouring particles are either separated by very small gaps or overlap slightly by less than $10^{-4}r$. In counting the contact number, if the gap between two adjacent particles is smaller than $10^{-2}r$, the two particles are considered to be in contact with each other. Simulation results show that the average contact number is also affected by the standard deviation of particle radii. Figure 5.19 shows the relationship between the standard deviation of particle radii and the average contact number. For equal particles the average contact number is 6.04 which is in very good agreement with Scott's experimental result. As the standard deviation increases the average contact number decreases. Figure 5.20 is the comparison of the contact number frequency of equal particles with that of normally distributed particles with standard deviation of 0.1. Figure 5.20 shows that for distributed particles the contact number has a wider range than that of equal particles.

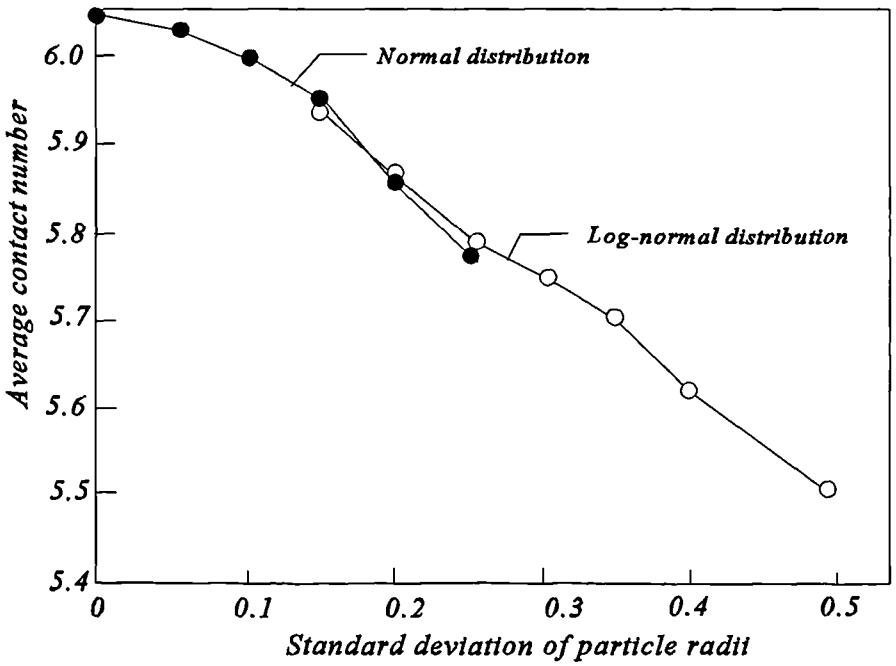

Figure 5.19 Average contact number vs standard deviation of particle radii.

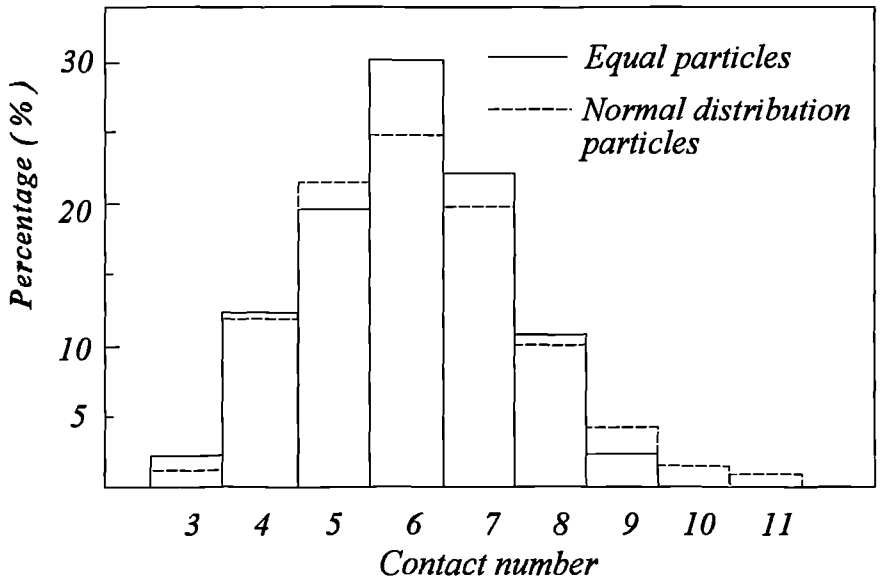

Figure 5.20 Percentage histogram of contact number.

The results also show that, for the random packing of distributed particles the contact number of large particles is higher than the contact number of small particles. To examine this trend, the average radius of the particles with the same contact number is calculated. Figure 5.21 shows this relationship.

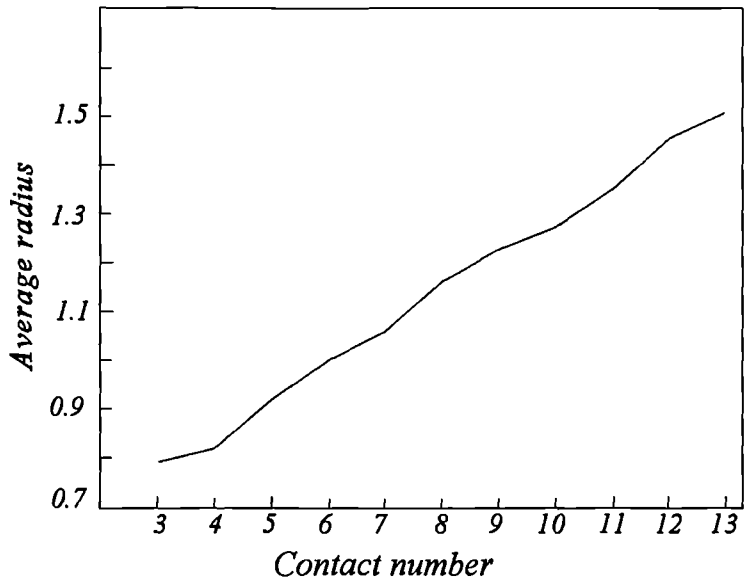

Figure 5.21 The relationship between contact number and average particle radius.

5.4.2 The micro-structure of dense suspensions

For a dense suspension of spherical particles with a given solid volume fraction, Eq. (5.24) through Eq. (5.28) are applied to separate the particles from the random packing to simulate the micro-structure. Figure 5.22 shows the three-dimensional view and the two-dimensional central-cross section view of the micro-structure of a dense suspension. It is obtained from the random packing, as shown in Figure 5.17, and the solid volume fraction is 0.5, the solid volume fraction of solder pastes used for stencil printing.

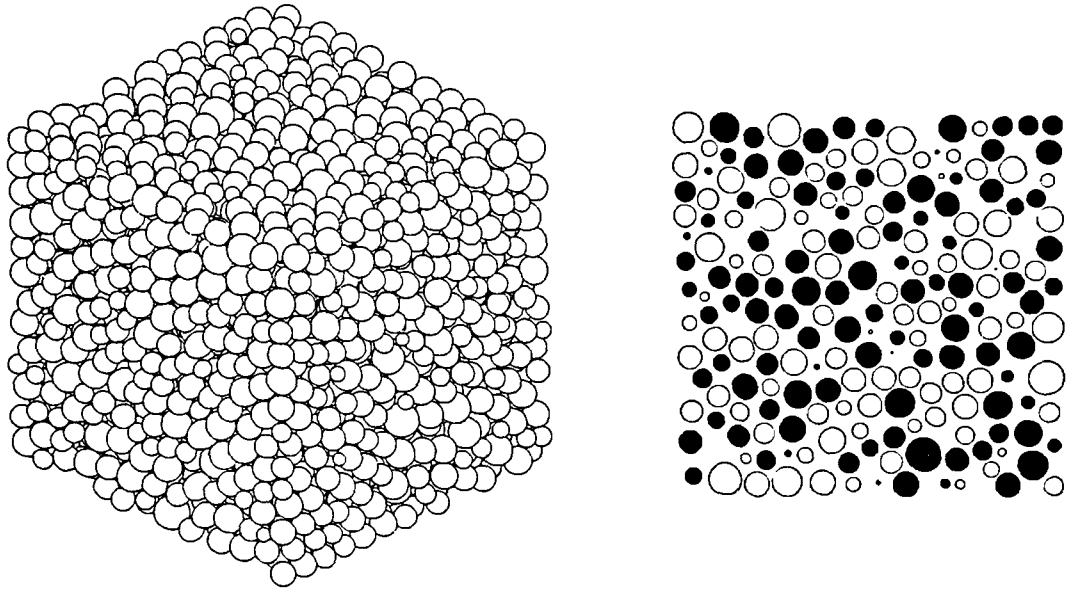

Figure 5.22 The micro-structure of a dense suspension of 0.5 solid volume fraction.

Two parameters, neighbour number and the average gap between neighbour particles, are used to characterize the micro-structure of a dense suspension. In the following analysis, if the gap between two particles is smaller than 0.3 times the average particle radius, then the two particles are taken as neighbour particles. If particle i is surrounded by N_i particles, then the neighbour number of particle i is N_i.

To comparing the effects of particle size distributions on the micro-structure of dense suspensions, the solid volume fractions of the dense suspensions with different particle size distributions are all equal to 0.5. Again the mean value of particle radii is one unit.

A. The neighbour number

Figure 5.23 shows the effect of particle size distribution on the average neighbour number. Comparing Figure 5.23 with Figure 5.19 it can be seen that the relationship between average neighbour number and standard deviation is similar to the relationship between the average contact number and standard deviation. However, the average neighbour number of the particles with low standard deviation is higher than the average contact number. For example, the average neighbour number of equal particles is above seven, while the average contact number is about six. The average number of the particles with high standard deviation is nearly equal to the average contact number. This is because that the random packing density of particles with low standard deviation is lower than the random packing density of particles with high standard deviation. For example, the packing density of equal particles is 0.603 while the packing density of particles, with standard deviation of 0.477, is about 0.65. To obtain the same solid volume fraction of 0.5, the separation factor for packing density of 0.603 is 1.06, calculated by Eq. (5.24), while the separation factor for packing density of 0.65 is 1.091. For low standard deviation, after separation there should be some neighbour particle pairs with gaps less than 0.3 although they did not contact each other before separation. For particles of high standard deviation, due to the high separation factor, the gaps between some large particles may be greater than 0.3 although they contacted each other before separation, while the gaps between some small particles may be smaller than 0.3 although they did not contact each other before separation. As a comprehensive result, the average neighbour number of a dense suspension of particles with high standard deviation is very near to the average contact number of the random packing.

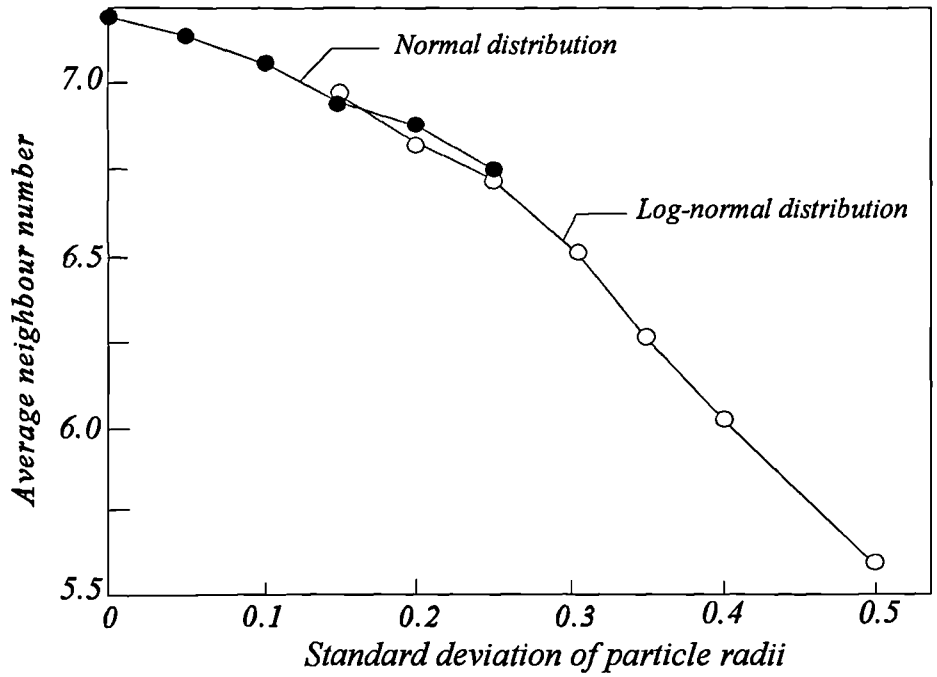

Figure 5.23 The average neighbour number vs particle standard deviation.

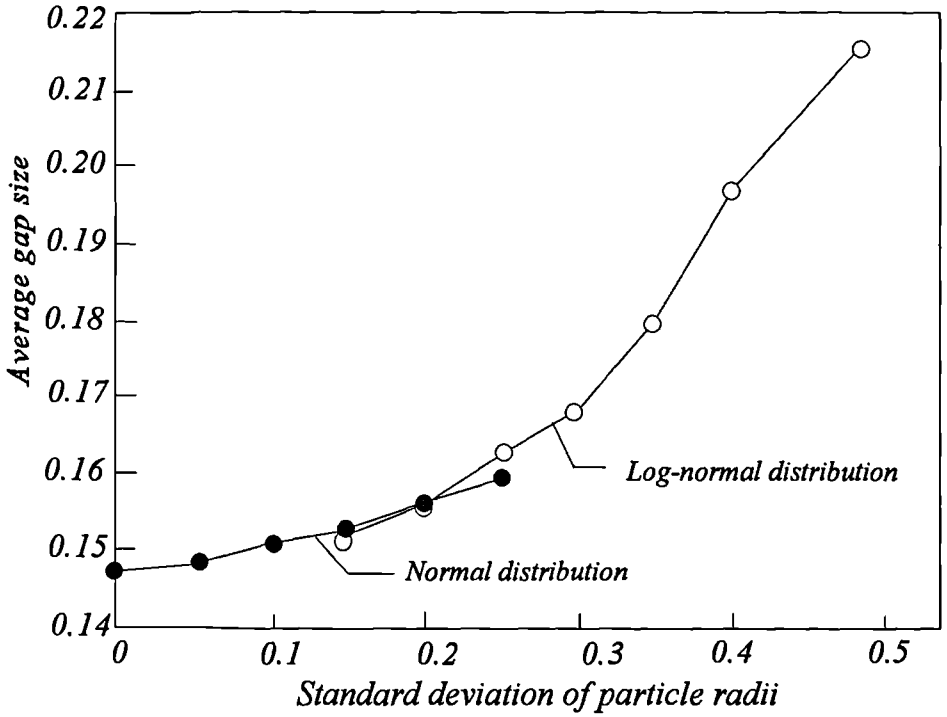

Figure 5.24 Average gap size between neighbour particles vs particle standard deviation.

B The average gap size

The average gap size between neighbour particles is another important parameter of a dense suspension. It affects the hydrodynamic interaction between neighbour particles, so the rheology of the dense suspension. Figure 5.24 shows the effect of particle size distribution on the gap size. It can be observed that, with the same solid volume fraction, 0.5, the average gap size between neighbour particles increases with the standard deviation of particle radii. Again this is because, for particles of high standard deviation, the separation factor, *S*, is larger than that of small standard deviation. As the standard deviation increases from zero (equal particles) to 0.477, the average gap size increases from 0.147 to about 0.215.

It should be mentioned that both the average neighbour number and the average gap size are counted using the definition, if the gap between two adjacent particles is smaller than 0.3 times of the mean value of the particle radii, then the two particles are considered neighbour particles. If the definition of gap increases, both the average neighbour number and the average gap size will increase too. However, this does not change the observation that, as the particle standard deviation increases the average neighbour number decreases and the average gap between neighbour particles increases.

5.5 Summary of chapter five

A novel simulation algorithm was introduced in this chapter. The first part of this algorithm was used to simulate the random loose packing of poly dispersed spherical particles. Then the second part of this algorithm was used to separate and disturb the particles of the random packing to simulate the micro-structure of a dense suspension of spherical particles. The random packing of dry solder particles and the micro-structure of solder paste, the distribution of solder particles in a flux/vehicle medium, were investigated by this simulation algorithm.

The packing density and the average contact number between neighbour particles are the two important parameters of random packing. Simulation results of the random packing of three thousand particles inside a cubic container showed that the packing density increases with the increase of the standard deviation of particle radii while the average contact number between neighbour particles decreases. This is attributed to small particles having the trend to fill into the voids among large particles for particles of high standard deviation.

The average gap between neighbour particles and the average neighbour number were used to characterize the micro-structure of the dense suspensions. Simulation results, with solid volume fraction of 0.5, showed that the average neighbour number decreases as the standard deviation of particle radii increases, while the average gap size increases. It may suggest that, in a dense suspension containing highly dispersed spherical particles, the small particles have many degrees of freedom to move in the liquid medium. It will be seen from the analysis of **Chapter six** that, the particle size distribution significantly influences the rheological properties of a dense suspension.

The algorithm developed in this study is applicable in the following fields: the simulation of powder compaction (He and Ekere, 1998), and the generation of solder particles packed inside cuboidal apertures. It may be also applicable for characterisation of anisotropic conductive adhesive used for SMT.

Chapter Six

The Effects of Particle Size Distributions on the Viscosity and on the Hydrodynamic Interaction between Particles in Solder Paste Flow

The effects of the particle size distributions on the random packing and on the micro-structure of dense suspensions were investigated in **Chapter five** using computer numerical simulation.

In this chapter, the effects of particle size distributions on the viscosity and on the particle interaction in dense suspension flow will be studied. Section **6.1**, presents viscosity models for dense suspensions and the model specially modified for the analysis of the effect of particle size distribution on the viscosity of non-colloidal dense suspensions, such as solder pastes. Section **6.2** covers the analysis of the hydrodynamic interaction between adjacent particles in dense suspension flow, and the effect of particle size distribution on the adjacent particle interaction. Section **6.3** gives a summary of the results of the study on effect of particle size distribution on viscosity and on the hydrodynamic interaction between particles in solder paste flow.

6.1 Effect of particle size distributions on the viscosity of dense suspensions

Viscosity is one of the most important rheological parameters of dense suspensions, such as solder paste. Manufacturing processes in which large volume of dense suspensions are handled, demand the understanding and control of the viscosity of the suspension. The application of solder paste for the reflow soldering assembly of printed circuit boards, and the transportation of various solid and liquid mixtures are typical examples of such processes. There are many reports in the literature on the study of the viscosity of suspensions. For convenience, viscosity is often represented by the relative viscosity, which

is the ratio of the viscosity of the suspension to the viscosity of the liquid medium.

6.1.1 Introduction of viscosity models of dense suspensions

Many viscosity models for dense suspensions have been developed either from theoretical analysis or from experimental results.

A. The analytical models

Early this century, Einstein (1911) studied the viscosity of infinitely dilute suspension. By classical analysis he derived that, a single isolated particle increases the viscosity of an infinitely dilute suspension as a simple function of the solid volume fraction, ϕ, of particles suspended in the liquid medium. According to Einstein, the relative viscosity of a dilute suspension can be written as:

$$\eta_r = \frac{\eta_s}{\eta_o} = (1 + 2.5 \phi) \qquad (6.1)$$

where η_r is the relative viscosity, η_s is suspension viscosity and η_o is the viscosity of the liquid medium. Einstein's model shows that the viscosity of dilute suspension is a linear function of the solid volume fraction of the particles. The differential form of Einstein's model gives:

$$d\eta_s = \eta_o \left(\frac{5}{2}\right) d\phi \qquad (6.2)$$

Following Einstein's work, attempts have been made to characterize dense suspensions and many viscosity models have been developed. In these models, the viscosities are expressed as functions of both the solid volume fraction and the maximum solid volume fraction of the suspended particles. Several of the most often used viscosity models are presented in this section. The first one is the Mooney's model (Ball et al, 1981):

$$\eta_r = \exp\left(\frac{5}{2}\,\frac{\phi}{1-\phi/\phi_m}\right) \tag{6.3}$$

where ϕ_m is the maximum solid volume fraction. The second model was developed by Krieger and Dougherty (1959) which gives the relative viscosity as:

$$\eta_r = \left(1 - \frac{\phi}{\phi_m}\right)^{-[\eta]\phi_m} \tag{6.4}$$

where $[\eta]$ is called the intrinsic relative viscosity of the suspension and its value ranges between 2.5 and 2.67 for rigid spheres depending on whether the particles are charged. The third one is the Maron-Pierce-Kitano model (1981) which gives the relative viscosity as:

$$\eta_r = \left(1 - \frac{\phi}{\phi_m}\right)^{-2} \tag{6.5}$$

Ball et al (1980) applied the average technique to modify Einstein's model. They assumed that the effect of all particles on the viscosity of a concentrated suspension is the sum of the effect of particles added to the suspension sequentially. By this assumption, they pointed out that Einstein's model can be modified in a differential form as:

$$d\eta_s = \eta_s \left(\frac{5}{2}\right) d\phi \tag{6.6}$$

It should be noted that, in Eq. (6.2) η_o is the viscosity of the liquid medium (constant), while in Eq. (6.6) η_s is the viscosity of the suspension (variable). Eq. (6.6) suggests that, if the present viscosity of a suspension is η_s, then further addition of a very small solid volume fraction, $d\phi$, of particles will induce a slight viscosity increment, $d\eta_s$. The final viscosity of the suspension is then obtained by integrating Eq. (6.6) which gives:

$$\eta_r = \frac{\eta_s}{\eta_o} = \exp\left(\frac{5}{2}\phi\right) \tag{6.7}$$

Ball et al also pointed out that the major limitation of Eq. (6.6) and Eq. (6.7) is that they omit the viscous effects resulting from the interactions between particles due to the finite

particle size. This means that, when a small volume of particles, $d\phi$, is added to a relatively concentrated suspension, it requires a space larger than $d\phi$ due to packing difficulties. When the solid volume fraction is increased by an amount $d\phi$, the particles that are already present in the suspension suffer a crowding effect. This crowding can cause a reduction in the available volume that can affect the change in viscosity by an amount proportional to (1 - $k\phi$), where k is called the crowding factor. Consequently, $d\phi$ in Eq. (6.6) is replaced with $d\phi/(1 - k\phi)$ to give:

$$(1 - k\phi)d\eta_s = \eta_s(\frac{5}{2})d\phi \qquad (6.8)$$

Integration of Eq. (6.8) gives:

$$\eta_r = \frac{\eta_s}{\eta_o} = (1 - k\phi)^{-\frac{5}{2k}} \qquad (6.9)$$

It should be noted that the initial condition of Eq. (6.7) and Eq. (6.9) is: $\phi = 0$, $\eta_s = \eta_o$. Comparing Eq. (6.9) with Eq. (6.4), it can be seen that, in Eq. (6.9), if 5/2 is replaced by $[\eta]$ and k is replaced by $1/\phi_m$, then Eq. (6.9) becomes the Krieger-Daugherty model.

After comparing the above viscosity models, Sudduth (1993) found that these models can be expressed in a common differential form. He rewrote Eq. (6.8) by giving an exponent to (1 - $k\phi$), then the common differential form is:

$$(1 - k\phi)^n d\eta_s = \eta_s(\frac{5}{2})d\phi \qquad (6.10)$$

If n equals one, the integration of Eq. (6.10) is the Krieger-Daugherty model. If n equals two and k equals $1/\phi_m$, the integration gives the Mooney's model, Eq. (6.3). If n equals zero, the integration becomes Arrhenius's model, Eq. (6.7). The Maron-Pierce-Kitano's model, Eq. (6.5), can also be derived from Eq. (6.10) by replacing 5/2 with $2/\phi_m$. Therefore, the above models can be placed in the same category.

Another class of analytical viscosity model were developed by Frankel et al (1967) and by Sengun et al (1989). Frankel et al applied an asymptotic technique to analyse the interaction between equal spherical particles in a high concentrated suspension. Then from the viscous dissipation of energy between adjacent particles they derived the relative viscosity as:

$$\eta_r = C[\frac{(\phi/\phi_m)^{\frac{1}{3}}}{1-(\phi/\phi_m)^{\frac{1}{3}}}] \tag{6.11}$$

where C is a constant of the magnitude of one unit dependent on the average neighbour number. By using a similar method as that used by Frankel et al, Sengun et al calculated the energy dissipated in a unit volume of suspension and the energy dissipated in a unit volume of pure liquid medium. Then the relative viscosity was defined as the ratio of the two energies:

$$\eta_r = 1+C_1\frac{3\pi}{8}\frac{\beta}{\beta+1}[\frac{3+4.5\beta+\beta^2}{\beta+1}-3(1+\frac{1}{\beta})\ln(\beta+1)]$$
$$\beta = \frac{(\phi/\phi_m)^{1/3}}{1-(\phi/\phi_m)^{1/3}} \tag{6.12}$$

where C_1 is also a constant of the magnitude of one unit.

B. Empirical models

Many experimental reports on the viscosity of dense suspensions can be found in the literature. An intensive review of the development in dense suspension rheology was made by Jomha et al (1991). They found that the experimental results obtained by different investigators have a significant spread. Eight points of the difficulties and complexities in the measurement of the viscosity of dense suspensions were summarised in this review.

Most of the empirical viscosity models were derived from experimental data by appropriate

extrapolation techniques. Thomas (1965) collected many experimental data from the literature. After careful examination, he noted that many of the experimental data could be expressed as a power series:

$$\eta_r = \frac{\eta_s}{\eta} = 1 + A_1\phi + A_2\phi^2 + A_3\phi^3 + \cdots + A_7\phi^7 \qquad (6.13)$$

where the constant A_1 is assumed to be 2.5 determined by Einstein's model for dilute suspension. By least squares analysis technique, Thomas obtained the values of the constants of Eq. (6.13), which were listed in his paper.

Sengun and Probstein (1989) compared their measurement of relative viscosity of styrene suspension in high shear rate with the data from other investigators, as shown in Figure 6.1. More experimental data can be found from Raffi et al' s paper (1992).

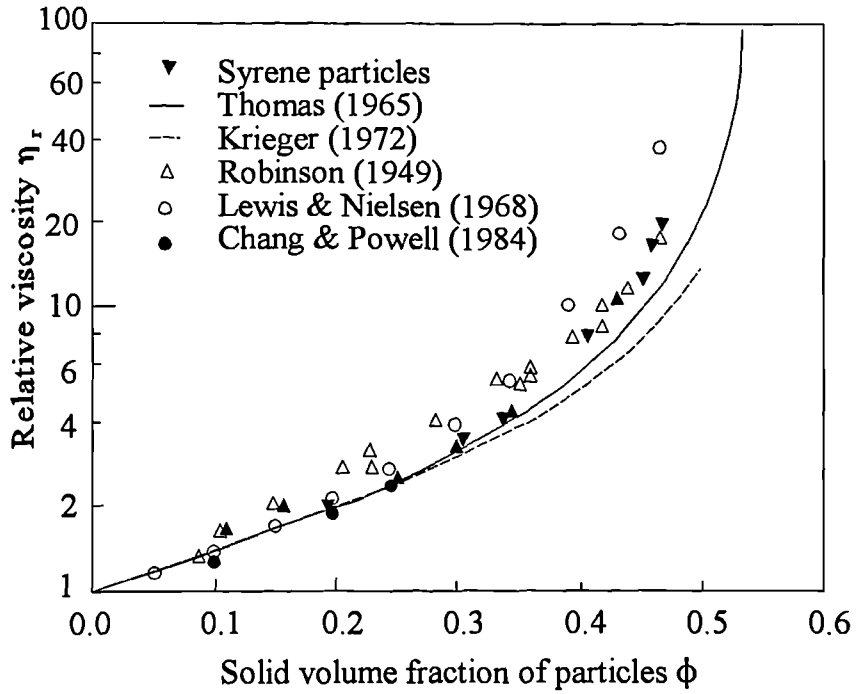

Figure 6.1 Relative viscosity vs solid volume fraction measured by different investigators.

C. The maximum solid volume fraction ϕ_m

It can be seen from most of the above models (Mooney model, Krieger and Daugherty model, Maron-Pierce-Kitano model, Frankel model and Sengun model) that, the viscosity of a dense suspension is not only dependent on the solid volume fraction, ϕ, it is also dependent on the maximum solid volume fraction, ϕ_m. Although ϕ_m does not appear in Eq. (6.13), it is incorporated into the constant. However, there is considerable variation of the value of ϕ_m in the literature. Taking equal spherical particles for example, ϕ_m is reported to range from 0.55 to 0.71 (Shapiro et al, 1992). It has been proved by many that, the close random packing density of equal spherical particles is about 0.633 (see **Chapter five**). Therefore, if equal particles are randomly suspended in a liquid medium, then the maximum solid volume fraction of the dense suspension must be smaller than the close random packing density. Higher values can be ascribed to greater degrees of ordering of the particles. Sudduth (1993) suggested that 0.602 would be the reasonable value of ϕ_m, which is the loose random packing density of equal particles. In Eq. (6.10) if k is replaced with ϕ_m, then as ϕ approaches ϕ_m, any further addition of particles can result in an infinite increase in the viscosity. As previously mentioned in **Chapter five**, the close random packing density, 0.633, was obtained by sufficient shaking of the container. Such a high solid volume fraction of particles cannot be obtained in a liquid medium. Therefore, in this work the loose random packing density is accepted as the maximum solid volume fraction of a dense suspension. Review of the experimental data published in the literature shows that the solid volume fraction of equal particles scarcely exceeds 0.60. This observation also suggests that the loose random packing density should be the suitable value of the maximum solid volume fraction of a dense suspension.

D. Comparison of viscosity models

As the loose random packing density is taken as the maximum solid volume fraction of the dense suspensions of equal spherical particles, then the viscosity models reviewed earlier above can be compared quantitatively. As shown in Figure 6.2, it can be seen that, if the solid volume fraction is lower than 0.3, the agreement among these models is reasonable.

However, as the solid volume fraction increases the disagreement among these models is significant. It should be noted that in Figure 6.2, the maximum solid volume fraction for Sengun model is 0.524, (see Shapiro et al, 1992), while 0.6 is taken as the maximum solid volume fraction in the other models.

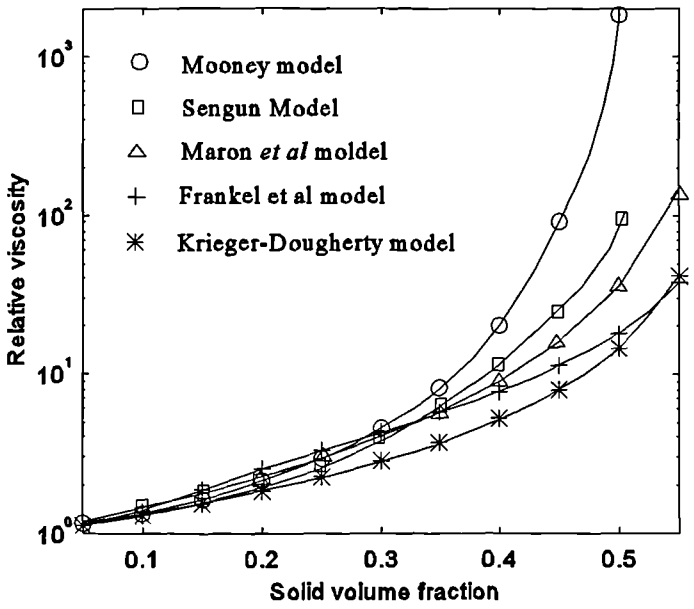

Figure 6.2 Comparison of viscosity models of suspension of equal particles.

6.1.2 A modified viscosity model

Figure 6.2 shows the high spread among different viscosity models at high solid volume fraction ($\phi > 0.3$). Recall that the Krieger-Daugherty model, the Mooney model and the Maron model were all derived from Eq. (6.10). The only difference is that, in Krieger-Daugherty model and Maron model the exponent, n, is 1.0, while in Mooney model the exponent is 2.0; and in Maron model the constant is $2/\phi_m$, while in Krieger-Daugherty model and Mooney model it is 5/2. The Frankel model is derived under the assumption that the particles are arranged in a regular pattern, such as cubic or hexahedral arrangement. Experimental observations show that, for a real dense suspension, such as solder paste, the

particles are arranged in a random order rather than in a regular pattern.

Recalling Eq. (6.10) again:

$$(1 - k\phi)^n \, d\eta_s = \eta_s(\frac{5}{2})d\phi \qquad (6.10)$$

Each term of this equation has its obvious physical meaning. However, restricting the exponent, n, to be an integer is unnecessary. The wide spread between Krieger-Daugherty model (n = 1) and Mooney model (n = 2) can be seen in Figure 6.2. In Eq. (6.10) if the exponent, n, is a real number and its value is varied between 1.0 and 2.0, then the integration form of Eq. (6.10), with condition: $\phi = 0$, $\eta_s = \eta$, becomes:

$$\eta_r = \frac{\eta_s}{\eta_0} = e^{\frac{5}{2k(n-1)}[(1-k\phi)^{-n+1} - 1]} \qquad 1< n \leq 2 \qquad (6.14a)$$

If k is replaced by $1/\phi_m$, then Eq. (6.14a) becomes:

$$\eta_r = \frac{\eta_s}{\eta_0} = e^{\frac{5\phi_m}{2(n-1)}[(1-\frac{\phi}{\phi_m})^{-n+1} - 1]} \qquad 1< n \leq 2 \qquad (6.14)$$

Eq. (6.14) is the modified viscosity model. If n = 2, it is the Mooney model, Eq.(6.3). Taking the maximum solid volume fraction to be 0.60, Figure 6.3 shows the effect of the value of n on the relative viscosity of dense suspensions of equal particles, in which the value of n is selected to be 2, 1.8, 1.6, 1.4 and 1.0 respectively.

Figure 6.3 shows that, By change of the value of the exponent, n, Eq. (6.14) can be applied to represent the relationship between relative viscosity and the solid volume fraction of suspensions. As the solid volume fraction, ϕ, increases the effect of the term $(1 - \phi/\phi_m)$ on the viscosity exponentially increases.

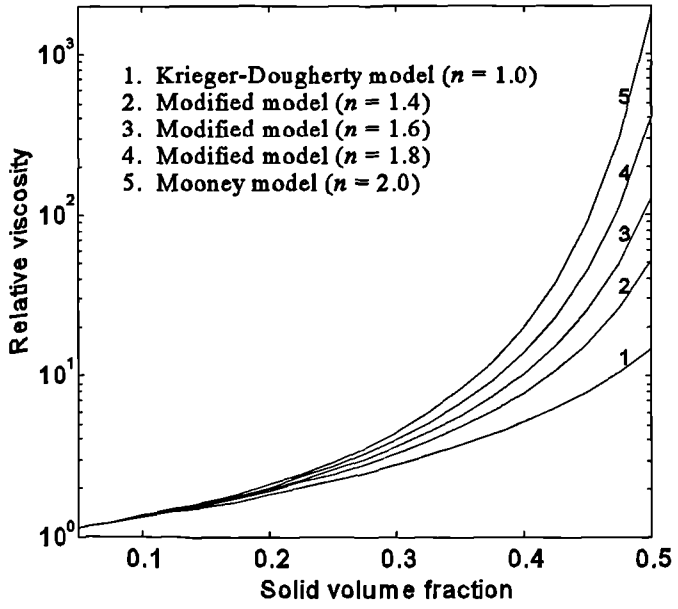

Figure 6.3 Comparison of the effect of n on the viscosity of dense suspensions.

6.1.3 The effect of particle size distribution on the viscosity of solder pastes

The viscosity models introduced in section **6.1.1** are only applicable for dense suspensions of equal spherical particles. In real life application, the industry always faces dense suspensions of unequal particles. It has also been found that, high solid volume fraction can be attained with a small increase in viscosity using a suspension that has a distribution of particle sizes rather than equal particles (Chang and Powell, 1994). It is therefore necessary to develop viscosity models which are suitable for dense suspensions with poly dispersed particles where the main difficulty is the determination of the maximum solid volume fraction (ϕ_m).

A. The viscosity of bimodal suspensions

A few studies of the viscosity of bimodal suspensions have been reported. Chong et al (1971) measured the flow rate and pressure drop of bimodal suspensions, which were

driven through an abrupt contracted orifice, and calculated the viscosity. In their study, two parameters, the diameter ratio of large to small particles, λ, and the volume fraction of small particles, $\xi\phi$, were identified as important factors to characterize bimodal suspensions. By fixing ξ to be 0.25, their experimental result showed that at a fixed ϕ, the viscosity decreased as λ increased from 1 to 7.5. They also suggested that there exists an optimum value of ξ as λ and ϕ are fixed at which the suspension viscosity is minimized. The experimental data were adequately represented by:

$$\eta_r = [\ 1 + 0.75\frac{\phi/\phi_m}{1 - \phi/\phi_m}\ ]^2 \qquad (6.15)$$

The value of ϕ_m was determined empirically in their experiment.

Storms et al (1990) measured the low shear rate viscosity of suspensions of bimodal polymethyl methacrylate beads. They proposed an expression for the relative viscosity as:

$$\eta_r = (\ 1 + \frac{R\phi}{1 - \phi/\phi_m}\ )^{3.3\phi_m} \qquad (6.16)$$

where R is varied from 0.7 to 1.25 depending on λ and ξ; ϕ_m is determined from a series of algebraic expressions that is also dependent upon λ and ξ.

Shapiro et al (1992) studied the viscosity of dense suspensions of bimodal spheres by Couette viscometer measurements. They employed the model developed by Sengun et al, Eq. (6.12), to fit their data. They found that, for bimodal particles, if the aspect ratio is not too far from one unit, the model is shown to correlate well with measurements made over a wide range of solid volume fractions, though this model was developed for equal particle suspensions. The comparison of their measurement with Eq. (6.14) is shown in Figure 6.4. Shapiro et al also studied the relationship between the random close packing density and the maximum solid volume fraction, which they called the lower bound fluidity limit, of suspensions of bimodal particles. Using an asymptotic technique the fluidity limit (the maximum solid volume fraction), were calculated from Couette viscometer measurements. It was found by Shapiro et al that the ratio of close random packing density to the fluidity

limit is 1.19, as shown in Figure 6.5. They also tabulated the values of the maximum solid volume fraction, ϕ_m, and the constant C of Eq. (6.12).

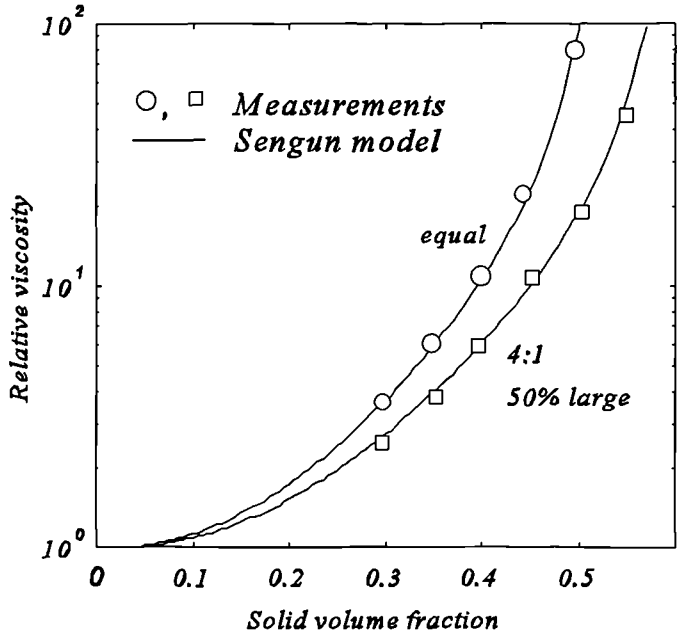

Figure 6.4 Relative viscosity of bimodal suspensions. (Shapiro)

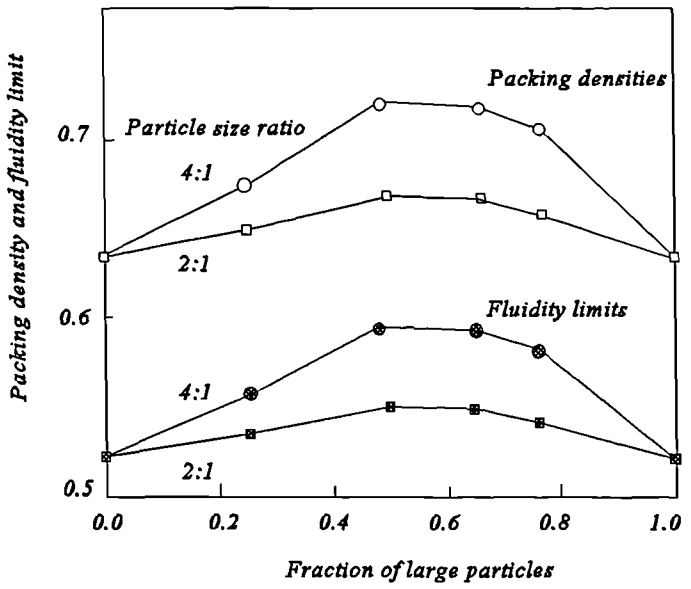

Figure 6.5 Comparison of close random packing density and fluidity limit. (Shapiro)

Chang et al (1994) measured the viscosity of bimodal suspensions using a parallel plate viscometer. The diameter of particles used by Chang et al was ranged from 40 μm to 50 μm and the proportion of small particles was between 0.07 and 0.9. They defined the ratio of solid volume fraction to the maximum packing density, ϕ/ϕ_m, as a dimensionless volume fraction. Figure 6.6 shows the relationship between the relative viscosity and the dimensionless volume fraction obtained by Chang et al.

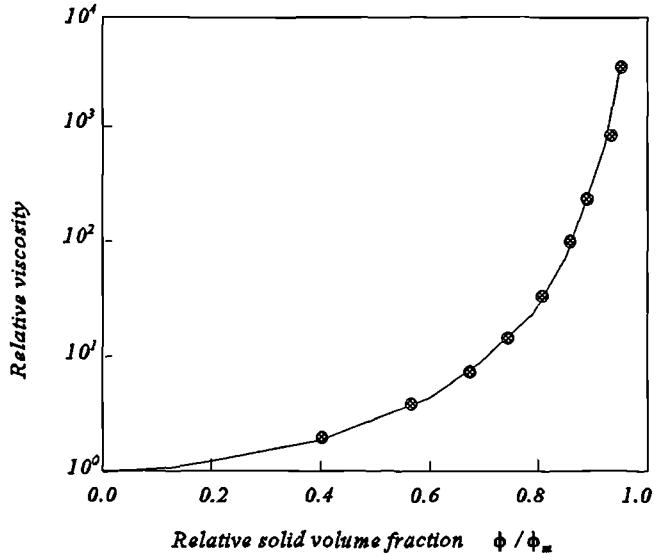

Figure 6.6 Relative viscosity vs relative solid volume fraction. (Chang et al)

B. The viscosity of poly dispersed suspensions

No viscosity models of poly dispersed suspensions are available in the literature. Recall the derivation of Eq. (6.14), where no restriction on the particle size distribution was made and which it can be employed to model the viscosity of poly dispersed suspensions. The task is to obtain the value of the exponent, n, and the maximum solid volume fraction, ϕ_m. As discussed early, taking the loose random packing density as the maximum solid volume fraction is reasonable. Observation of Figure 6.6 shows that, if 0.6 is taken as the maximum solid volume fraction, ϕ_m, of equal particles, the viscosity of Figure 6.6 agrees with that of

Figure 6.4. Comparing these two figures and using a least square regression technique, the exponent, *n*, of Eq. (6.14) can be shown to be 1.5. Then Eq. (6.14) can be rewritten as:

$$\eta_r = \frac{\eta_s}{\eta_o} = e^{5\phi_m[(1-\frac{\phi}{\phi_m})^{-0.5} - 1]} \qquad (6.17)$$

For equal particles, taking 0.6 as ϕ_m in Eq. (6.17), Figure 6.7 shows the excellent agreement between this model and Sengun's model.

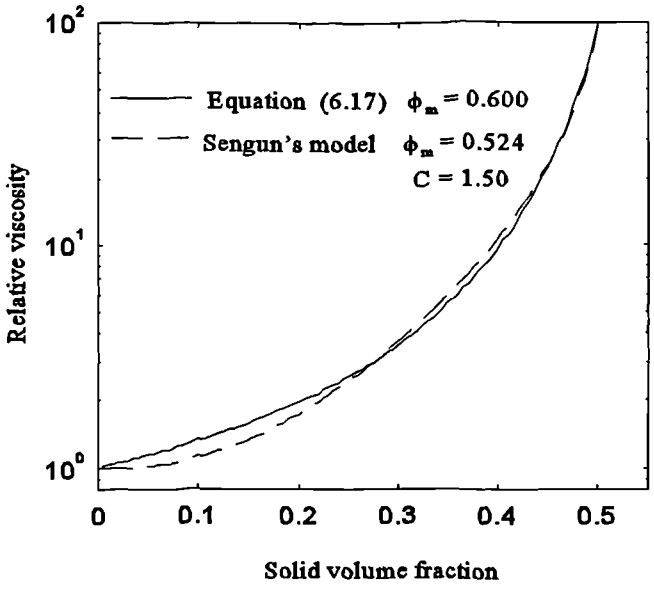

Figure 6.7 The agreement between Eq. (6.17) and Eq. (6.12).

Therefore, these two models are used in the study to investigate the effect of particle size distributions on the viscosity of dense suspensions. As defined by Shapiro et al (1992), the fluidity limit of Sengun's model is 0.524 for equal particles. So in the use of Sengun's model for unequal particles the fluidity limit should be $\phi_m = \rho / (0.6 / 0.524) = \rho / 1.145$, where ρ is the loose random packing density obtained in **Chapter five**. In contrast, in Eq. (6.17) the loose random packing density, ρ, is taken as the maximum solid volume, ϕ_m.

Figure 6.8 and Figure 6.9 show the effect of particle size distributions on the viscosity of dense suspensions obtained by Sengun's model and by Eq. (6.17) respectively. In Eq. (6.17) the maximum solid volume fractions are 0.6, 0.62 and 0.63, while in Sengun's model they are 0.524, 0.541 and 0.550, which correspond to the particle standard deviations of 0.0, 0.22 and 0.30 respectively.

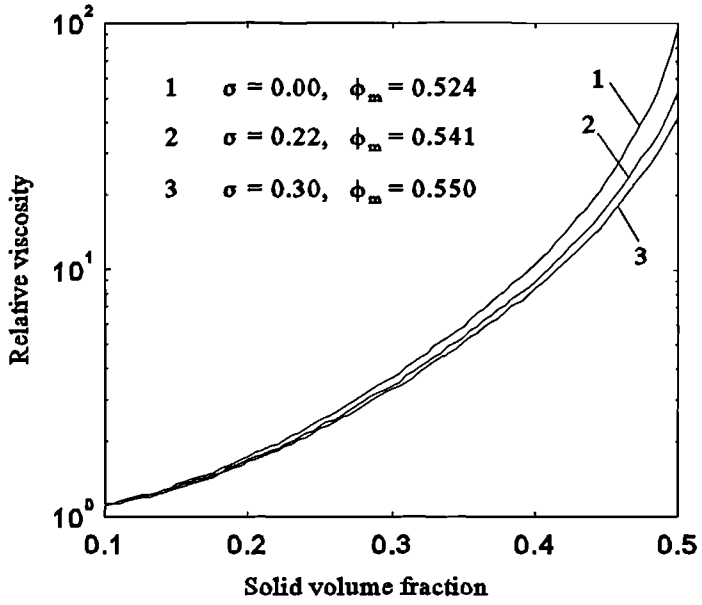

Figure 6.8 Effect of particle size distributions on suspension viscosity Sengun's model.

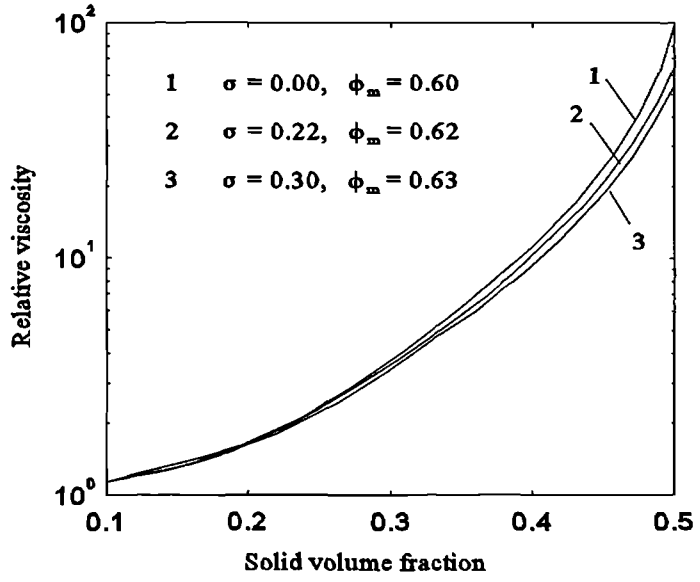

Figure 6.9 Effect of particle size distributions on suspension viscosity by Eq.(6.17).

Figure 6.8 and Figure 6.9 demonstrate that the particle size distributions significantly affect the viscosity of dense suspensions, and the higher the solid volume fraction the more significant the effect. Taking a solid volume fraction of 0.50 for example, Figure 6.8, the Sengun's model, shows that, the relative viscosity of suspension with equal particles is about 1.78 times that with standard deviation of 0.22 ($\rho = 0.62$), and is about 2.28 times that with standard deviation of 0.30 ($\rho = 0.63$). Figure 6.9, Eq. (6.17), shows that, the relative viscosity of suspensions with equal particles is 1.49 times that with standard deviation of 0.22 ($\rho = 0.62$), and is about 1.76 times that with standard deviation 0.30 ($\rho = 0.63$). Table 6.1 is the comparison of the relative viscosities of dense suspensions with different particle size standard deviations.

Table 6.1 Comparison of viscosity of dense suspensions of different particle standard deviations.

Models	Solid Volume Fraction = 0.50			Solid Volume Fraction = 0.48		
	$\eta_{0.00}/\eta_{0.22}$	$\eta_{0.00}/\eta_{0.30}$	$\eta_{0.22}/\eta_{0.30}$	$\eta_{0.00}/\eta_{0.22}$	$\eta_{0.00}/\eta_{0.30}$	$\eta_{0.22}/\eta_{0.30}$
Sengun's	1.78	2.28	1.28	1.46	1.71	1.18
Eq.(6.17)	1.49	1.76	1.18	1.37	1.55	1.14

* The subscript of η is the standard deviation of particle size.

It can be calculated by Sengun model and by Eq. (6.17) (see Figure 6.8 and Figure 6.9), that the relative viscosity of suspension with particle standard deviation of 0.35, at solid volume fraction of 0.5, is nearly equal to that with equal particles at solid volume fraction of 0.483.

The solid volume fraction of solder pastes used for surface mount assembly is about 0.48 to 0.50. Researchers have been continuously appealing for pastes of high solid volume fractions with workable rheology (Hwang, 1989). The above study suggests that, solder pastes of high solid volume fractions can be attained with a small increase in viscosity using solder powder of widely distributed particles. However, it must be kept in mind that the trade cost of high solid volume fraction and small viscosity increase is the wide spread of

solder particle sizes. In practice, it has been demonstrated that, to obtain a good reflow soldering quality, the particle size must be controlled in a reasonable range. For example, the range of solder particles for fine pitch printing should be between 20 μm and 45 μm. Using the simulation algorithm developed in **Chapter five**, the random packing of particles that come from two normal distributions was studied. In this simulation, 2400 particles obey (23, 2.0^2) normal distribution and 600 particles obey (42,^{2} 2.0) normal distribution. Simulation results show that the maximum particle is about 49 μm and the minimum particle is about 15 μm. The particles that are out of the range between 20 μm and 45 μm is less than 6% and the random loose packing density obtained is about 0.63. Employing Sengun's model or Eq. (6.17) the relative viscosity can be calculated, which is near the value of log-normal distributed particles with mean diameter of 31 μm and standard deviation of 9 μm. The distributions are compared in Figure 6.10. Although the relative viscosities of the two suspensions are similar, for log-normal distribution, the rate of particles smaller than 16 μm or bigger than 46 μm is much higher than that of the combination of the two normal distributions, see the shadows of Figure 6.10. Small particles may cause smears during reflow, while big particles may block the apertures during stencil printing. Therefore, the use of solder powder with two narrow normal distributions is better than the use of powder

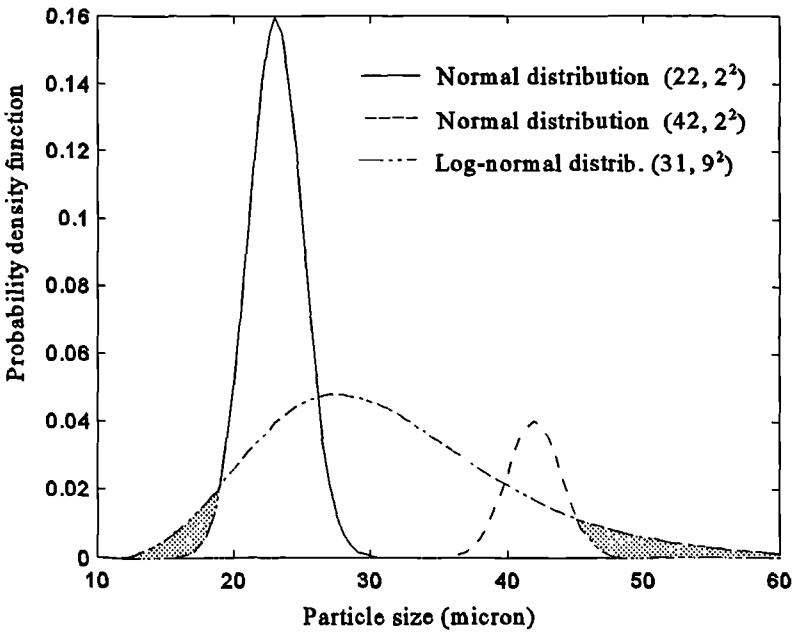

Figure 6.10 Comparison of different particle size distributions.

with one wide spread log-normal distribution. In fact, solder powder with two peaks particle size distribution has been measured (Mannan et al, 1994).

6.2 The effect of particle size distribution on the neighbour particle interaction

In section **6.1** the effect of particle size distributions on the viscosity of dense suspensions was investigated. Analytical results showed that, with the same solid volume fraction, the relative viscosity of a dense suspension of equal particles is higher than that of distributed particles.

In general, the viscosity, or the response of a dense suspension to shear rate, can be considered as the overall interactions among individual particles induced by the shear rate. Therefore, understanding the interactions between neighbouring particles is necessary.

6.2.1 Modelling of particle interaction in suspensions

A. Influence factors on particle interaction

The forces that dominate the particle motion of dense suspensions are dependent on many factors. The characteristics of the suspension are important factors, such as the particle diameter (d), the solid volume fraction of the particles (ϕ), the shape of the particles and the liquid viscosity (η_o). Another factor is shear rate (γ'). Two dimensionless parameters are usually used to judge the flow of suspensions. One is the Peclet number:

$$Pe = \frac{\eta_o d^3 \gamma'}{KT} \tag{6.18}$$

where T is the absolute temperature, K is the Boltzmann constant. The Peclet number is a judgement of the forces that dominate the flow of a suspension. If the Peclet number is much higher than one unit (high liquid viscosity, large particle size or high shear rate), hydrodynamic forces dominate the particle motion (Shapiro *et al,* 1992). If it is much lower

than one, very small particles, low shear rates and very high temperature, then the colloidal forces and thermal dynamic forces are important. The particle motion induced by colloidal and thermal dynamic forces is called the Brownian motion. For Brownian motion the particle size is of sub microns (Bossis and Brady, 1984). The range of solder particles is between 20 μm and 75 μm. Therefore, the Brownian forces can be ignored. The other dimensionless parameter is the Reynold number:

$$Re = \rho_o \frac{\gamma' d^2}{\eta_o} \tag{6.19}$$

Where ρ_o is the mass density of the liquid medium. At low Reynold number the inertia of the particles can be ignored.

B. Modelling of hydrodynamic force in dense suspensions

The hydrodynamic forces acting on a particle suspended in a liquid can be classified to the interaction between liquid and particle and between particles.

If a spherical particle moves in a liquid medium with relative velocity u_r, then the hydrodynamic force exerting on the particle by the liquid medium is given by:

$$F_{liq} = 6 \pi \eta_o u_r r \tag{6.20}$$

where η_o is the viscosity of the liquid and r is the radius of the particle. Considering the high concentrated suspensions, such as solder paste, 0.5 solid volume fraction, according to the simulation results of **Chapter five**, one particle is averagely surrounded by six to seven particles and the average gap between neighbouring particles is less than 10% of particle diameter. Therefore, it can be expected that both the particle velocity and the velocity of the liquid surrounding the particle should take the average value of the velocities of the surrounding particles. So the relative velocity between the particle and the liquid, u_r, is smaller compared with the relative velocity between two neighbour particles (Frankel and Acrivos, 1967).

The hydrodynamic interaction between two particles almost in contact has been studied using asymptotic technique and lubrication theory (Frankel and Acrivos, 1967; Cox et al, 1967, 1974; O'Neill et al, 1967; Adler, 1985). If two spheres, suspended in a liquid medium and almost in contact, move with a relative velocity $u_{//}$ along the central to central line, as shown in Figure 6.11, then the hydrodynamic interacting force between the two particles is given by:

$$F_{\parallel} = 6\pi\eta_o u_{\parallel} \frac{r_1^2 r_2^2}{(r_1 + r_2)^2} \frac{1}{\delta} \qquad \delta \ll r_1 \quad and \quad \delta \ll r_2 \qquad (6.21)$$

where r_1 and r_2 are the radii of particle 1 and particle 2 respectively, δ is the gap between the two particles and η is the liquid viscosity. Eq. (6.21) is also applicable for particles of equal radius, r, and in such case Eq. (6.21) is reduced to:

$$F_{\parallel} = 1.5\pi\eta_o u_{\parallel} \frac{r^2}{\delta} \qquad \delta \ll r \qquad (6.22)$$

If the relative velocity is perpendicular to the central to central line of the two particles, $u_{\perp}$, then the force exerting on particle 1 by particle 2 is given by:

$$F_{\perp} = -\frac{2\pi\eta_o u_{\perp} r_1 r_2}{(r_1 + r_2)} \left[\frac{3(r_1 - r_2)^2}{5(r_1 + r_2)^2} + 1\right] \ln(\epsilon) \qquad \epsilon \ll 1 \qquad (6.23)$$

where ϵ is the ratio of the gap size to the particle radius, for equal particles, $\epsilon = \delta/r$, for unequal particles r is replaced by a equivalent radium r_e, which is defined as:

$$r_e = 2\left(\frac{1}{r_1} + \frac{1}{r_2}\right)^{-1} \qquad (6.24)$$

Examining Eq. (6.23), if the difference between the two particles radii is not significant, then the term $3(r_1-r_2)^2/5(r_1+r_2)^2$ is much smaller than one unit and is negligible. In such case Eq. (6.23) can be simplified to:

$$F_{\perp} = -\frac{2\pi\eta_o u_{\perp} r_1 r_2}{(r_1 + r_2)} \ln(\epsilon) \tag{6.25}$$

Applying Eq. (6.23) to equal particles leads to:

$$F_{\perp} = -\pi\eta_o u_{\perp} r \ln(\epsilon) \tag{6.26}$$

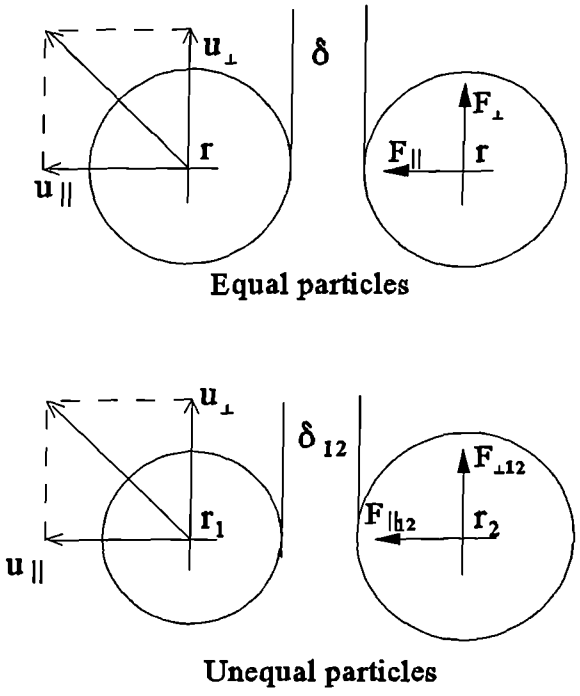

Figure 6.11 Hydrodynamic interaction between neighbour particles.

C. Modelling of electrostatic repulsive force in dense suspensions

For dense suspensions with particles larger than a micron in diameter, and the gap between two neighbour particles is much smaller than the particle radius, then according to Takamura et al (1981) the pairwise electrostatic repulsive force between two equal particles can be written as:

$$F_{rep} = F_0 \frac{\tau e^{-\tau\epsilon}}{1 - e^{-\tau\epsilon}} \tag{6.27}$$

where ϵ is dimensionless gap, $\epsilon = \delta / r$, τ is the dimensionless radius of the particle, $\tau = kr$, and k^{-1} is the Debye length. F_0 is the amplitude of the electrostatic force and is given by:

$$|F_0| = 2 \pi \nu \psi^2 \tag{6.28}$$

where ν is the electrical permittivity of liquid medium and ψ is the surface potential of the particles as $\epsilon \to \infty$. It is assumed that, in Eq. (6.27) the surface potentials of the two particles are the same and the surface charge densities remain constant as the particles move to each other. For ϵ greater than $4.5\tau^{-1}$ the electrostatic force will generally be negligible compared with the hydrodynamic force, and as $\tau \to \infty$ there is essentially no electrostatic force. The parameters, k, ψ and ν, of a dense suspension are dependent on the materials of the particles and the liquid medium.

D. The dominant force in solder paste flow

The Brownian forces, the hydrodynamic forces and the electrostatic force in a dense suspension flow have been introduced above. The range of solder particle size is between 25 μm and 75 μm and the solid volume fraction of solder pastes for stencil printing is about 50%. The stencil printing is carried out at room temperature, about 20~25 °C. Therefore, the Brownian forces are negligible compared with hydrodynamic forces. Frankel et al (1967) suggested that, for high concentration suspensions, the relative velocity between a particle and the surrounding liquid is lower than the relative velocity between two neighbouring particles. So the hydrodynamic force exerting on the solder particles by the flux/vehicle system, Eq. (6.20), can also be negligible. As a metal dense suspension, the surface charge of solder particles should be taken into account because the electrostatic force may significantly affect the relative motion between neighbouring particles, hence the bulk flow of solder paste. Recall that in Krieger-Daugherty viscosity model, see Eq. (6.4), the value of the intrinsic relative viscosity, $[\eta]$, is dependent on the particle surface charge

density, which again shows that, particle surface charge affects the solder paste flow. However, due to the shortage of the values of the physical parameters, k, ψ and ν, analysing the effect of the electrostatic force is not available. Therefore, only the hydrodynamic force between neighbour particles is taken into consideration in the following analysis.

6.2.2 Hydrodynamic interaction between solder particles in paste flow

From the point of view of relative viscosity of dense suspensions, see **6.1**, the solder paste flow is influenced by two parameters, the solid volume fraction of solder particles and the particle size distribution. These two parameters also influence the hydrodynamic interaction between neighbouring particles, which are discussed below respectively.

A. Effect of solid volume fraction on the hydrodynamic interaction

The lubrication forces between two neighbouring particles have been modelled in **6.2.1**. For convenience, the equations of hydrodynamic forces between two particles are re-written here. The force along the central to central line between two unequal particles is:

$$F_{\parallel} = 6\pi\eta_o u_{\parallel} \frac{r_1^{\,2}\, r_2^{\,2}}{(r_1 + r_2)^2} \frac{1}{\delta} \qquad \delta \ll r_1 \ \textit{and} \ \delta \ll r_2 \qquad (6.21)$$

and between two equal particles is:

$$F_{\parallel} = 1.5\pi\eta_o u_{\parallel} \frac{r^2}{\delta} \qquad \delta \ll r \qquad (6.22)$$

The force perpendicular to the central to central line between two unequal particles is:

$$F_{\perp} = \frac{2\pi\eta_o u_{\perp} r_1 r_2}{(r_1 + r_2)} \ln(\epsilon) \qquad (6.25)$$

and between two equal particles is:

$$F_{\perp} = -\pi \eta_o u_{\perp} r \ln(\epsilon) \tag{6.26}$$

In Eq. (6.26), $\epsilon = \delta/r$, and in Eq. (6.25), $\epsilon = \delta/r_e$. r_e is defined by Eq. (6.24). To avoid confusion, in the following analysis $F_{||}$ and δ of Eq. (6.21) are replaced by $F_{||12}$ and δ_{12}, $F_{\perp}$ and ϵ of Eq. (6.25) are replaced by $F_{\perp 12}$ and ϵ_{12}.

Now the effect of solid volume fraction on the hydrodynamic forces can be examined. For reason of comparability two assumptions are made in the following analysis. The first assumption is that the total volume of the two equal particles equals the total volume of the two unequal particles that is: $2r^3 = r_1^3 + r_2^3$. The second assumption is that the central to central distance between two equal particles equals that between two unequal particles that is: $2r + \delta = r_1 + r_2 + \delta_{12}$. Let $r_1 = \alpha r$, then from the first assumption it can be derived that $r_2 = (2 - \alpha^3)^{1/3} r = \beta r$, and from the second assumption there is $\delta_{12} = (2 + \epsilon - \alpha - \beta)r = \Delta r$. Substituting r_1, r_2 and δ_{12} by αr, βr and Δr respectively, then Eq. (6.21) becomes:

$$F_{||12} = 6\pi \eta_o u_{||} \frac{\alpha^2 \beta^2 r}{(\alpha + \beta)^2 \Delta} \tag{6.29}$$

and Eq. (6.25) becomes:

$$F_{\perp 12} = -2\pi \eta_o u_{\perp} r \frac{\alpha \beta}{\alpha + \beta} \ln\left[\frac{\Delta}{2}\left(\frac{1}{\alpha} + \frac{1}{\beta}\right)\right] \tag{6.30}$$

In Eq. (6.22), Eq. (6.26), Eq. (6.28) and Eq. (6.29), there are only two independent variables, the ratio of particle sizes, α, and the ratio of the gap to the radius of the equal particles, ϵ. β and Δ are derived from the two assumptions.

For dense suspensions, as the solid volume fraction increases the average gap between neighbouring particles decreases. Therefore, to examine the effect of the solid volume fraction on the particle interaction, the hydrodynamic interacting forces can be taken as functions of the gap to radius ratio, ϵ. Figure 6.12 and Figure 6.13 show the effects of ϵ on the neighbouring particle hydrodynamic interactions. Notice that, in these two figures the

forces are all dimensionless, which eliminates the effects of the relative velocity, the particle radius and the liquid viscosity. Figure 6.12 shows that, for equal particles, as ϵ is smaller than 0.20, $F_{||}$ significantly increases with the decrease of ϵ. Recall the simulation results of **Chapter five**, which showed that for equal particles with a solid volume fraction of 0.5, the average gap is about 0.15 times of the particle radius. It was shown in section **6.1** that as ϕ approaches 0.5, the relative viscosity significantly increases. This demonstrates that, as the solid volume fraction increases, the increase in the viscosity of a solder paste is attributed to the increase in the hydrodynamic interactions between neighbouring solder particles. Figure 6.12 and Figure 6.13 also prove that, if $u_{||}$ equals $u_{\perp}$, then $F_{||}$ is much higher than $F_{\perp}$.

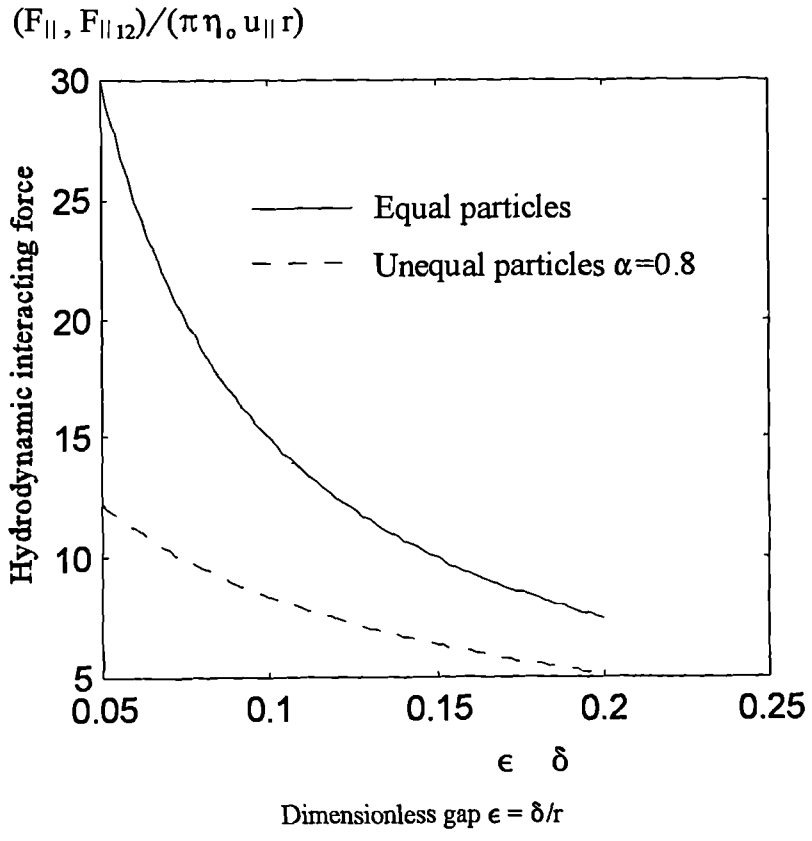

Figure 6.12 Effect of ϵ on $F_{||}$ and $F_{||12}$.

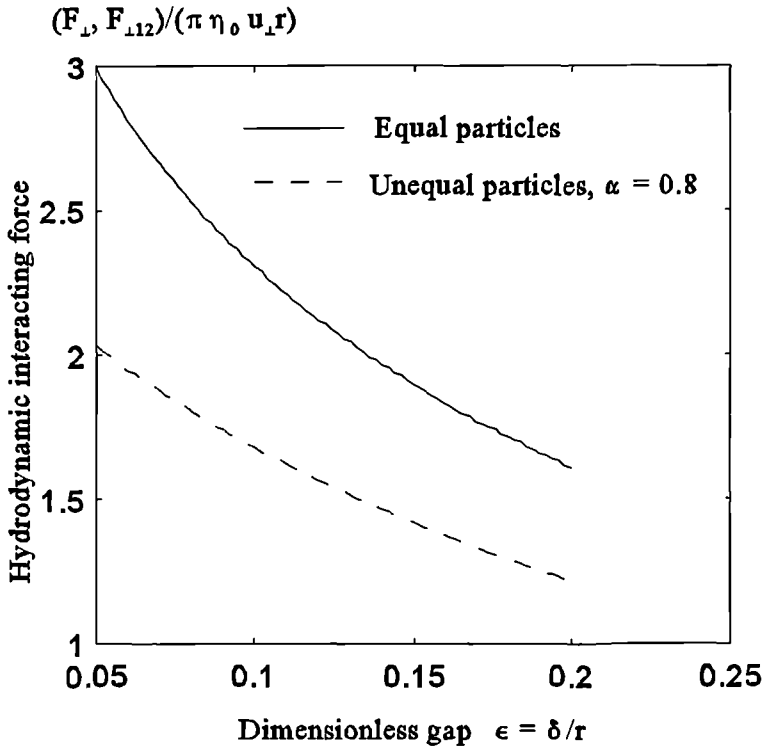

Figure 6.13 Effect of ϵ on $F_\perp$ and $F_{\perp 12}$.

B. Effect of particle size distribution on the particle hydrodynamic interaction

The effect of particle size distribution on the hydrodynamic interactions between neighbouring can be observed in Figure 6.12 and Figure 6.13. Recall that, the total volume of two equal particles is assumed equal the total volume of two unequal particles, and the central to central distance between two equal particles is assumed equal that between two unequal particles. Figure 6.12 and Figure 6.13 show that as α (r_1/ r) is fixed to 0.8, the hydrodynamic force $F_{\|12}$ is much smaller than $F_{\|}$ and $F_{\perp 12}$ is much smaller than $F_\perp$.

To investigate the effect of particle size distribution on the particle interaction further, two force ratios can be constructed as:

$$f_{\|} = \frac{F_{\|12}}{F_{\|}} = \frac{4\ \alpha^2\beta^2\ \epsilon}{(\ \alpha + \beta\ )^2\ \Delta} \qquad (6.31)$$

and as:

$$f_{\perp} = \frac{F_{\perp 12}}{F_{\perp}} = \frac{2\alpha\beta}{\alpha + \beta} \frac{\ln[\frac{\Delta}{2}(\frac{1}{\alpha}+\frac{1}{\beta})]}{\ln(\epsilon)} \tag{6.32}$$

Eq. (6.31) is the force ratio along the central to central line and Eq. (6.32) is the force ratio perpendicular to the central to central line. The typical solid volume fraction of solder pastes is about 0.5. Simulation result of **Chapter five** showed that, for dense suspensions of 0.5 solid volume fraction of equal particles, the average gap between neighbour particles is about 0.15 times the particle radius. Therefore, to examine the effect of particle distributions on the hydrodynamic interaction, let ϵ equal 0.15. Then Eq. (6.31) and Eq. (3.32) are functions of α only. Figure 6.14 shows the effect of α on $f_{||}$ and $f_{\perp}$. It suggests

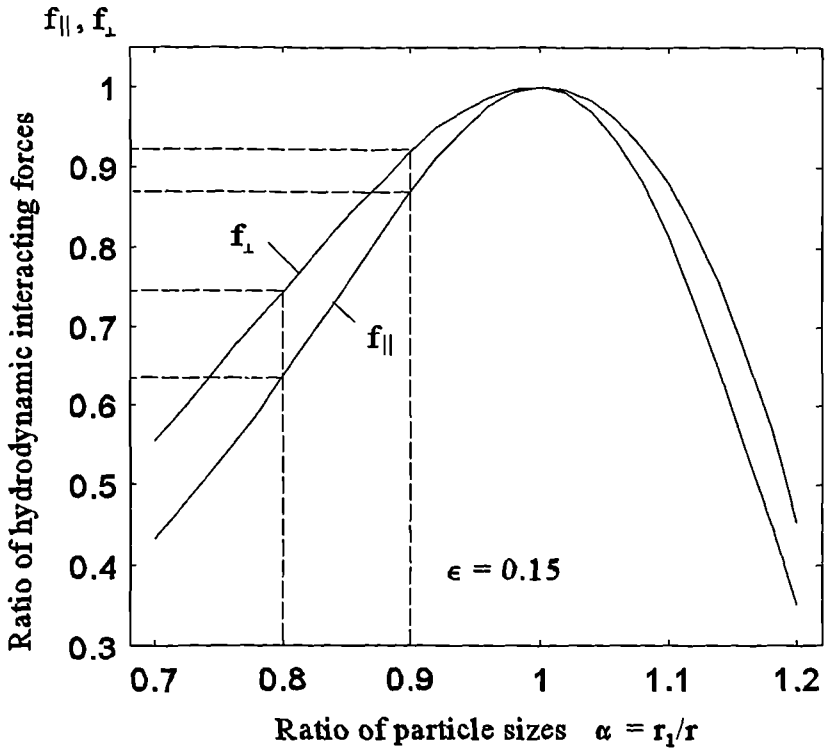

Figure 6.14 Effect of α on $f_{\perp}$ and $f_{||}$.

that the particle size distributions significantly affect the hydrodynamic interaction between neighbouring particles in solder paste flow. Both the forces parallel and perpendicular to the central to central line between two neighbouring particles decrease as the particle size ratio, α, diverges from 1.0. For example, if α equals 0.9, from Figure 6.14 it can be seen that, $f_{||}$ is about 0.88 and $f_{\perp}$ is about 0.92, and if α equals 0.8, then $f_{||}$ is about 0.64 and $f_{\perp}$ is about 0.74. Comparing Figure 6.14 with Figure 6.8 and Figure 6.9, the following can be seen. If ϵ is a constant, which implies the solid volume fraction of a dense suspension is constant, then the relationship between α and $f_{||}/f_{\perp}$ corresponds to the relationship between the relative viscosity and the particle standard deviation. This demonstrates that, for dense suspensions with the same solid volume fraction, the decrease in the relative viscosity with the increase of the particle standard deviation is attributed to the decrease of the hydrodynamic interaction as α diverges from 1.0.

6.3 Summary of Chapter six

In this chapter, the effects of particle size distributions on the relative viscosity of dense suspensions and on the particle hydrodynamic interaction in dense suspension flow were studied.

Examination of different viscosity models for dense suspensions showed that at high solid volume fraction, $\phi > 0.3$, a wide spread of viscosity exists among these models. A modified viscosity model was developed, which agrees well with Sengun's model and with experimental data in a wide range of solid volume fractions. In this model the loose random packing density of spherical particles obtained in **Chapter five** is taken as the maximum solid volume fraction, while in Sengun's model, this value is scaled down by 1.145. Employing the modified model and the model developed by Sengun et al, the effect of particle size distributions on the relative viscosity of dense suspensions was studied. Result showed that the standard deviation of particle size significantly affects the relative viscosity. For example, with solid volume fraction of 0.5, the relative viscosity of dense suspension with equal particles is about 50% to 80% higher than that with particles with standard deviation of 0.22. This study showed that solder pastes of high solid volume fraction can

be attained with a small increase in viscosity by using solder powders with highly dispersed particles. However, for fine-pitch printing, the solder particle size must be controlled between 20 μm and 45 μm. Study showed that, under such restriction, solder pastes of high solid volume fraction are still attainable by the use of solder powder with two narrow particle size distributions.

Analysis of the forces between particles in dense suspension flow showed that the solder paste flow in stencil printing is dominated by the hydrodynamic interactions between neighbouring particles. Comparison showed that, with the same solid volume fraction, the hydrodynamic interacting force between two unequal particles is smaller than that between two equal particles. As the solid volume fraction increases, this effect becomes more significant. This result proved that the increase in solder paste viscosity with the increase of the solid volume fraction is attributed to the hydrodynamic interaction between particles. Analysis suggested that, for dense suspensions of metal particles, such as solder pastes, the particle surface charges may induce electrostatic repulsive force between neighbouring particles. However, due to the shortage of data of the physical parameters, such as the surface potential, the Debye length and the electrical permittivity of liquid medium, the electrostatic force was not given consideration in this study. It should be taken into account in future work.

Chapter Seven

Summary and Suggestion for Future Work

7.1 Summary

The research work on the modelling and computer simulation of the behaviour of solder pastes in stencil printing for SM assembly of PCB's was reported in this thesis.

The motivation of this work is that, the stencil printing of solder paste is governed by the complex interactions of many variables, and among these variables, the rheology of solder pastes is the most complicated one. Although there are several reports on research on the stencil printing of solder pastes in the literature, the rheology of solder pastes is still poorly understood and there is very little on the correlation of paste properties to the stencil printing process performance. Some reports show that up to 60% of the PCB's assembly defects originate from the printing process and this is likely to continue as the electronics manufacturing industry moves towards further minimisation. To meet the challenge of minimisation requires a better understanding of the rheology of solder pastes as impact on the printing process and further improvements to stencil printing process.

The results of this work can be divided into five main areas:

i. Literature review

A detailed review of the literature on the stencil printing of solder pastes used for the reflow soldering of SM assembly. The review includes the characterisation of solder paste, and the modelling of solder paste printing and the experimental investigations;

ii. A theoretical study of stencil printing using a vibrating squeegee

This concerns the response of solder paste to the vibrating squeegee and the

development of the model correlating the vibration parameters to the printing quality.

iii. Experimental investigation of pastes' response to vibration

The aim of this part of work is to validate the theoretical prediction of solder pastes' response to the vibrating squeegee and to find out the suitable vibration parameters. It includes three sets of experiment: oscillatory shear measurements on solder paste, printing test on a prototype of vibrating squeegee system and test of paste response inside a vibration container.

iv. Computer simulation of random packing of solder powder and the microstructure of solder paste

This involves the development of the computer simulation algorithms for the study of the random packing of solder powder and the microstructure of solder paste. The aim of this part of the work of this part is to investigate the effects of particle size distribution and the solid volume fraction of solder powder on the microstructure of solder paste. The simulation result obtained in this part of work can be used for the study of the viscosity of solder paste and for numerical simulation of paste flow in printing process.

v. Investigation of the effect of particle size distribution on solder viscosity and on particle hydrodynamic interaction in paste flow

This part of the work includes the development of a viscosity model for dense suspensions, which can be used to predict the relative viscosity of a dense suspension with given particle size distribution and solid volume fraction. It also includes the modelling of the effect of particle size distribution on hydrodynamic interaction between adjacent particles in dense suspension flow.

7.2 Detailed discussion

7.2.1 The behaviour of solder pastes in stencil printing using a vibrating squeegee

The idea of the use of the vibrating squeegee is taken directly from that a mason oscillating a float to level and pack the mortar. The vibrating squeegee utilises the same principle. In stencil printing, under the impact of the vibrating squeegee, the solder particles at the squeegee and paste interface will move in towards the bulk of the paste roll. This motion of the solder particle will lead to the generation of a liquid rich layer at the interface between the squeegee leading edge and the paste roll. Based on lubrication theory, it is predicted that this liquid rich layer could reduce the squeegee resistance on the paste roll.

As a of viscoelastic material, under oscillatory shear, the dynamic viscosity of solder paste decreases as the oscillatory frequency increases. Compared with constant shear rate, the superimposition of an oscillatory shear rate on a constant shear rate can reduce the shear stress in a dense suspension. As the vibrating squeegee passes over the stencil apertures the paste packed inside the apertures experience an oscillatory shear by the squeegee tip. Under the action of the vibrating squeegee, the dynamic viscosity of the paste inside the apertures decreases. Hence the fluidity increases which will lead to higher particle packing density inside the apertures.

If the vibration velocity amplitude, $A\omega$, is kept constant, then using a combination of a relatively high frequency, ω, and a small amplitude, A, will enhance the rolling action of the paste in front of the squeegee, enhance the packing of powder particles inside the apertures and also help to reduce the amount of paste sticking on the squeegee as it is lifted at the end of the printing stroke.

7.2.2 Experimental validation of the theoretical predictions

The result of frequency sweep oscillatory shear measurement showed that the dynamic

viscosity of solder paste decreases as the frequency increases. Under high oscillatory frequency (50 Hz to 90 Hz) the storage modulus of solder paste is much smaller than the loss modulus. Therefore, under oscillatory shear the behaviour of solder paste is more like viscous liquid than an elastic solid. The result also showed that the storage modulus of solder paste under high shear stress (large shear strain), is smaller than that under low shear stress (small shear strain).

The experimental result of the vibrating squeegee system proved that the application of a vibrating squeegee can generate a liquid rich layer at the squeegee blade and paste roll interface. This liquid rich layer acts as lubricating agent between squeegee blade and paste roll that could reduce the squeegee resistance on the paste roll. There is empirical evidence to show that a good paste roll is essential for the proper filling of the apertures, for achieving good paste withdrawal, and thus more consistent printing deposits. The formation of a liquid rich layer can also help to reduce the potential for paste roll to stick on the squeegee blade at the end of the printing stroke. This experiment also showed that the vibrating squeegee can reduce the time it takes to form the paste roll at the start of a printing stroke. The quick formation of paste roll can help to reduce the length of printing stroke, and hence the cycle time. The result also showed that, for the paste used in this experiment, the suitable range of frequency is from 80 Hz to 200 Hz and the suitable range of amplitude is from 0.10 mm to 0.37 mm.

The third experiment concerns the study of the behaviour of solder paste under vibration inside a container. Experimental result showed that under vibration liquid rich layers can be generated at the container wall and the sample interface and at the sample surface. The liquid rich layer at the wall and paste interface can help the withdrawal of solder paste from the stencil apertures and the liquid rich layer at the surface can help to achieve level paste deposit on the substrate. Scanning Electron Microscope observation showed that under vibration the particles arrangement is more uniform than without vibration. This uniform particle arrangement may reduce the viscosity of solder paste. Uniform arrangement of particles can also help to improve the soldering quality and obtain reliable connections

between components and substrate.

7.2.3 The random packing of solder particles and the microstructure of solder pastes

The packing density and the average contact number between neighbour particles are the two important parameters of random packing. Computer simulation results showed that the packing density increases with the increase of the standard deviation of particle radii while the average contact number between neighbouring particles decreases. This is attributed to the fact that, in the packing of particles of high standard deviation, the smaller particles tend to fill the voids between large particles.

The average gap between neighbour particles and the average neighbouring number are used to characterize the micro-structure of the solder pastes. Simulation results, with solid volume fraction of 0.5, showed that the average neighbouring number decreases as the standard deviation of particle radii increases, while the average gap size increases. It may suggest that, in a dense suspension containing highly dispersed spherical particles, the smaller particles have high degree of freedom to move within the liquid medium.

7.2.4 Solder paste viscosity and solder particle hydrodynamic interaction

A modified relative viscosity model was developed in this work, which agrees well with Sengun's model and with experimental data in a wide range of solid volume fractions. Compared with other models, this modified model is simpler, and the physical meaning of the parameters of this model are clear.

The effect of the particle size distribution on the relative viscosity of solder paste was studied by this model and by Sengun's model. Results showed that the particle size distribution significantly affects the viscosity. For solder paste of 50% solid volume fraction, the relative viscosity of that of equal particles is about 50% higher than that of particles with standard deviation of 0.22. This suggests that solder pastes of high solid volume fraction

can be attained with a small increase in viscosity by using solder powder of highly dispersed particles. However, for fine-pitch printing, the range of particle size distribution must be rigorously controlled. In such case, analysis showed that the use of the combination of solder particles that come from two narrow distributions can also attain a high solid volume fraction with a small increase in viscosity.

Under high shear rate, analysis showed that, in stencil printing, the solder paste flow is dominated by the hydrodynamic interactions between adjacent particles. With the same solid volume fraction, the study showed that the hydrodynamic interaction force between distributed adjacent particles is smaller than that between equal particles. As the solid volume fraction increases, this effect becomes more significant. This result may explain, from the point of particle interaction, why the relative viscosity of a dense suspension with highly dispersed spherical particles is smaller than that with equal particles.

7.3 Suggestion for future work

Future work is suggested in the following two areas:

i. Due to the difficulty encountered in manufacturing a special stencil, the prediction of the packing of solder paste inside the apertures was indirectly verified by vibrating the solder paste sample inside a cylindrical container. There is concern that the use of a vibrating squeegee may induce paste flow beneath the stencil, which could lead to bridging defects. Therefore, further experiments are necessary to investigate whether or not bridging will be induced by use of the vibrating squeegee. If bridging occurs what methods can be used to prevent it.

ii. As a metallic powder, the surface of the solder particles may be charged, which will induce electrostatic repulsive forces between adjacent particles in the solder paste flow. The electrostatic force will also affect the viscosity of the solder paste.

However, due to the shortage of the physical parameters of solder pastes, such as the surface potential of the solder particles, the electrical permittivity of the flux/vehicle system, the electrostatic force was not taken into consideration in this work. In future study, it should be taken into account to verify the magnitude of electrostatic force compared to the hydrodynamic force.

Appendix 1

Programme for simulation of particle random packing

```
**************************************************************
*   This programme  simulates the random packing of poly-dispersed  spheres     *
*   within a cubic container. Subroutine GENERATE generates the particle radii  *
*   and the initial positions. The particle distribution is dependent on the value of  *
*   the integer variable flag, for equal particles flag=1, for particles obey normal   *
*   distribution flag=2, for particles obeying log-normal distribution flag = 3 and   *
*   for bimodal particles flag=4.                                                      *
**************************************************************
      real x(4,10000), mean(4),meanr, devir,devi(4), l, r, xigma,
     +     density, meanva, meanno, l2, ra
      integer n, n1, ns, judge, flag
      write(* , *) 'please type in simulated number of spheres'
      read(* , *) n
      write(*,*)'Equal spheres type 1, normal distribution type 2,'//
     +          ' lognormal distribution type 3 and bimodal type 4 '
      read(* , *)  flag
      if (flag .lt. 4) then
        write(* , *) 'please give mean radius and standard deviat'//
     + 'ion of spheres( for equal spheres standard deviation equals 0)'
         read(* , *) r, xigma
      else
        write(*,*) ' please give rs/rl and ns'
        read (*,*) ra, ns
      end if
      write (*,*)'          The initail generated result '
      write (*,*)' '
```

```
   call generate ( x, n, ns, l, r, xigma, devi, density, mean,
  +  ra, flag )
   write (*,*)' The radius of the container = ',l
   write( *, * ) '  n     mean(r)   devi(r)   density ',
  + ' mean(x)   mean(y)   mean(z)'
   write (*,20) n, mean(1), devi(1), density, mean(2),
  +            mean(3), mean(4)
   write (*,*)'     '
   write (*,*)'              The intermediate results '
   write( *, * ) '  n     mean(r)   devi(r)   density ',
  + ' meanva    meanno     l'
   call sequence ( x, n )
   n1 = 15
   i=1
   call moving(x,n,n1,l,i)
   call vibrate(x,n,judge, meanr,l,i)
   do 15 i = 1, 30
     call moving( x, n, n1, l, i )
     call sequence ( x, n )
     call statisti(x, n, mean, devi, flag, density,l)
     l2 = l
     call check ( x, n, meanva, meanno, l, judge )
     if (judge.eq.1) then
       if ( i .eq. 20 ) then
         n1 = 20
       else
         n1 = 15
       end if
       write (*,20) n, mean(1), devi(1), density, meanva,
  +            meanno, l2
       call vibrate(x,n,judge,meanr,l,i)
```

```
      else
        n1 = 12
        write (*,20) n, mean(1), devi(1), density, meanva,
     +          meanno, l2
        call sequence (x, n)
       do 12 j = 15 , 20
        call vibrate( x, n, judge, meanr, l, j )
        call moving( x, n, n1, l, j )
        call statisti( x,n,mean,devi,flag,density,l)
        l2 = l
        call check ( x, n, meanva, meanno, l,judge)
        write (*,20) n, mean(1), devi(1), density, meanva,
     +          meanno, l2
12        continue
        goto 30
       end if
       call vibrate( x, n, judge, meanr, l, i )
15     continue
20     format(i7, 6f10.5)
30     open ( unit = 2, file = 'cube1.dat' )
      write (*,*) n, l2
      do 50 i = 1, n
        write(*,*) x(1,i), x(2,i), x(3,i), x(4,i)
50     continue
      close(2)
      open ( unit = 2, file = 'cube01.dat' )
      write(*,*)'        The final simulation result   '
      write(*,*)' '
      write(*,*)'  Total particles: n =',n,'packing dimension: l=',l
      write(*,*)' '
      write(2,*)'  n    mean(x)   mean(y)   mean(z)   mean(r) ',
```

```
     +' stdev(r)'
      write(2,*)' '
      write(2,40) n, mean(2), mean(3), mean(4), mean(1), devi(1)
      write(2,*)' '
40     format(i7,5f10.5)
      call result( x, n, density, l2 )
      close(2)
      end

C---------- End of the main programme ----------

      subroutine generate (x,n,ns,l,r,xigma,devi,density,mean,ra,flag)
************************************************************
*  This subroutine randomly generates the particle radii and the initial positions *
************************************************************
      real x(4,n), s1, s2, l, r, xigma, density, mean(4), devi(4),
         r1, rb, ro
      integer n, flag
      parameter ( pi = 3.14159 )
      density = 0
      do 110 i = 1, 4
        mean(i) = 0
        devi(i) = 0
 110    continue
      call date_time_seed@
      if (flag .eq. 4) then
        ro = ns/n
        do 70 i = 1, n
          rb = random()
          if (rb. lt. ro) then
            x(1,i) = n*ra/(ns*ra+n-ns)
```

```
        else
          x(1,i) = n/(ns*ra+n-ns)
        end if
        density = density + x(1,i)**3
        mean(1) = mean(1) +x(1,i)
        devi(1) = devi(1) + x(1,i)*x(1,i)
70      continue
      else
       do 80 i = 1, n
85        s1 = random()
          s2 = random()
        if ( flag .eq. 1 ) then
          x(1,i) = r
          density = density + x(1,i)**3
        else if ( flag .eq. 2 ) then
          x(1,i) = r + xigma*cos(pi*2*s1)*sqrt(-2*log(s2))
          if (x(1,i) .lt. 0.0)then
            goto 85
          end if
          density = density + x(1,i)**3
          mean(1) = mean(1) +x(1,i)
          devi(1) = devi(1) + x(1,i)*x(1,i)
        else
          x(1,i) = exp(r+xigma*cos(pi*2*s1)*sqrt(-2*log(s2)))
          density = density + x(1,i)**3
          mean(1) = mean(1) +x(1,i)
          devi(1) = devi(1) + x(1,i)*x(1,i)
        end if
80     continue
      end if
      density = density*pi*4.0/3.0
```

```
      l = (density/0.85)**(1.0/3.0)
      density = density/l**3
      do 100 i = 1, n
        do 90 j = 2, 4
          x(j,i) = l*random()
          mean(j) = mean(j) + x(j,i)
          devi(j) = devi(j) + x(j,i)*x(j,i)
**  x(2,i), x(3,i) and x(4,i) are x y z coordinates of ith sphere centre
**  and l is the cubic container size
90            continue
100     continue
      if ( flag .eq. 1 ) then
        devi(1) = 0
        mean(1) = r
        k = 2
      else
        k = 1
      end if
      do 130 j = k, 4
        mean(j) = mean(j)/n
        devi(j) = devi(j)/n
        devi(j) = sqrt (devi(j)-mean(j)*mean(j))
130     continue
      return
      end

C---------------------- end of GENERATE -------------------------
```

```
      subroutine statisti(x, n, mean, devi, flag, density, l)
************************************************************
*  This subroutine calculates the mean radius and standard deviation of the  *
*   particles, the mean values and the standard deviations of particle centre  *
*   coordinates, and the packing density.                                      *
************************************************************
      real x(4,n), mean(4), devi(4), density, l
      integer n, flag
        density = 0
      do 200 j = 1, 4
        mean(j)=0
        devi(j)=0
200     continue
      if ( flag .eq. 1) then
         k = 2
         mean(1) = x(1,1)
         devi(1) = 0
      else
         k = 1
      end if
      do 220 i = 1, n
        density = density + x(1,i)**3
        do 210 j = k, 4
          mean(j) = mean(j) + x(j,i)
          devi(j) = devi(j) + x(j,i)*x(j,i)
210       continue
220     continue
      do 230 j = k, 4
        devi(j) = devi(j)/n
        mean(j) = mean(j)/n
        devi(j)=sqrt(devi(j)-mean(j)*mean(j))
```

```
230    continue
       density = density*3.14159*4.0/3.0/l**3
       return
       end

C------------------ end of STATISTI ----------------------------

       subroutine sequence ( x,  n )
*************************************************************
*  This subroutine randomly generates the particle moving sequence.   *
*************************************************************
       real x(4,n), x1(4,10000), juge(10000)
       integer n,  m
       call date_time_seed@
       do 25 i = 1, n
          juge(i) = 1000.0*random()
          do 15 j = 1, 4
             x1(j,i)=x(j,i)
15         continue
25     continue
       do 55 i = 1, n
          m = 1
          do 35 j = 1, n
            if ( j .eq. i ) then
              go to 35
            else if ( juge(i) .GT. juge(j) ) then
              m = m + 1
            end if
35          continue
          do 45 k = 1, 4
             x(k,i) = x1(k,m)
```

```
45          continue
55      continue
        return
        end

C-------------------- end of SEQUENCE ----------------------------

        subroutine moving ( x , n, n1, l, i )
*****************************************************************
*       This subroutine relocates particles to reduce the overlap values between    *
*       adjacent particles.                                                         *
*****************************************************************
        real x(4,n),l, r1, r2, sum(3)
        integer n, n1, i, i1, j1, k1, m1, m
        do 400 k = 1, n1
        do 390 i1 = 1, 10
          do 380 j1 = 1, n
            m = 1
            sum(1) = 0
            sum(2) = 0
            sum(3) = 0
            r2 = x(1,j1)
           do 350 k1 = 1, n
             if (k1 .eq. j1) then
               go to 350
             end if
             if (abs(x(2,k1)-x(2,j1)) .lt. r2+x(1,k1)) then
               if (abs(x(3,k1)-x(3,j1)) .lt. r2+x(1,k1)) then
                 if (abs(x(4,k1)-x(4,j1)) .lt. r2+x(1,k1)) then
                   r1 = (x(2,k1)-x(2,j1))**2 +
     +                 (x(3,k1)-x(3,j1))**2 +
```

```
     +                (x(4,k1)-x(4,j1))**2
                    r1 = sqrt(r1)
                    if ( r1 .lt. r2+x(1,k1))then
                      if ( r1 .gt. 0 ) then
                        r1 = (r2+x(1,k1))/r1
                        do 340 m1 = 1, 3
                          sum(m1)=sum(m1)+x(m1+1,k1)
     +                    +(x(m1+1,j1)- x(m1+1,k1))*r1
340                       continue
                        m = m + 1
                      end if
                    end if
                  end if
                end if
              end if
350           continue
            if ( m.gt.1 ) then
              m = m - 1
              do 360 m1 = 1, 3
                x(m1+1,j1)=sum(m1)/m
360             continue
            end if
            do 370 m1 = 2, 4
              if ( x(m1,j1) .lt. x(1,j1) ) then
                x(m1,j1)=x(1,j1)
              else if ( x(m1,j1) .gt. l-x(1,j1) ) then
                x(m1,j1) = l-x(1,j1)
              end if
370           continue
380         continue
          if (n1 .eq. 5) then
```

```
          goto 390
        else if ( i .gt. 2 ) then
          if ( k .gt. 1 ) then
            if ( i1 .eq. 6 ) then
              call grow(x,n,l)
            end if
          end if
        end if
390     continue
          call sequence(x,n)
400     continue
      return
      end
C -------------------------end of moving-----------------------------


      subroutine check ( x,n,meanva,meanno,l,judge )
*****************************************************************
*  This  subroutine examines the overlap number of each sphere and the overlap  *
*  value. If the average overlap value is higher than the tolerance, then it shrinks  *
*  the particles according to the average overlap value. Otherwise it goes back to *
*  main programme to output the simulation results.                              *
*****************************************************************
      real x(4,n), overva(10000), shrink, r1, l, meanva, meanno, dl
      integer n, overno(10000)
      meanva = 0
      meanno = 0
      do 500 i = 1, n
        overva(i) = 0
        overno(i) = 0
500     continue
      do 530 i = 1, n-1
```

```
      do 520 j = i+1, n
        if (abs(x(2,j)-x(2,i)) .lt. x(1,j)+x(1,i))then
          if (abs(x(3,j)-x(3,i)) .lt. x(1,j)+x(1,i))then
            if(abs(x(4,j)-x(4,i)) .lt. x(1,j)+x(1,i))then
              r1 = (x(2,j)-x(2,i))**2 +
     +             (x(3,j)-x(3,i))**2 +
     +             (x(4,j)-x(4,i))**2
              r1 = sqrt(r1)
              if ( r1 .lt. x(1,i)+x(1,j))then
                overva(i)=overva(i)+(x(1,i)+x(1,j)-r1)/x(1,i)
                overva(j)=overva(j)+(x(1,i)+x(1,j)-r1)/x(1,j)
                overno(i)=overno(i)+1
                overno(j)=overno(j)+1
              end if
            end if
          end if
        end if
  520   continue
        meanva = meanva + overva(i)
        meanno = meanno + overno(i)
  530   continue
      meanva = (meanva + overva(n))/n
      meanno = (meanno + overno(n))/n
      meanva = meanva/6
      if ( meanva .gt. 0.0005) then
        if ( meanva .gt. 0.10) then
          shrink = 1.0 - meanva**1.2/7.0
        else if ( meanva .gt. 0.0250 ) then
          shrink = 1.0 - meanva/5.0
        else
          shrink = 1.0 - meanva**.93/5.0
```

```
        end if
        dl= l/shrink - l
        l = l/shrink
        do 550 i = 1, n
          do 540 j= 2, 4
            x(j,i) = x(j,i)+dl/2.0
540         continue
550       continue
        judge = 1
      else
        judge = 0
      end if
      return
      end
C---------------------- end of check ------------------------------
          subroutine vibrate(x, n, judge, meanr, l, i)
************************************************************
*    This subroutine vibrates the particles by randomly disturbing the    *
*    the coordinates of the particle centres.                              *
************************************************************
      real x(4,n), meanr, l, r, scale
      integer n, judge, i
      scale = sqrt(real(i))
      call date_time_seed@
      do 720 j = 1, n
        do 710 j1 = 2, 4
          if ( x(j1,j) .lt. 1.5*x(1,j)) then
            goto 710
          else if ( x(j1,j) .gt. l-1.5*x(1,j) ) then
            goto 710
          else
```

```
            x(j1,j)=x(j1,j)+(.05 -.1*random())/scale
          end if
710       continue
720     continue
      return
      end
C---------------- the end of vibrate ----------------------

       subroutine grow (x, n, l)
************************************************************
*      Subroutine grow slightly increases the radii of the particles whose    *
*      contact number is less than 2.                                         *
************************************************************
      real x(4,n), l, r, r1, r2, dr(4), sum(3)
      integer n, contact
      contact = 0
        do 980 i = 1, n
          r2 = sqrt(x(2,i)**2+x(3,i)**2+x(4,i)**2) + 1.5*x(1,i)
          if ( r2 .gt. l ) then
            goto 980
          end if
          r = x(1,i)
          contact = 0
          do 910 j = 1, n
            if ( j .eq. i ) then
              goto 910
            end if
          r1 = sqrt((x(2,j)-x(2,i))**2 +
     +            (x(3,j)-x(3,i))**2 +
     +            (x(4,j)-x(4,i))**2 )
            if ( r1 .lt. r+x(1,j))then
```

```
            contact = contact + 1
          end if
910       continue
        if ( contact .gt. 1 ) then
          goto 980
        end if
        r2 = 1.5*x(1,i)
        dr(1) = 0.1*x(1,i)
        dr(2) = 0.2*x(1,i)
        dr(3) = 0.3*x(1,i)
        dr(4) = 0.4*x(1,i)
        do 930 j = 1, n
          if ( j .eq. i ) then
            goto 930
          end if
          r1 = sqrt((x(2,j)-x(2,i))**2 +
     +          (x(3,j)-x(3,i))**2 +
     +          (x(4,j)-x(4,i))**2 )
          if ( r1 .lt. r2+x(1,j))then
            if ( r1-x(1,i)-x(1,j) .lt. dr(1)) then
              dr(2)=dr(1)
              dr(3)=dr(2)
              dr(4)=dr(3)
              dr(1)= r1-x(1,i)-x(1,j)
            else if ( r1-x(1,i)-x(1,j) .lt. dr(2)) then
              dr(3)=dr(2)
              dr(4)=dr(3)
              dr(2)= r1-x(1,i)-x(1,j)
            else if ( r1-x(1,i)-x(1,j) .lt. dr(3)) then
              dr(4)=dr(3)
              dr(3)= r1-x(1,i)-x(1,j)
```

```
          else if ( r1-x(1,i)-x(1,j) .lt. dr(4)) then
            dr(4)= r1-x(1,i)-x(1,j)
          end if
        end if
930     continue
        x(1,i) = x(1,i) + ( dr(1)+dr(2)+dr(3)+dr(4))/4.2
      r = x(1,i)
      sum(1) = 0
      sum(2) = 0
      sum(3) = 0
      contact = 0
      do 960 j = 1, n
        if ( j .eq. i ) then
          goto 960
        end if
        r1 = sqrt((x(2,j)-x(2,i))**2 +
     +       (x(3,j)-x(3,i))**2 +
     +       (x(4,j)-x(4,i))**2)
        if ( r1 .lt. r+x(1,j))then
          if ( r1 .gt. 0 ) then
            r1 = (r+x(1,j))/r1
            do 950 m1 = 1, 3
              sum(m1)=sum(m1)+x(m1+1,j)
     +         +(x(m1+1,i)- x(m1+1,j))*r1
950           continue
            contact = contact + 1
          end if
        end if
960     continue
      if ( contact .gt. 0 ) then
        do 970 m1 = 1, 3
```

```
            x(m1+1,i)=sum(m1)/contact
970         continue
          end if
980     continue
        return
        end

C-------------------end of grow-----------------


        subroutine result( x, n, density, l )
************************************************************
*     This subroutine counts the statistic results of the random packing    *
*     simulation and writes the results to a data file.                     *
**************************************** ******************
        real x(4,n), l,r1,r2,density,meancon,maxr,minr,dr,meanr(60)
        integer n, n1, frequen(60), maxcon, mincon, contact, distri(11)
        meancon =0
        maxcon = 0
        maxr = 0.0
        n1 = n
        minr = 10.0
        mincon = 10
        do 810 i = 1, 11
          distri(i) = 0
810     continue
        do 820 i = 1, 60
          frequen(i)=0
          meanr(i)=0
820     continue
        do 840 i = 1, n
          if ( x(1,i) .gt. maxr ) then
```

```
          maxr = x(1,i)
        end if
        if ( x(1,i) .lt. minr ) then
          minr = x(1,i)
        end if
        do 825 j = 2, 4
          if( x(j,i) .lt. 1.75*x(1,i) ) then
            n1 = n1 - 1
            goto 840
          else if ( x(j,i) .gt. l-1.75*x(1,i)) then
            n1 = n1 - 1
            goto 840
          end if
825       continue
        contact = 0
        r1=x(1,i)+0.005
        do 830 j = 1, n
           if ( j .eq. i ) then
             goto 830
           end if
          if (abs(x(2,j)-x(2,i)) .lt. x(1,j)+r1)then
            if (abs(x(3,j)-x(3,i)) .lt. x(1,j)+r1)then
              if(abs(x(4,j)-x(4,i)) .lt. x(1,j)+r1)then
                r2 = (x(2,j)-x(2,i))**2 +
     +               (x(3,j)-x(3,i))**2 +
     +               (x(4,j)-x(4,i))**2
                r2 = sqrt(r2)
                if ( r2 .lt. x(1,j)+r1)then
                  contact=contact+1
                end if
              end if
```

```
            end if
          end if
830       continue
        meancon =meancon + contact
        if ( contact .gt. maxcon ) then
          maxcon = contact
        end if
        if ( contact .lt. mincon ) then
          mincon = contact
        end if
        do 850 k = 1, 60
          if ( contact .eq. k-1 ) then
            frequen(k) = frequen(k)+1
            meanr(k) = meanr(k)+x(1,i)
            goto 840
          end if
850       continue
840   continue
      meancon = meancon / n1
      dr = (maxr - minr)/11
      do 865 i = 1, n
        do 860 j = 1, 11
          if ( x(1,i) .lt. minr+.0001*dr + j*dr ) then
            distri(j) = distri(j) + 1
            goto 865
          end if
860       continue
865   continue

      write ( *,845 ) maxcon, mincon
845   format('  maximum contact =',i4,'  minimun contact =',i3)
```

```
      write(2,*) ' '
      write(2,*)' packing density       =',density
      write(2,*) ' '
      write(2,*)' average contact number =',meancon
      write(2,*) ' '
      write(2,*)' The distribution of contact number:'
      write(2,*) ' '
      do 870 i = 1, maxcon+1
        if ( frequen(i) .eq. 0 )then
           goto 870
        end if
        meanr(i)=meanr(i)/frequen(i)
        write(2,880) i-1, frequen(i), i-1, meanr(i)
870     continue
880     format(' frequency(',I2,') =',I4,'   meanr(',i2,') = ',f8.5)
      write(2,*)' '
      write(2,*)' '
      write(2,*)' The particle size distribution'
      write(2,*)' '
      do 890 i = 1, 11
        write(2,895) minr+(i-1)*dr, minr+i*dr, i, distri(i)
890     continue
895     format(' ',f8.5,'--',f8.5,'  ','f',i2,' =',i4 )
      return
      end
```

Appendix 2

Programme for simualtion of dense suspension's microstructure

```
************************************************************
*    This programme reads data from file 'cube1.dat' which contains the data   *
*    of particle random packing. Then it deparates the particles to simulate the  *
*    the micro-structure of a dense suspension with 0.5 solid volume fraction.  *
*    Finally it draws three and two dimensional views of the dense suspension.  *
*    If the separation parameter 'sep' is set to be 1.0, then the three and two  *
*   dimensional views are of the random packing.                                 *
************************************************************
      real x(4,10000), x1(4,10000), l, x2(4), x3(4,5000), sep,
     +     meanr, pi, cita, phi, dx, dy, dz, mx, my, mz, den1, den2
      double precision dl, delta1, delta2
      integer  ix,iy, ir, n, n1
      character *(*) a, b
      parameter (a = '(a)')
      parameter (b = '(b)')
      pi = 3.1416
      cita =  pi/4.0
      phi =  pi/6.0
      n1 = 0
      mx = 0
      my = 0
      mz = 0
      dx = 0
      dy = 0
      dz = 0
      den1 = 0.0
```

```
      den2 = 0.50
      meanr = 0
      open ( 1, file = 'cube1.dat' )
      read (*,*) n,l
      do 20 i = 1, n
        read(*,*) x(1,i), x(2,i), x(3,i), x(4,i)
        den1 = den1 + x(1,i)**3*4*pi/3
20     continue
      close(1)
      den1 = den1/l**3
           sep = (den1/den2)**(1.0/3.0)
      l = l*sep
      call date_time_seed@
      do 25 i = 1, n
        dl=random()*x(1,i)*(sep -1.0)
        delta1=random()*2.0*pi
        delta2=random()**1.732*pi/2.0
        if (random() .gt. 0.5) then
          delta2 = - delta2
        end if
        dx=dl*cos(delta2)*cos(delta1)
        dy=dl*cos(delta2)*sin(delta1)
        dz=dl*sin(delta2)
        x(2,i) = x(2,i)*sep + dx - l/2.0
        x(3,i) = x(3,i)*sep + dy - l/2.0
        x(4,i) = x(4,i)*sep + dz - l/2.0
        if (abs(x(2,i)) .lt. x(1,i)) then
          n1 = n1 + 1
          x3(1,n1) = sqrt(x(1,i)**2 - x(2,i)**2)
          do 15 j = 2, 4
            x3(j, n1) = x(j,i)
```

```
15          continue
          end if
          meanr = meanr+x(1,i)
          x1(2,i) = x(2,i)*cos(cita)- x(3,i)*sin(cita)
          x1(3,i) = x(2,i)*sin(cita)+ x(3,i)*cos(cita)
          x(2,i) = x1(2,i)
          x1(2,i) = x(4,i)*sin(phi) + x(2,i)*cos(phi)
          x1(4,i) = x(4,i)*cos(phi) - x(2,i)*sin(phi)
          x1(1,i) = x(1,i)
25        continue
        open ( unit = 2, file = 'dense.dat')
        write(*,*) n, l
        do 26 i = 1, n
          write (*,*) x(1,i), x(2,i), x(3,i), x(4,i)
26        continue
        close(2)
        meanr = meanr/n
        do 40 i =1, n
          do 30 j = 1, 4
            x(j,i)=x(j,i)/meanr
30          continue
40        continue
        l=l/meanr
        do 80 i = 1, n-1
          do 70 j = 1+1, n
            if ( x1(2,j) .lt. x1(2,i) ) then
              do 60 k = 1, 4
                x2(k) = x1(k,j)
                x1(k,j)=x1(k,i)
                x1(k,i) = x2(k)
60              continue
```

```
          end if
 70       continue
 80     continue
       call select_pcl_printer@(203,'A4',300,nhorz,nvert)
       call set_pcl_bitplanes@(0,error_code)
       call set_pcl_landscape@(0,nhorz,nvert,error_code)
       call open_gprint_device@(1,error_code)

       do 120 i = 1, n-1
         ix=450*x1(3,i)/l+1200
         iy=450*x1(4,i)/l+800
         ir=450*x1(1,i)/l
         call ellipse@( ix, iy, ir, ir, 7)
         call fill_ellipse@(ix,iy,ir-1,ir-1, 0)
 120     continue
       do 130 i = 1, n1
         ix = 519*x3(3,i)/l + 1200
         iy = 519*x3(4,i)/l + 1600
         ir = 519*x3(1,i)/l
         call ellipse@( ix, iy, ir, ir, 7)
         if (x3(2,i) .gt. 0.0) then
           call fill_ellipse@(ix, iy, ir-1, ir-1, 7)
           else
           call fill_ellipse@(ix, iy, ir-1, ir-1, 0)
         end if
 130     continue
       call set_text_attribute@(3, 3.0, 0.0, 0.0)
       call draw_text@ (a,1170, 1260, 7)
       call draw_text@ (b,1170, 1970, 7)
       call close_graphics_printer@
       end
```

Reference

Adler P. M., Zuzovsky M. and Brenner H., "Spatially periodic suspensions of convex particles in linear shear flows. II. Rheology," *International Journal of Multiphase Flow*, **11** (1985) 387.

Anon, "New innovative stencil printing technology developed by Gunter Erdmann and his team of experts at HTI engineering," *Surface Mount Technology*, Dec. (1994) 22

Ball R. C. and Richmond P., "Dynamics of colloidal dispersions," *Physics and Chemistry of Liquids*, **9** (1980) 99.

Barnes H. A., Edwards M. F. and Woodcock L. V., "Applications of computer simulations to dense suspension rheology," *Chemical Engineering Research*, **42** (1987) 591.

Batchelor G. K. and Green J. T., "The hydrodynamic interaction of two small freely-moving spheres in a linear flow field," *Journal of fluid mechanics*, **56** (1972) 375.

Bennett C. H., "Serially deposited amorphous aggregates of hard spheres," *Journal of Applied Physics*, **43** (1972) 2727.

Bernal J. D. and Mason J., "Co-ordination of randomly packed spheres," *Nature*, **188** (1960) 910.

Berryman G. J., "Random close packing of hard spheres and disks," *Physical Review A*, **27** (1983) 1053.

Bossis G. and Brady J. F., "Dynamic simulation of sheared suspensions. I. General method," *Journal of Chemical Physics*, **80** (1984) 5141

Brady J. F., Phillips R. J., Lester J. C. and Bossis G., "Dynamic simulation of hydrodynamically interacting suspensions," *Journal of Fluid Mechanics*, **195** (1988) 257.

Brady J. F. and Bossis G., "Stokesian Dynamics," *Annual Review of Fluid Mechanics*, **20** (1988) 111.

Chang C and Powell R L, "Dynamic simulation of bimodal suspensions of hydrodynamically interacting spherical particles," *Journal of Fluid Mechanics*, **253** (1993) 1.

Chang C. and Powell R. L., "Effect of particle-size distribution on the rheology of bimodal suspensions," *Journal of Rheology*, **38** (1994) 85.

Clarke A. S. and Wiley J. D., "Numerical simulation of the dense random packing of a binary mixture of hard spheres: Amorphous metals," *Physical Review B*, **35** (1987) 7350.

Clouthier R., "Appraising stencils for fine-pitch printing," *Surface Mount Technology*, March, (1995) 60.

Cox R. G., "The slow motion of a sphere through a viscous fluid towards a plane surface–II small gap widths, including inertial effect," *Chemical Engineering Science*, **22** (1967) 1753.

Cox R. G., "The motion of suspened particles almost in contact," *International Journal of Multiphase Flow*, **1** (1974) 343.

Cummings P. T. and Evans D. J., "Nonequilibrium molecular dynamics approaches to transport properties and non-newtonian fluid rheology," *Ind. Eng. Chem. Res.*, **31** (1992) 1237.

Currie M. A., "Characterization of solder pastes for surface mount assembly," PhD Thesis, Salford University, 1997.

Currie M. A., Ekere N. N., Mannan S. H. and Ismail I., "Solder paste characteristics and their effect on fine pitch printing," *Proceedings of 4th International Conference FACTORY 2000*, (1994) 552.

Daebler D., "Specifying solder paste materials for stenciling applications on thick circuits," *Electronic Packaging and Production*, **21** (1981) 5.

Durlofsky L., Brady J. F. and Bossis G., "Dynamic simulation of hydradynamicall interacting particles," *Journal of Fluid Mechanics*, **180** (1987) 21.

Ekere N. N. and Lo E. K., "New chalenges in solder-paste printing," *Journal of Electronics Manufacturing*, **1** (1991) 29.

Ekere N. N., Ismail I., Lo E. K. and Mannan S. H., "Experimental study of stencil/substrate separation speed in on-contact solder paste printing for reflow soldering," *Journal of Electronics Manufacturing*, **3** (1993) 25.

Ekere N. N., Mannan S. H. and Lo E. K., "Mapping of manufacturing process modelling," *Soldering and Surface Mount Technology Jounal*, **17** (1994) 4.

Evans J. W. and Beddow J. K., "Characterization of particle morphology and rheological behavior in solder paste," *IEEE Transactions on Components, Hybrids, and Manufacturing Technology*, **10** (1987) 224.

Gadala-Maria F. and Acrivos A., "Shear-induced structure in a concentrated suspension of solid spheres," *Journal of Rheology*, **24** (1984) 799.

Gamba A., "Random packing of equal spheres," *Nature*, **256** (1975) 521.

Ginsberg G., *Surface Mount and Related Technologies, Chapter 10*, Marcel Dekker Inc., New york, 1989.

Gotoh K. and Finney J. L., "Statistical geometrical approach to random packing density of equal spheres," *Nature*, **252** (1974) 202.

Gotoh K. and Finney J. L., "Repply to Gamba A.," *Nature*, **256** (1974) 522.

Hanrahan T. F., Monaghan P. F. and Babikian R. D., "Modelling of a solder paste flow with a free surface in stencil printing," *Advances in Electronic Packaging, ASME*, (1992) 587.

Haslehurst L. and Ekere N. N., "Parameter interactions in stencil printing of solder paste," *Journal of Electronics manufacturing*, **6** (1996) 307.

Head L. M., Rogers V., Sahay C. and Constable J., "Determination of shear stress at a solder paste/stencil interface," *Material Research Society Symposium Proceedings*, **323** (1994) 425.

Hwang J. S., *Solder Paste in Electronics Packaging*, Van Nostrand Reinhold, New York, (1989) 137-139.

Hwang J. S., "Solder/Screen printing", *Surface Mount Technology*, March (1994) 44.

Jeffrey D. J. and Acrivos A., "The rheological propertis of suspensions of rigid particles," *AIChE Journal*, **22** (1976) 417.

Jodrey W. S. and Tory E. M., "Computer simulation of isotropic, homogeneous, dense random packing of equal spheres," *Powder Technology*, **30** (1981) 111.

Jodrey W. S. and Tory E. M., "Computer simulation of close random packing of equal spheres," *Physical review A*, **32** (1985) 2374.

Jomha A. I. and Woodcock L. V., "Effects of oscillatory shear on the steady-flow of shear thickening suspensions," *Chemical Engineering Research and Design*, **68** (1990) 550.

Jomha A. I., Merrington A., Woodcock L. V., Barnes H. A. and Lips. A., "Recent developments in dense suspension rheology," *Powder Technology*, **65** (1991) 343.

Kitano T., Kataoka T. and Shirota T., "An empirical-equation of the relative viscosity of polymer melt filled with various inorganic fillers," *Rheology Acta*, **20** (1981) 207.

Kolli V. G., Gadala-Maria F. and Anderson R., "Rheological characterization of solder paste for surface mount applications," *IEEE Transactions on Components, Packaging, and Manufacturing Technology-Part B*, **20** (1997) 416.

Konakawa Y. and Ishizaki K., "The particle size distribution for the highest relative density in a compacted body," *Powder Technology*, **63** (1990) 241.

Krieger I. M. and Dougherty T. J., "A mechanism for non-newtonian flow in suspensions of rigid spheres," *Transaction of the Society of Rheology*, **3** (1959) 137.

Krieger I. M., "Rheology of monodisperse latices," *Adv. Colloid Interface Science*, **3** (1972) 113.

Lapasin R., "Rheological characterization of solder pastes," *Journal of Electronic Materials*, **23** (1994) 525.

Lee N., Xiao M., Lawless K. J., Slattery J. A. and Sovinsky J. R., "Solder paste for tommorow's electronics manufacturing technology," *Journal of Electronics Manufacturing*, **4** (1994) 181.

Li Y., Mahajan R. L. and Nikmanesh N., "Fine pitch stencil printing process modelling and optimization," *Transactions of the AMAE: Journal of Electronic Packaging*, **118** (1996) 1.

Lu G. Q. and Shi X., "Computer simulation of isostatic powder compaction by random packing of monosized particles," *Journal of Mterials Science Letters*, **13** (1994) 1709.

Lu G. Q., Ti L. B. and Ishizaki K., "A new algorithm for simulating the random packing of monosized powder in CIP processes," *Materials and Manufacturing Processes*, **9** (1994) 601.

Mackay C. A., "Solder creams and how to use them," *Electronic Packaging and Production*, **21** (1981) 11.

Mannan S. H., Ekere N. N., Lo E. K. and Ismail I., "Application of ink screen printing models to solder paste printing in SMT assembly", *Journal of Electronics Manufacturing*, **3** (1993) 113.

Mannan S. H., Ekere N. N., Ismail I. and Lo E. K., "Squeegee deformation study in the stencil printing of solder pastes," *IEEE Transctions on Components, Packaging, and Manufacturing Technology-Part A*, 17 (1994) 470.

Mannan S. H., Ekere N. N., Ismail I. and Currie M. A., "Computer simulation of solder paste flow. Part I: Dense suspension theory", *Journal of Electronics Manufacturing*, **4** (1994) 141.

Mannan S. H., Ekere N. N., Ismail I. and Currie M. A., "Computer simulation of solder paste flow. Part II: Flow out of a stencil aperture", *Journal of Electronics Manufacturing*, **4** (1994) 149.

Mannan S. H., Ekere N. N., Ismail I. and Currie M. A., "Flow processes in solder paste during stencil printing for SMT assembly," *Journal of Materials Science: Materials in Electronics*, **6** (1995) 34.

Matheson A. J., "Computation of a random packing of hard spheres," *Journal of Physics C: Solid State Physics*, 7 (1974) 2569.

Metzner A. B., "Rheology of suspensions in polymeric liquids," *Journal of Rheology*, **29** (1985) 739.

Morris J. R. and Wojcik T., "Stencil printing of solder paste for fine-pitch surface mount assembley," *Soldering & Surface Mount Technology*, June (1990) 5.

Myklak P. R. and Coleman W. E., "Hybrid stencil: a laser cut/chem-etch stencil to optimize fine pitch stencil printing," *Proceedings of the Technical Program -National Electronic Packaging and Production Conference*, (1995) 1116.

Nolan G. T. and Kavanagh P. E., "Computer simulation of random packing of hard spheres," *Powder Technology*, **72** (1992) 149.

Nolan G. T. and Kavanagh P. E., "Computer simulation of random packings of spheres with log-normal distributions," *Powder Technology*, **76** (1993) 309.

Onoda G. Y. and Liniger E. G., "Random loose packing of uniform spheres and the dilatancy onset," *Physical Review letters*, **64** (1990) 2727.

Owczarek J. A. and Howland F. L., "A study of the off-contact screen printing process-Part I: Model of the printing process and some results derived from experiments," *IEEE Transactions on Components, Hybrids, and Manufacturing Technology*, **13** (1990) 358.

Owczarek J. A. and Howland F. L., "A study of the off-contact screen printing process-Part II: Analysis of the model of the printing process," *IEEE Transactions on Components, Hybrids, and Manufacturing Technology*, **13** (1990) 368.

Rajewski K., "Defect minimization for no clean," *Surface Mount Technology*, February (1996) 48.

Riemer D. E., "Analytical engineering model of the screen printing process: Part I," *Solid State Technology*, August (1988) 107.

Riemer D. E., "Analytical engineering model of the screen printing process: Part II," *Solid State Technology*, September (1988) 85.

Rooskozel B., "Designing solder paste materials for the attachment of surface mounted components," *Proceedings of the Technical Program -National Electronic Packaging and Production conference*, (1983) 334.

Rooskozel B., "Controlling pad bridging in SMD attachment," *Circuits Manufacturing*, **24** (1984) 68.

Rubin, "Solder creams and vapour soldering in hybrid technology," *Electronic Production*, **12** (1983) 13.

Rumpf H., *Particle Technology*, Chapman and Hall, London, (1990) 20-28.

Schultz M. A. and Struble L. J., "Use of oscillatory shear to study flow behaviour of fresh cement paste," *Cement and Concrete Research*, **23** (1993) 273.

Schütt J., "Ultra-fine-pitch solder paste printing," Surface Mount Technology, June (1993) 27.

Scott G. D., "packing of equal spheres," *Nature*, **188** (1960) 908.

Sengun M. Z. and Probstein R. F., "High-shear-limit Viscosity and the Maximum Packing Fraction in Concentrated Monomodal Suspensions," *PhysicoChemical Hydrodynamics*, **11** (1989) 229.

Sengun M. Z. and Probstein R. F., "Bimodal model of slurry viscosity with application to coal-slurries. Part 2. High shear limit behaviour," *Rheology Acta*, **28** (1989) 394.

Shapiro A. P. and Probstein R. F., "Random packing of spheres and fluidity limits of monodispersed and bidisperse suspensions," *Physical Review Letters*, **68**, (1992) 1422.

Sudduth R. D., "A generalized model to predict the viscosity of solutions with suspended particles," *Journal of Applied Polymer Science*, **48** (1993) 25.

Sudduth R. D., "A new method to predict the maximum packing fraction and the viscosity of solutions with a size distribution," *Journal of Applied Polymer Science*, **48** (1993) 37.

Takamura K., Goldsmith H. L. and Mason S. G., "The microrheology of colloidal dispersions. 12. Trajectories of orthokinetic pair-collisions of latex spheres in a simple electrolyte," *Journal of and Interface Science*, **82** (1981) 175.

Tanner R. I., *Engineering Rheology*, Clarendon Press, Oxford, (1985) 52-62.

Thomas D. G., "Transport characteristics of suspension: VIII. A note on the viscosity of Newtonian suspensions of uniform spherical particles," *Journal of Colloid Science*, **20** (1965) 267.

Tory E. M., Cochrane N. A. and Waddell S. R., "Anisotropy in simulated random packing of equal spheres," *Nature*, **220** (1968) 1023.

Trankel N. A. and Acrivos A., "On the viscosity of concentrated suspension of solid spheres," *Chemical Engineering Science*, **22** (1967) 847.

Tsai S. C. and Viers B., "Effect of liquid polarity on rheology of noncolloidal suspensions," *Journal of Rheology*, **31** (1987) 483.

Turian R. M., Hsu F., Avramidis K. S., Sung D. and Allendorfer R. K., "Settling and rheology of suspensions of narrow-sized coal particles," *AIChE Journal*, **38** (1992) 969.

Visscher W. M. and Bolsterli M., "Random packing of equal and unequal spheres in two and three dimensions," *Nature*, **239** (1972) 504.

Woodcock L. V. and Angell C. A., "Diffusivity of the hard-sphere model in the region of fluid metastability," *Physics Review Letters*, **47** (1981) 1129.

Yerazunis S., Cornell S. W. and Wintner B., "Dense random packing of binary mixtures of spheres," *Nature*, **207** (1965) 835.

Zwick K. J., Ayyaswamy P. S. and Cohen I. M., "Die-bonding in micro-electronic packaging by oscillatory squeezing," *Advances in Electronic Packaging, ASME 1997*, **1** (1997) 373.